Province of British Columbia
Ministry of Energy, Mines and
Petroleum Resources

MINERAL RESOURCES DIVISION
Geological Survey Branch

EVOLUTION OF THE IRON MASK BATHOLITH AND ITS ASSOCIATED COPPER MINERALIZATION

By Y. T. J. Kwong

BULLETIN 77

MINERAL RESOURCES DIVISION
Geological Survey Branch

Canadian Cataloguing in Publication Data
Kwong, J.
Evolution of the iron mask batholith and its associated copper mineralization

(Bulletin, ISSN 0226-7497 ; 77)

Bibliography: p.
ISBN 0-7718-8603-9

1. Batholiths — British Columbia — Thompson-Nicola. 2. Copper ores — British Columbia — Thompson-Nicola. 3. Gold ores — British Columbia — Thompson-Nicola. 4. Geology, Economic — British Columbia — Thompson-Nicola. I. British Columbia. Geological Survey Branch. II. Title. III. Series: Bulletin (British Columbia. Ministry of Energy, Mines and Petroleum Resources) ; 77.

QE187.K86 1987 553.4 C87-092181-9

VICTORIA
BRITISH COLUMBIA
CANADA

September 1987

TABLE OF CONTENTS

		Page
SUMMARY		v
1	INTRODUCTION	1
	Location, Access, and Physical Features	1
	Previous Work	1
	Acknowledgments	1
2	GEOLOGY OF THE IRON MASK BATHOLITH	3
	Regional Setting	3
	General Geology	3
	Nicola Group	3
	Intrusive Rocks of the Iron Mask Batholith	3
	Iron Mask Hybrid Unit	4
	Pothook Unit	4
	Picrite Unit	4
	Sugarloaf Unit	4
	Cherry Creek Unit	5
	Kamloops Group Volcanic and Sedimentary Rocks	5
3	AFTON MINE — LOCAL GEOLOGY AND DISTRIBUTION OF MINERALS	7
	Introduction	7
	Local Geology and Petrography of the Afton Open Pit	7
	General Aspects	7
	Detailed Pit Petrography	7
	Mineral Distribution and Alteration Patterns	11
	Introduction	11
	Lateral Distribution of Minerals	13
	Vertical Distribution of Minerals	13
	Details of Ore Mineralization	18
	Discussion and Interpretation	18
	Summary and Conclusions	21
4	MAJOR ELEMENT GEOCHEMISTRY	23
	Introduction	23
	Results of Major Element Analyses	23
	Discussion and Interpretation	28
	Evolution of the Iron Mask Batholith	28
	Evolution of Copper Mineralization Within the Iron Mask Batholith	29
	Summary and Conclusions	32
5	A THERMODYNAMIC SIMULATION OF SUPERGENE ALTERATION AT AFTON MINE	35
	Introduction and Method of Approach	35
	Specifications for Computer Runs	35
	Results and Interpretation	36
	General Aspects	36
	Enrichment Versus Nonenrichment and Dominance of a Particular Phase	37
	Discrepancies between Theoretical and Observed Mineral Assemblages	41
	Other Considerations	42
	Summary and Conclusions	43
6	ASSESSING THE MINERAL POTENTIAL OF THE IRON MASK BATHOLITH	45
	Commodities of Interest	45
	Indicators of Mineralization	46
	Summary and Conclusions	47
BIBLIOGRAPHY		48
APPENDICES		
IA.	Major element geochemistry and brief sample descriptions of the major intrusive phases of the Iron Mask pluton and rocks in its vicinity	51
IB.	Major element geochemistry and brief sample descriptions of rocks collected from the Afton property	52
II.	Results of microprobe analyses of selected minerals	54
III.	A list of major mineral occurrences in the Iron Mask batholith	55
TABLES		
1.	Petrographic characteristics of various rock units of the Iron Mask batholith	24
2.	Major element geochemistry of various rock units making up or associated with the Iron Mask pluton	25
3A.	Composition of starting material (in modal per cent)	35
3B.	Composition of hypothetical rain water used in simulation runs	36
4.	Composition of northwest pit wall seepage water, March 14, 1979 (courtesy of Afton Mines Ltd.)	43
5.	Metal production from the Iron Mask batholith prior to 1970	45
6.	Precious metals content of selected samples from the Iron Mask batholith by emission spectrographic analysis	46
7.	Copper and gold contents of a suite of samples from the Joker claim: a systematic chip-sampling of a small portion of the west side of a gully along Anderson Creek	47
FIGURES		
1.	Generalized geology of south central British Columbia (modified from Geological Survey of Canada, Map 232A)	4
2.	Generalized geology of the Iron Mask batholith	In pocket
3.	A geological map (A) and geological section (B) of the Afton property (after Carr and Reed, 1976)	8

TABLE OF CONTENTS — *Continued*

Page

4. A geological section across the eastern half of the Afton open pit, illustrating the complexity of the host rocks involved ... 9
5. A highly generalized geological plan of the Afton open pit at the 610–640-metre levels as of June 1979 ... 9
6. Mineral distribution within the Afton open pit at the 613-metre level, as revealed by X-ray diffraction analyses of blasthole composite samples ... 12

7(a-c). Distribution of selected minerals as determined from petrographic examination of 173 specimens from the 613–640-metre levels of the Afton open pit ... 14

7(d). Distribution of ore and accessory minerals in the 613–640-metre levels of the Afton open pit ... 15

8. Hydrothermal alteration observed in a geological section (11 on Figure 5) across the eastern portion of the orebody ... 16
9. An illustration of vertical distribution of minerals at Afton mine; distribution of high temperature alteration minerals in a geological section (18 on Figure 5) across the western portion of the orebody ... 17
10. Distribution of copper and gold at various benches in the Afton pit ... 20
11. Harker plots of analyses of the major intrusive phases of the Iron Mask pluton ... 26
12. A total alkali – total iron – magnesia plot of analyses of the four major intrusive phases of the Iron Mask pluton ... 28
13. A comparison of analyses of various rock groups related to the Iron Mask batholith with those of the four major intrusive phases of the batholith ... 30

Page

14. A total-alkali versus silica plot for analyses of various rock groups within the Iron Mask pluton ... 32
15. Changes in solution chemistry and the production and destruction of minerals as a result of rain water – rock interactions at 25°C and a pressure of 1 bar (east pit) ... 37
16. Changes in solution chemistry and the production and destruction of minerals as a result of rain water – rock interactions at 25°C and a pressure of 1 bar (west pit) ... 38
17. Changes in solution chemistry and the production and destruction of minerals as a result of rain water – hypothetical monzonite interactions at 25°C and a pressure of 1 bar ... 39
18. The evolutionary paths of the reacting solutions for the three simulation runs over the stability fields of minerals in the Cu-Fe-S-O system at 25°C and a pressure of 1 bar ... 40
19. Distribution of sulphur species at 25°C and 100°C as a function of oxygen fugacity, f_{O_2}, and solution pH ... 41
20. Paragenesis of product minerals resulting from the rainwater-rock interaction calculations ... 42
21. Commodities of interest in mineral claims of the Iron Mask batholith ... 45

PLATES

1. Native gold coating chalcocite which incompletely replaces bornite ... 19

SUMMARY

The Iron Mask batholith is an elongated composite intrusion that extends northwesterly across Kamloops Lake in south central British Columbia. It consists of two major intrusive bodies, the Cherry Creek pluton to the northwest and the Iron Mask pluton to the southeast; these consist of four major intrusive phases: the Iron Mask Hybrid, Pothook, Sugarloaf, and Cherry Creek units. The composition and texture range from coarse-grained gabbro to microsyenite. As a whole, this intrusion has alkaline affinity, is considered to be subvolcanic, and is comagmatic and coeval with Upper Triassic rocks of the Nicola Group that it intrudes. Locally, intrusive picrite is also prominent. While the picrite is probably not genetically related to the batholith, its presence may have affected the ore deposition in the batholithic rocks.

Afton mine, a major copper and gold producer, is located at the northwestern end of the Iron Mask pluton. It is at the western extremity of a west-trending, intensely brecciated zone and is hosted entirely by rocks of the Cherry Creek unit. Supergene native copper with subordinate chalcocite accounts for 80 per cent of the 30.8-million-tonne orebody; hypogene mineralization consists mainly of bornite and chalcopyrite. A detailed study of the distribution of minerals in the Afton open pit indicates that primary mineralization took place in a roof pendant environment characterized by a diversified array of rock types. Hydrothermal alteration proceeded under a condition of low fluid/rock ratio such that primary mineralogy controlled the appearance of the secondary minerals. Whereas little meteoric water was involved in the hypogene mineralization, supergene alteration was dominated by irreversible mineral-solution (groundwater) interactions.

Based on major element geochemical data, petrographic observations and field evidence, the four major phases of the batholith are related by the process of fractional crystallization. The magmatic differentiation took place under conditions of high oxidation state with continual magnetite separation; this affected the solubility and composition of subsequently separated sulphides. The Afton protore is likely a byproduct of magmatic differentiation, generated at the early Cherry Creek stage when portions of the fractionating magma were intruded into a subvolcanic environment. Local trapping of late magmatic fluids remobilized and concentrated sulphides, which were disseminated in the pluton, to form the hypogene ore.

Supergene alteration at Afton is unique; a thermodynamic simulation demonstrates that the dominance of native copper and the lack of copper enrichment in the supergene zone relate to the relatively mafic composition of the wallrocks, and to the paucity of sulphides produced during hypogene mineralization. Supergene alteration of porphyry copper deposits in general can be interpreted in the framework of a log f_{O_2} versus log f_{S_2} plot within two arbitrary "limiting" curves characterized by extreme values of acidic and basic conditions respectively. If a reacting fluid evolves parallel and close to the upper or acidic " limiting" curve, it is more likely to give rise to a well-developed leached cap with an enriched supergene ore blanket underneath. In contrast, a reacting fluid evolving parallel and close to the lower or basic "limiting" curve will lead to a spectrum of copper oxides, native copper, and little enrichment.

Upon reassessing the mineral potential of the batholith, attention is drawn to the possibility of recovering palladium as a byproduct in the mining of major commodities like copper, gold and silver. Furthermore, subeconomic concentrations of ore minerals throughout the batholith may be amenable to recovery by heap leaching. While feldspathization, carbonatization, and association with altered picrite may provide indications of hypogene mineralization, careful examination of reddish ochreous oxidation products and geochemical sampling of stream sediments and old drainage systems are recommended in the search for supergene ore. The southeastern end of the Iron Mask pluton appears to have the right geological environment to host another Afton-type deposit and thus deserves further detailed examination.

CHAPTER 1

INTRODUCTION

The Iron Mask batholith is one of several large alkaline intrusions in the Intermontane Belt that contain porphyry copper deposits. It is a subvolcanic, multiple intrusion which is comagmatic and coeval with Upper Triassic rocks of the Nicola Group. Five different phases of the batholith have been recognized and all contain some copper mineralization. At this time, Afton mine is the only major copper-gold producer located within the batholith. The proven start-up reserves of the Afton orebody were 30.84 million tonnes grading 1.0 per cent copper, 0.58 gram per tonne gold and 4.19 grams per tonne silver at a cutoff grade of 0.25 per cent copper. Besides being hosted by dioritic rocks of alkaline affinity, salient characteristics of the deposit include two unique features; these are the absence of a well-defined hypogene alteration pattern about the orebody, and the abundance of native copper in the supergene zone without apparent copper enrichment.

This bulletin is a synthesis of studies completed to date on the Iron Mask batholith and the Afton deposit. Emphasis is placed on geochemical and mineralogical aspects of the batholith and the copper-gold deposit, that shed light on their derivation and evolution. Through theoretical modelling with pertinent thermodynamic data, the unique supergene alteration features of the Afton orebody are explained. Applications of the major findings of this study are briefly discussed with respect to other copper ± gold occurrences in the batholith.

LOCATION, ACCESS, AND PHYSICAL FEATURES

The Iron Mask batholith, centred at latitude 50.6 degrees north and longitude 120.5 degrees west, is located 230 kilometres northeast of Vancouver, near the city of Kamloops in south central British Columbia. The batholith comprises two major northwesterly trending plutons separated by 6 kilometres of younger volcanic and sedimentary rocks just south of Kamloops Lake. The larger pluton, the 18-kilometre-long southern part of the batholith, is called the Iron Mask pluton*. The smaller Cherry Creek pluton farther northwest outcrops on either side of Kamloops Lake. The combined exposure of the batholith, including the intervening younger rocks, is about 33 kilometres long and 5 kilometres wide.

Afton mine is located at the northwestern end of the Iron Mask pluton, along the south side of the relocated Trans-Canada Highway. Excellent access to the rest of the batholith is provided by the Trans-Canada Highway and secondary gravel or dirt ranching and mining roads. Rolling summits and broad uplands are the prominent topographic features, with elevations lying between 610 and 1100 metres. The batholith is situated within the dry belt of British Columbia. Annual precipitation recorded in Kamloops averages about 26 centimetres. Vegetation is dominated by sagebrush; there is local, park-like forest with little underbrush. Whereas outcrops within the batholith are generally adequate to reveal the overall geology of the component units, outcrops at its outer contacts are rare.

PREVIOUS WORK

Early geological literature relevant to the Iron Mask batholith (Dawson, 1877 and Young and Uglow, 1926) is mainly concerned with its magnetite occurrences. Since then, most exploration on the batholith has been directed toward discovery of porphyry copper mineralization. The thesis of Mathews (1941) and the memoir of Cockfield (1948) furnished the early descriptions of the geology of the Iron Mask batholith. Subsequently, Carr (1956) and Preto (1967) studied the Iron Mask pluton in more detail and summarized the exploration activities then prevalent in the batholith. Recently, Northcote (1974, 1976, and 1977) continued the study and furnished valuable information on the structure and general geology of the Iron Mask pluton. The mineral potential of the various phases of the pluton was also briefly discussed.

The Afton claims were first staked in 1949 but the Afton orebody was not discovered until 1971, after extensive percussion drilling by C.F. Millar for Afton Mines Ltd. Based on field mapping, core logging, and mine records, Preto (1972) provided the first published comprehensive account on the geology and structure of the Afton deposit. As a contribution to the understanding of porphyry deposits of the Canadian Cordillera, Carr and Reed (1976) described the overall salient features of the deposit. Meanwhile, the discovery of the Afton orebody and the subsequent start of open-pit mining in 1977 have stimulated three thesis research projects toward advanced degrees in geology. Hoiles (1978) studied the nature and genesis of the Afton orebody, and furnished sulphur isotope data on the prevalent sulphides. Cann (1979) studied the geochemistry of magnetites in the Iron Mask batholith and made special reference to its significance in the genesis of the Afton orebody. Kwong (1982) presented a new look at the copper mine in light of the distribution of minerals, host rock geochemistry and irreversible mineral solution interactions. The paper of Reed (1983) on the structural geology and geostatistical parameters of the Afton copper-gold mine makes up the latest piece of information on the deposit.

ACKNOWLEDGMENTS

This bulletin is based mainly on a dissertation submitted to the Faculty of Graduate Studies, The University of British Columbia, in 1982. Fieldwork on Afton was done mainly in June 1979. A brief examination of other mineral occurrences

*Northcote (1974, 1976, and 1977) refers to this pluton alone as the Iron Mask batholith.

in the summer of 1982 further clarified the overall style of mineralization in the batholith. The writer wishes to acknowledge the support of the British Columbia Ministry of Energy, Mines and Petroleum Resources in granting the permission to complete the thesis research on a part-time basis. Drs. H.J. Greenwood, T.H. Brown, C.I. Godwin and K.C. McTaggart of The University of British Columbia provided many helpful suggestions during thesis research and writing. Dr. W.J. McMillan and J.M. Newell critically read the revised manuscript. Discussions on the geology of the batholith and Afton mine by previous workers, especially K.E. Northcote, V.A. Preto, A.J. Reed, and the late J.M. Carr, have been freely drawn upon in this report; their contributions are acknowledged.

CHAPTER 2

GEOLOGY OF THE IRON MASK BATHOLITH

REGIONAL SETTING

The Iron Mask batholith lies in the southern part of the Quesnel trough, which is also known as the Nicola belt. The Quesnel trough, located in the Intermontane structural belt of British Columbia, is 1200 kilometres long, 30 to 60 kilometres wide and consists of Lower Mesozoic volcanic and related rocks enclosed between older rocks. It is much invaded by batholiths and smaller intrusions and is copper rich (Campbell and Tipper, 1970). Porphyry copper mines in the trough include, from north to south, Bell, Granisle, Gibraltar, Afton, the Highland Valley deposits, Brenda, Ingerbelle, and Copper Mountain.

The Nicola belt extends from south of Kamloops Lake 200 kilometres to the International Boundary. The most important pre-Tertiary rocks in this belt are Late Triassic volcanic and sedimentary rocks of the Nicola Group. The Nicola belt is divided into a series of narrow northerly trending blocks by several large, high-angle, northerly trending faults (Figure 1). These faults are interpreted to be basement structures which controlled the distribution of volcanic centres and flanking sedimentary basins (Preto, 1977). Preto *et al.* (1979) identified four groups of major plutonic events in the belt. They are characterized by the ages of 200 million years (Ma), 160 Ma, 100 Ma, and 50–70 Ma respectively. The Iron Mask batholith is one of the larger alkaline plutons of the 200-Ma age group. It is situated along the southwest side of a regional northwest-trending fracture zone and is itself cut by numerous northwesterly faults. Northcote (1976) and Preto (1977) suggested that the batholith and other alkaline plutons in the same group are likely centres of Nicola volcanism.

GENERAL GEOLOGY

The Iron Mask batholith consists of two related plutons, namely the Iron Mask pluton and the Cherry Creek pluton, formerly believed to be a single connected body (Cockfield, 1948). The Iron Mask pluton comprises four major, successively emplaced units designated as the Iron Mask Hybrid, Pothook, Sugarloaf, and Cherry Creek units. Locally, an additional Picrite unit also occurs which is probably not genetically related to the batholith. The smaller Cherry Creek pluton consists entirely of Cherry Creek unit. Isotopic dates (194 to 204 $\pm$ 6 Ma) furnished by Preto *et al.* (1979) indicate that all of these units are of Late Triassic or earliest Jurassic age.

Figure 2 (in pocket) depicts the generalized geology of the Iron Mask batholith and its vicinity. The following abridged description is taken mainly from the detailed studies of Preto (1967) and Northcote (1974, 1976, and 1977) and augmented by observations made by the writer during short field studies in the summers of 1979 and 1982.

NICOLA GROUP

The two plutons of the Iron Mask batholith are emplaced in Upper Triassic strata of the Nicola Group. In the vicinity of the batholith, the Nicola Group is dominated by volcanic and volcaniclastic sedimentary rocks. They are generally recognized by albitization of feldspars, occurrence of patchy epidote, and/or rare hematite alteration.

On the southwestern flank of the Iron Mask pluton, well-indurated, massive and bedded tuff, breccia, and interbedded flows and flow breccia are prominent. All of these rocks are weakly metamorphosed and most of them show a fairly uniform green-grey colour. On the northeast flank, less well-indurated and less altered tuff and tuff breccia predominate. However, adjacent to the intrusive contact, these rocks are also well indurated and epidotized and are locally mineralized with sulphides. Fragments found in the tuff breccia include some belonging to the intrusive Cherry Creek unit. This apparently contradictory observation is readily explained if the batholithic rocks and the Nicola volcanic rocks are comagmatic and coeval, such that during the evolution of the common parent magma, the prevalence of an intrusive phase or its volcanic equivalent is dependent on whether or not the magma reached the surface.

At the southeastern tip of the Iron Mask pluton and locally along the southwestern flank, the Nicola rocks comprise distinctive porphyritic augite-hornblende basalt, very similar to varieties of the Sugarloaf unit that occur along the southwest flank of the pluton. Locally, basaltic breccia that is porphyritic with 10 to 25 per cent olivine and augite phenocrysts is also prominent. North of Hughes Lake near the northwestern end of the pluton, the volcanic breccia contains occasional argillite and limestone blocks. Adjacent to the Cherry Creek pluton farther north, rocks of the Nicola Group consist mainly of porphyritic plagioclase andesite with occasional interbedded tuffs.

INTRUSIVE ROCKS OF THE IRON MASK BATHOLITH

The multiphase batholith is believed to have been emplaced in a subvolcanic environment. All component units except the Picrite unit are thought to be genetically related. Their distribution is largely controlled by major systems of northwesterly, northerly, and northeasterly trending fractures or faults. Most units show some degree of alteration and/or contamination which may be intense locally. Weak to moderate saussuritization is ubiquitous in all batholithic rocks while potassium feldspathization is more prominent in rocks of the Cherry Creek unit. Rock units and varieties are mainly distinguished in the field by original textures which, in most cases, are still visible despite alteration. The average modal composition of these rock units will be presented and discussed in conjunction with major element geochemistry in a later chapter. Here, the individual

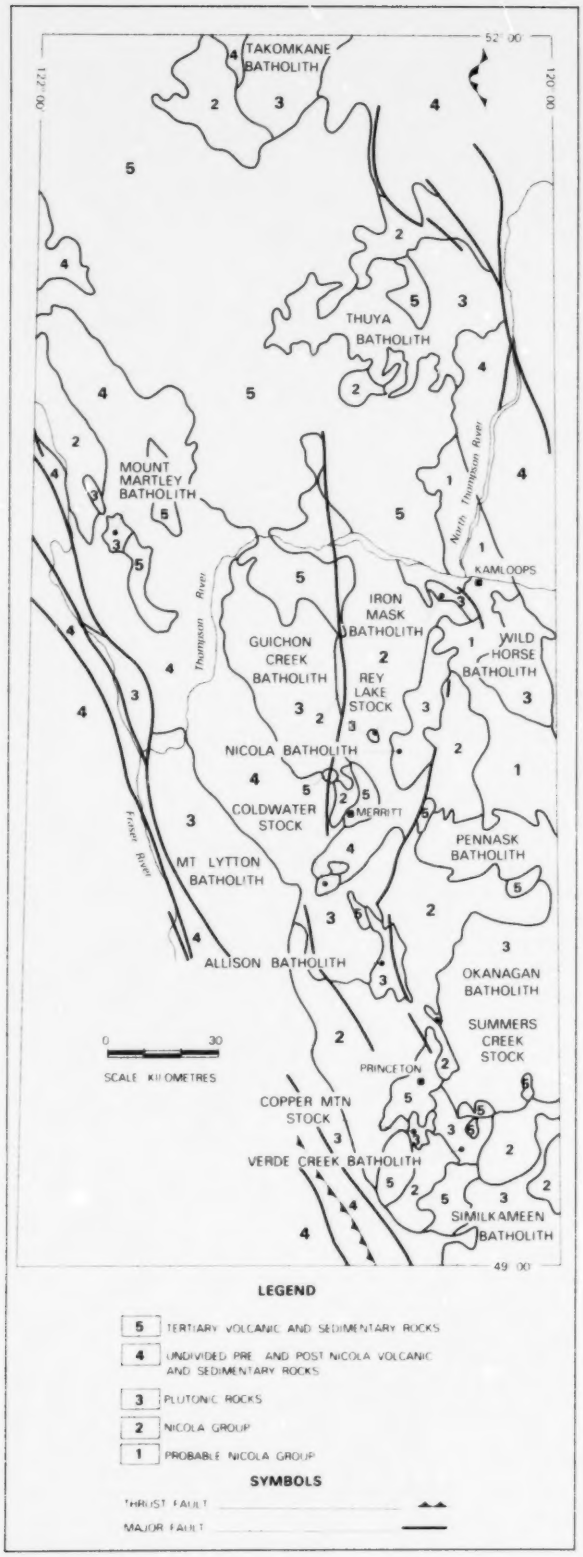

Figure 1. Generalized geology of south central British Columbia (modified from Geological Survey of Canada, Map 232A).

units are briefly described in order of oldest to youngest, as determined mainly on crosscutting relationships.

Iron Mask Hybrid Unit

The Iron Mask Hybrid unit, the oldest intrusive phase of the batholith, forms the spine of the Iron Mask pluton and accounts for about 40 per cent of its exposures. In the northwestern half of the pluton, this unit is cut and partially enclosed by the Cherry Creek unit, the youngest phase of the batholith. In the southeastern half of the pluton, rocks of the Iron Mask Hybrid unit form a margin about 1.2 kilometres wide along the southwest side; they also occur in the northern portion, as an elongated pendant in Cherry Creek rocks, from east of Coal Hill southeasterly toward Knutsford Hill.

The Iron Mask Hybrid unit is mostly agmatitic, consisting of rounded to angular fragments of various sizes, texture and composition in a dioritic matrix. The fragments, which make up more than 80 per cent by volume of a typical outcrop, include mainly coarse and fine-grained diorite and coarse-grained gabbro with lesser amounts of medium to coarse grained hornblendite and scattered xenoliths of Nicola Group volcanic rocks. They are interpreted to represent slightly older intrusive equivalents of lower Nicola volcanic rocks carried up to a higher level by resurgence of magmatic activity. Mineralization, particularly of iron and copper, is almost ubiquitous in the Iron Mask Hybrid unit. In fact, except where Nicola xenoliths are predominant, all rock varieties in the unit contain magnetite which is often more than 10 per cent by volume. The Iron Mask mine, a former copper producer, is located in this unit, but is also associated with picrite.

Pothook Unit

The Pothook unit occurs mainly in the northwestern half of the Iron Mask pluton, appearing frequently as narrow, gradational zones between the Iron Mask Hybrid and Cherry Creek units. Rocks of this unit are uniformly of dioritic composition and are medium to coarse grained. Many of the coarse-grained rocks exhibit cumulate texture (Cann, 1979). The Pothook unit is locally mineralized with copper and iron. Magnetite occurring in uniformly dipping veins is prominent south and southeast of the Afton deposit.

Picrite Unit

The Picrite unit consists of rocks of basaltic composition with abundant clinopyroxene and serpentinized olivine phenocrysts. These rocks generally occur as steeply dipping, poorly exposed and relatively small lenticular bodies in many parts of the batholith. They appear to be associated with recurring, northwesterly trending fracture systems and copper mineralization frequently occurs in their vicinity. The genetic relationship of the Picrite unit with the other phases of the batholith is not clear. Because picrite basalt has been observed far from the two component plutons of the batholith (for example, north of Kamloops Lake at both Carabine and Watching Creeks; Cockfield, 1948; Carr, 1956), it is probable that this unit is not part of the batholith.

Sugarloaf Unit

The Sugarloaf unit occurs mainly along the southwest side of the Iron Mask pluton and as small enclosed bodies in the southern half of the pluton. Rocks of this unit are mainly

porphyritic with hornblende, minor clinopyroxene, and plagioclase in a greyish green matrix. They are of fairly uniform diorite-andesite composition. Fine-grained varieties are not readily distinguished from the Nicola volcanic flows. Several copper occurrences are hosted by the Sugarloaf rocks. For example, the Ajax property east of Jacko Lake is located within brecciated and albitized Sugarloaf rocks (Preto, 1967).

Cherry Creek Unit

The Cherry Creek unit is the most widely distributed phase of the batholith. It constitutes the entire Cherry Creek pluton and also accounts for about 50 per cent of the exposure of the Iron Mask pluton. The unit consists of rocks with composition ranges from diorite, monzonite, syenite, to their porphyritic and fine-grained equivalents as well as local intrusive breccias. These rocks are believed to represent small, localized, differentiating offshoots intruded into widely varied physical and chemical environments during the later stages of evolution of the batholith.

Copper and minor iron mineralization is prominent in the Cherry Creek unit, particularly in zones of intense brecciation associated with alkali metasomatism. Afton mine, for example, lies at the western termination of a narrow, 4-kilometre-long, easterly trending zone of intense intrusive brecciation that is located at the northern edge of the Iron Mask pluton. The brecciation is considered to have resulted from high-level venting events. Similar breccia, consisting largely of Cherry Creek fragments, has also been observed on the Kimberley copper property northwest of Knutsford (Preto, 1967) and at the extreme southeastern tip of the Iron Mask pluton.

KAMLOOPS GROUP VOLCANIC AND SEDIMENTARY ROCKS

Early Tertiary sedimentary and volcanic rocks of the Kamloops Group unconformably overlie the Nicola rocks and the Iron Mask batholith. These include tuffaceous sandstone, siltstone, and shale with minor conglomerate, as well as basaltic to andesitic flows and agglomerates with minor dacite, latite, and trachyte. The Iron Mask pluton and the Cherry Creek pluton are separated by a thick sequence of Kamloops Group rocks occupying what appears to be a graben structure resulting from renewed fault movement around the margins of the plutons during Paleocene or Early Eocene time. The geology of these rocks has been described in detail by Ewing (1982).

CHAPTER 3

AFTON MINE – LOCAL GEOLOGY AND DISTRIBUTION OF MINERALS

INTRODUCTION

Afton mine is located beside the Trans-Canada Highway, 13 kilometres west of Kamloops and 420 kilometres northeast of Vancouver at latitude 50° 39'N and longitude 120° 31'W. Start-up reserves were 30.84 million tonnes of open-pit ore grading 1.0 per cent copper, 0.58 gram per tonne gold and 4.19 grams per tonne silver at a 0.25 per cent copper cutoff grade. It comprises two distinct zones: a reddish supergene zone which accounts for 80 per cent of the ore and a greyish hypogene zone which contains the rest of the ore reserves.

The Afton deposit is one of the alkaline suite of porphyry copper deposits that occur in the Intemontane Belt. It is situated at the northwestern extremity of the Iron Mask pluton and is hosted by Cherry Creek rocks. Deformation in post-Triassic time, during the Coast Mountain orogeny, took place around the margin of the pluton and led to the emergence of a high-relief terrain of structurally bounded plateaus and adjoining graben structures where thick sequences of Kamloops Group rocks accumulated (Preto, 1972; Carr and Reed, 1976; and Ewing, 1982). Deep weathering at the plateau margins promoted the supergene alteration at Afton until the elimination of extreme relief by the gradual filling of the basins by the Middle Eocene (Carr and Reed, 1976). These Eocene strata served to protect the orebody from abrasion by Pleistocene glaciers.

The development history, general geology, and structural geology of the Afton deposit have been described in literature summarized in Chapter 1. This chapter focuses on the petrography of the Afton orebody and on the significance of the distribution of several minerals not previously delineated.

LOCAL GEOLOGY AND PETROGRAPHY OF THE AFTON OPEN PIT

GENERAL ASPECTS

Figures 3A and B (after Carr and Reed, 1976) depict the local geology and a vertical geological section of the Afton property. As shown, the orebody, which generally strikes west-northwest, dips southward at 55 degrees and has an overall length of 520 metres, lies completely within the Cherry Creek unit of the Iron Mask pluton. It is separated from the Tertiary rocks to the north mainly by faults and locally by a rather flat-lying unconformity which postdates the supergene event (Carr and Reed, 1976). The Cherry Creek rocks intrude the Nicola Group rocks; the contact is steep, southward dipping and partly sheared. Within this simplified framework, local complications arise because of the highly fractured and altered nature of the host rocks, similarity of both texture and composition of the intrusive and extrusive rocks, gradational contacts between various phases of the intrusive rocks, and the inclusion of large slabs of one rock type in another. Consequently, geological contacts in many cases are drawn rather subjectively. The amount of potassium feldspar present has been utilized by Northcote (1974, 1976, and 1977), Carr and Reed (1976), and Preto (1972) to differentiate various phases of the Iron Mask pluton and between the extrusive and intrusive rocks where brecciation precludes easy identification of primary features (G.P.E. White, personal communication). In view of the fine grain size of most rocks found on the Afton property, two additional criteria are used here in the classification of rock types. Intrusive rocks are distinguished from the extrusive ones by their holocrystalline texture and by lack of fragments of different composition or contrasting textures. Applying these rules in field mapping and core logging, it became evident that close to the Afton orebody, there is no continuity of any single rock unit over a reasonable distance to serve as a marker, at least as far as the upper 600 metres of the orebody is concerned. Figure 4, depicting a geological section across the eastern portion of the orebody, illustrates the complexities involved. Because structural deformation within the Triassic rocks rarely involved large, readily recognizable displacements (Carr and Reed, 1976), the discontinuity of rock types must reflect an intrusive roof-pendant environment, where successive intrusive events would cause brecciation of the early solidified units and lead to intricate interrelationships. Under the circumstances, a rigorous definition and assignment of rock types to various phases of the Iron Mask pluton would not be as fruitful as the mapping of alteration mineralogy, which is more closely related to the copper mineralization. Therefore, the generalized geological map of the Afton open pit as of June 1979 (Figure 5) has been constructed and subsequently used to discuss mineral distributions. Similarly, the geological sections shown on Figures 3B and 4 will be used to describe the mineral distribution patterns in relation to the copper mineralization.

DETAILED PIT PETROGRAPHY

Figure 5 is a highly generalized geological map of the Afton open pit at the 610 to 640-metre levels. It was constructed based on field mapping carried out by the writer in the summer of 1979, petrographic and X-ray diffraction studies of samples collected and supplied, to December of 1979, by A. Reed (then Chief Mine Engineer of Afton Mines Ltd.) and G.P.E. White (District Geologist at Kamloops, British Columbia Ministry of Energy, Mines and Petroleum Resources) during various stages of stripping of the orebody, preliminary company maps of the relevant levels and drill hole data. Readily discernible rock units are described as follows:

Southwest of the open pit, excavation in 1979 exposed a narrow strip of picrite basalt. It comprises brownish green,

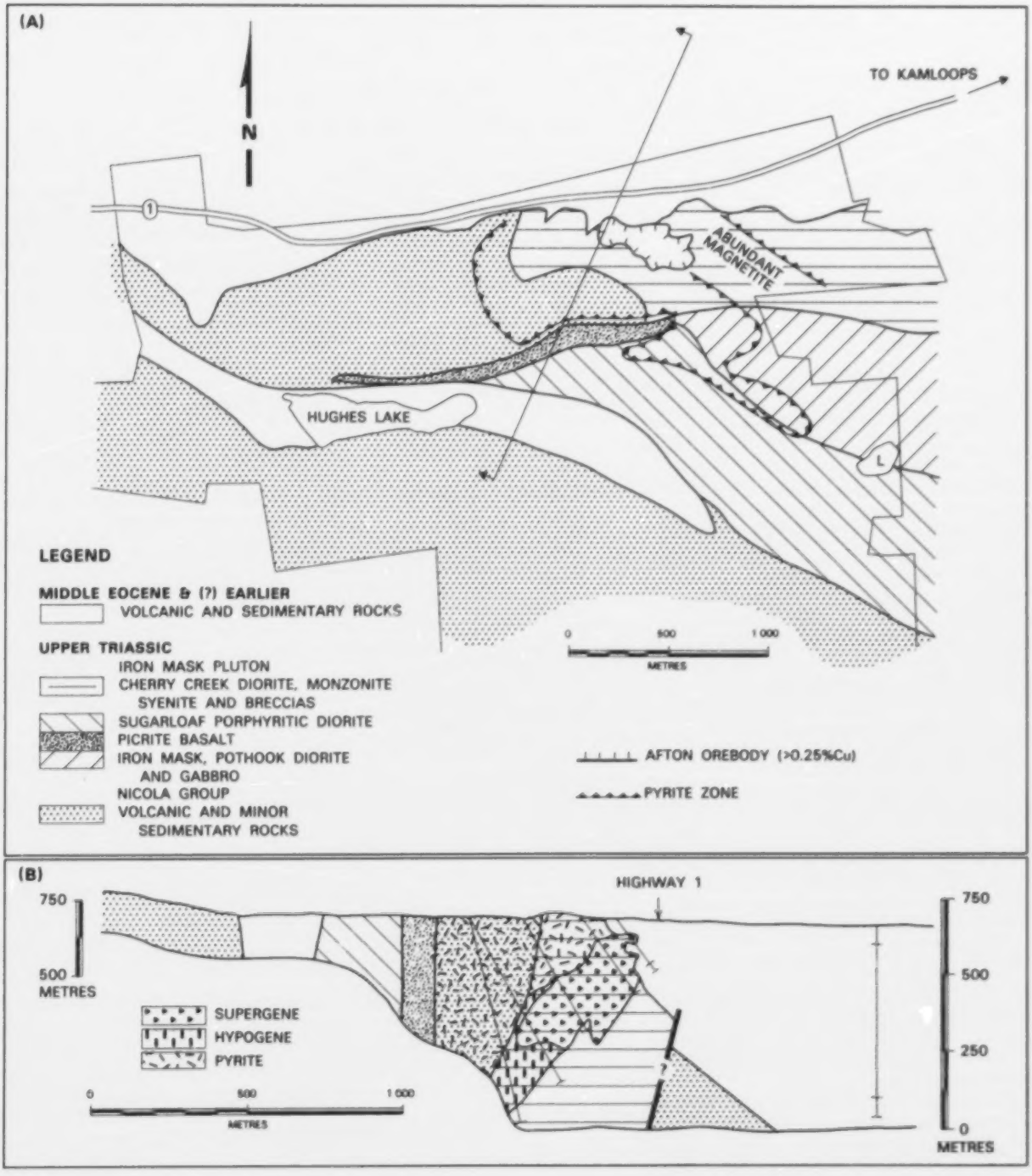

Figure 3. A geological map (A) and geological section (B) of the Afton property (after Carr and Reed, 1976).

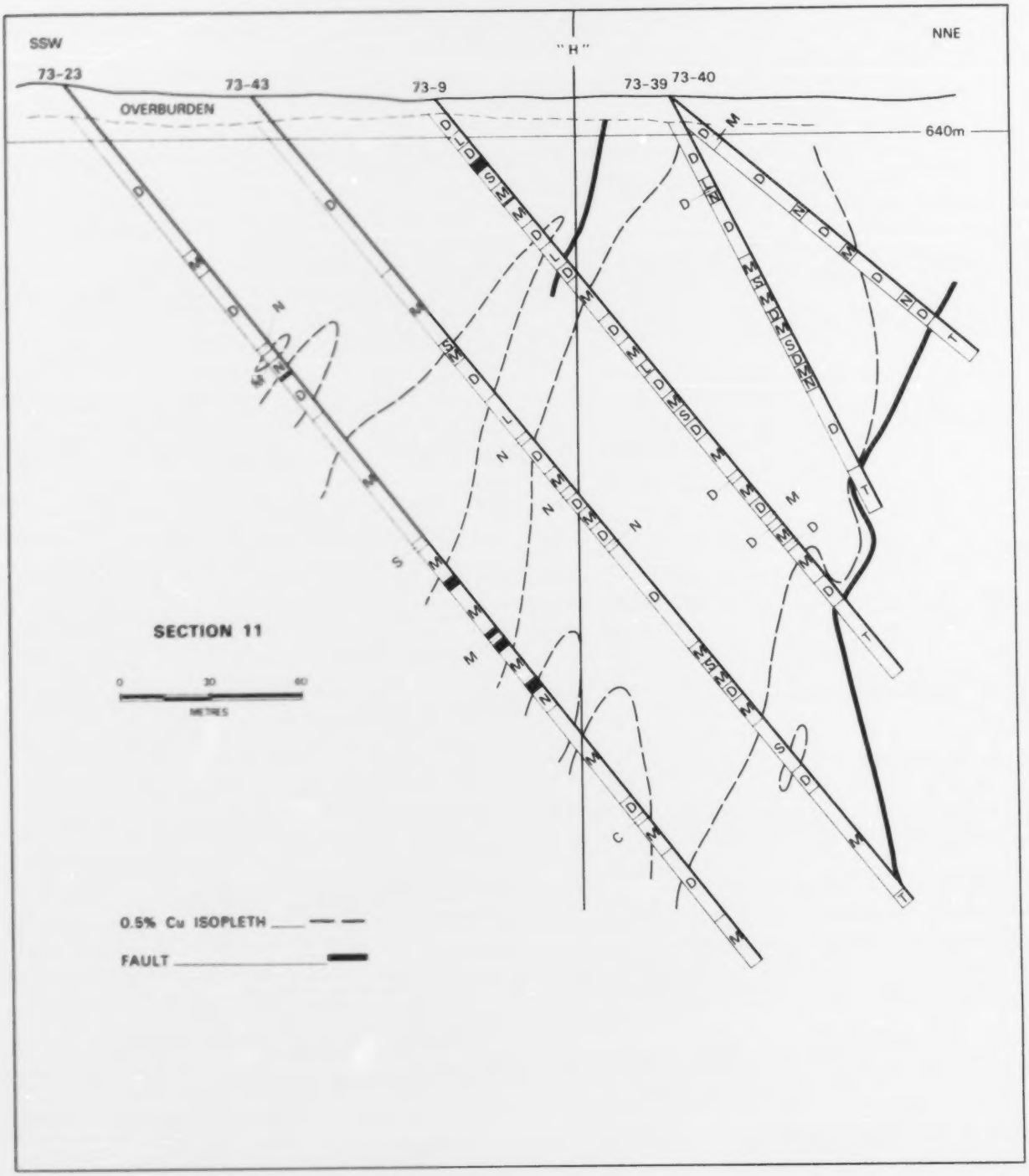

Figure 4. A geological section across the eastern half of the Afton open pit, illustrating the complexity of the host rocks involved. The orebody at the 0.5% Cu isopleth is depicted in broken lines. (Symbols: D, diorite; M, monzonite; S, syenite; L, latite dyke; N, Nicola Group volcanic rocks; T, Tertiary volcanic and sedimentary rocks; C, ankerite; solid black, magnetite). Note the apparent lack of vertical or lateral continuity of any single rock type.

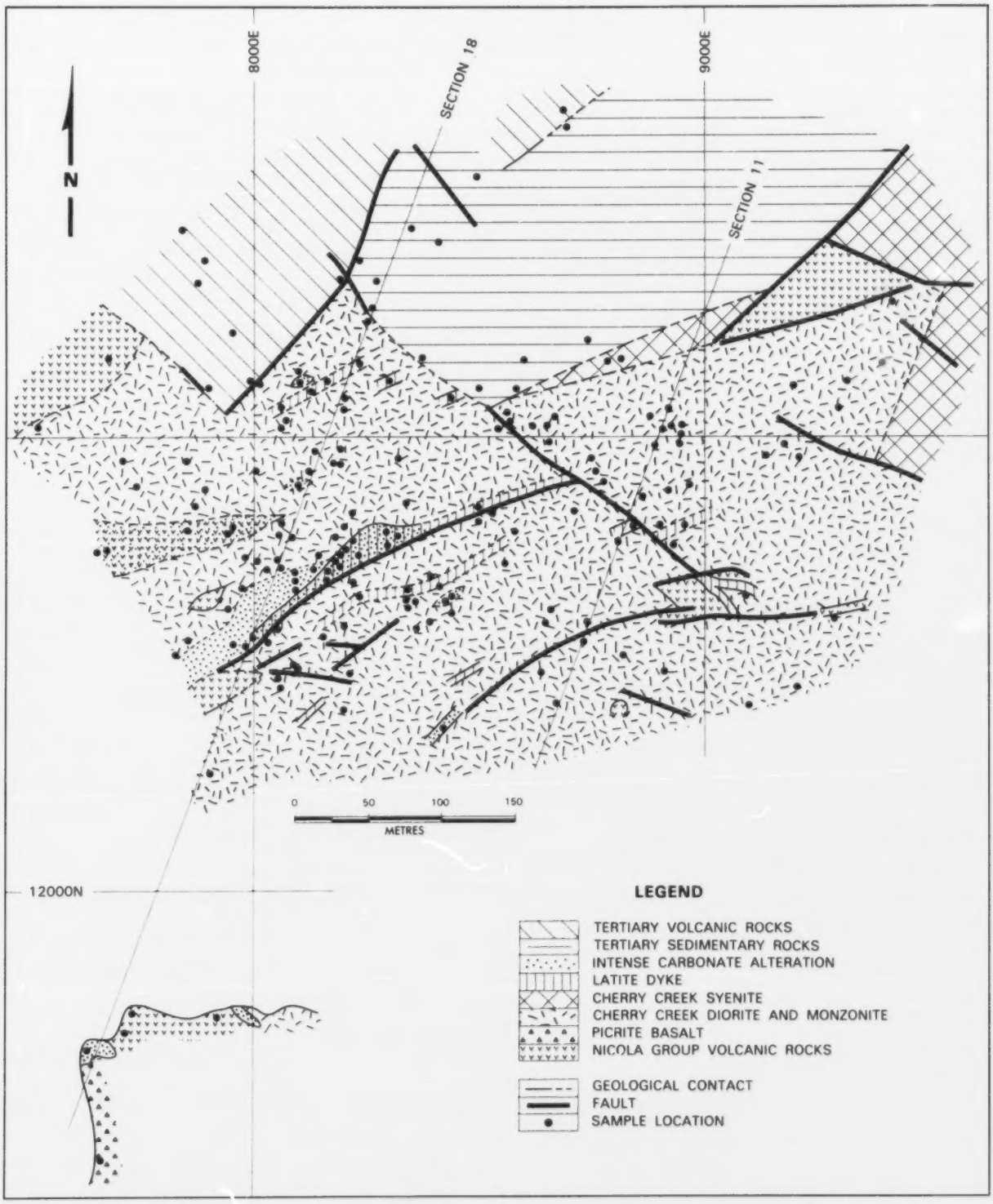

Figure 5. A highly generalized geological plan of the Afton open pit at the 610-640-metre levels as of June 1979.

slightly elongated nodules, with diameters up to half a metre, aligned in a yellowish, friable matrix; the matrix also forms continuous bands of varying thickness between the nodule-rich layers. The nodules consist mainly of serpentinized olivine and rather fresh clinopyroxene with small but varying amounts of phlogopite. The yellow matrix is similar in composition but is fine grained and shows alteration to sepiolite. Possibly, the rock unit was formed by the intrusion of an ultramafic crystal mush to near surface conditions, resulting in the rough alignment of the nodules and fast quenching of the matrix. Subsequent differential weathering of the nodules and the matrix gave rise to the layered appearance of the whole assemblage. As a result of intensive carbonate alteration and poor exposure, the contact between the picrite basalt and the Nicola volcanic breccia to the immediate north is obscure. The volcanic breccia is made up almost entirely of fine-grained hornblendite fragments. Epidote veinlets, some of which carry pyrite and chalcopyrite, are common. Progressing toward the east, the breccia becomes so deficient in matrix that it could easily be mistaken for hornblendite except where localized intense carbonate replacement emphasizes the fragmental texture of the rock. With a gradual increase in grain size and the disappearance of fragmental structure further east, contact with the medium-grained diorite is again obscure.

Within the open-pit itself, six rock units are distinguished. They are designated as Cherry Creek diorite and monzonite, Cherry Creek syenite, Nicola volcanic rocks, latite dykes, Tertiary sediments, and Tertiary volcanic rocks respectively.

The Cherry Creek intrusive rocks, the most abundant rock type in the open pit, are typically fine grained, slightly porphyritic in texture and range from syenite to diorite in composition; diorite generally predominates over the other varieties. Grain size increases and the extent of development of porphyritic texture decreases southward and eastward. Rocks with 50 per cent or more by volume of grains smaller than 1 millimetre in the largest dimension are described as the micro varieties. Even after brecciation, these fine-grained intrusive rocks may be distinguished from the Nicola volcanic rocks on the basis of overall uniformity of composition, holocrystallinity, and lack of evidence of pre-existing glass. The Cherry Creek rocks contain 50 to 70 per cent feldspars. Plagioclase grains in all varieties of rock are completely albitized. Potassic feldspar, typically microcline, occurs mainly in the fine-grained matrix, frequently rims plagioclase and rarely occurs as phenocrysts. In the dioritic and monzonitic varieties, potassium feldspar frequently occurs in a patchy habit including and grading into aggregates of epidote or biotite. Discrete potassium feldspar veins commonly show a chloritic envelope. Sericite, carbonate, and clay replacements are present in feldspars but are rarely very intense. Partially altered clinopyroxene forms up to 10 per cent of the rock in the eastern portion of the pit while amphibole and its alteration products are the principal mafic minerals elsewhere. Equigranular, medium-grained and more "normal" looking intrusive rocks were observed only in drill cores recovered from moderate depth.

Nicola volcanic rocks within the Afton pit and its vicinity are of several varieties. In the southern portion of the open pit, hard massive green volcanic breccia, with predominantly hornblendite fragments, is particularly abundant. This breccia commonly contains epidote ± carbonate ± sulphides veins and is locally pervasively replaced by carbonate ± chlorite. In the northeastern portion, the Nicola volcanic rocks consist of highly saussuritized andesite, which is hardly distinguishable in hand-specimen from the neighbouring fine-grained Cherry Creek intrusive rocks. Elsewhere and in drill cores, the Nicola Group rocks range from fine-grained andesite, generally darker in colour than most Cherry Creek rocks, to pebbly sandstone made up entirely of igneous clasts that are generally cemented by iron oxides.

Latite dykes observed in the Afton pit are invariably massive, fine-grained, and very slightly porphyritic rocks. The total feldspar varies from 50 to 65 per cent but is generally greater than 60 per cent. Like many Cherry Creek rocks, potassium feldspar is concentrated in the matrix. Amphibole is the predominant mafic mineral; it usually exceeds 20 per cent and occurs mainly as phenocrysts. Quartz ranges up to 10 per cent and is essentially interstitial. Hornblende can be fresh, or replaced by chlorite, carbonate, and rarely hydromica. Plagioclase is typically albitized. Some rocks show signs of oxidation in the form of an overall reddish tone and several samples contain native copper. They are most readily distinguished from the Cherry Creek intrusive rocks by the presence of quartz and potassium feldspar "eyes". Based on mineralogy and alteration, it is concluded that these latites are probably of pre-Tertiary age.

Arranged in order of decreasing abundance, sandstone, arkose, conglomerate, lithic wacke, carbonaceous argillite, and streaks of coal are among the Tertiary sedimentary materials observed in the Afton pit. In the central part of the pit, adjacent to the inferred fault contact between the Tertiary and Cherry Creek rocks, lithic wackes with heavy iron staining and iron oxide cement contain clasts carrying native copper. It has not been possible to determine the exact age of these lithic wackes.

Tertiary volcanic rocks occurring on the Afton property include dacite, trachytic flow breccia, amygdaloidal andesite, and massive andesite. Whereas most plagioclase grains in these rocks remain intact, mafic minerals are typically replaced by ankerite.

MINERAL DISTRIBUTION AND ALTERATION PATTERNS

INTRODUCTION

Compared to other porphyry copper deposits, the Afton deposit does not exhibit well-defined hydrothermal alteration patterns. Other than the pyrite and magnetite zoning about the orebody (*see* Figures 3A and 3B) that was noted by Carr and Reed (1976), various classical hydrothermal alteration assemblages were reported to be present but not delineated (*see*, for example, Preto, 1972 and Hoiles, 1978). However, in the preceding petrographic description, it has already been mentioned that within the Cherry Creek rocks in the Afton open pit, clinopyroxene is limited to the eastern portion while amphibole is more abundant to the south. As far as carbonate alteration is concerned, calcite predominates over ankerite in the eastern portion of the pit and the reverse is true elsewhere. Thus, it appears that both primary and alteration mineral

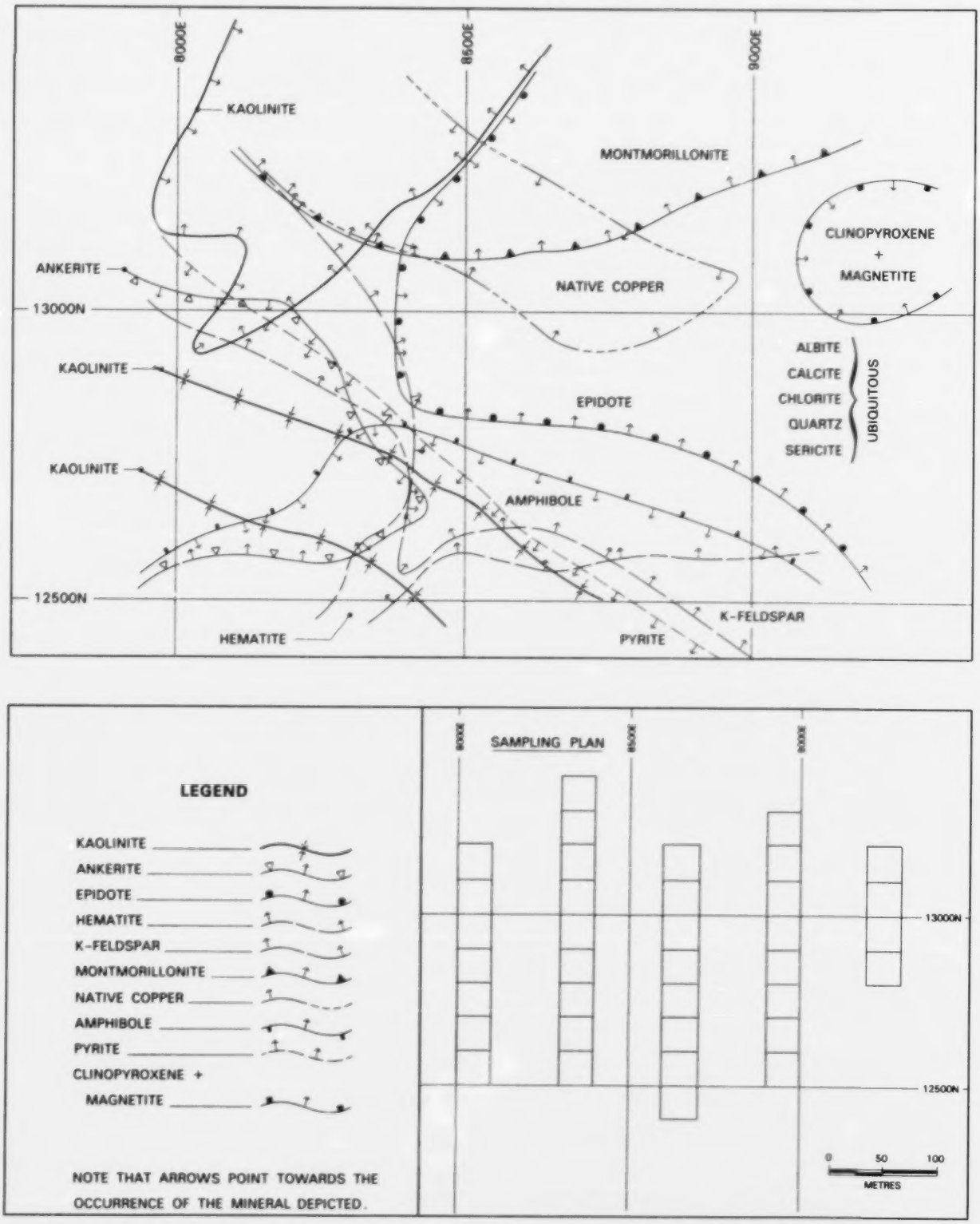

Figure 6. Mineral distribution within the Afton open pit at the 613-metre level as revealed by X-ray diffraction analyses of blasthole composite samples. The samples analysed here are provided through the courtesy of Afton Mines Ltd.

zoning are present even within the orebody. Here, an attempt is made to define the horizontal zoning by analyses of blasthole samples from a chosen level, and vertical zoning through detailed examination of selected samples from two geological cross-sections.

LATERAL DISTRIBUTION OF MINERALS

Figure 6 illustrates the distribution of minerals within the Afton pit at the 613-metre level, as revealed by X-ray diffraction analysis of blasthole composite samples supplied by Afton Mines Ltd. The plan of sampling is included in the legend of the diagram. Within each sampling block, barren Tertiary rocks were deliberately excluded from the composite. Interference problems precluded quantitative estimation of mineral abundance. Boundaries of mineral domains are based on positive identification of the mineral from diffractograms of nonoriented mounts of the composite samples. For most minerals, this means a detection limit of about 5 per cent by weight, except for calcite, quartz, mica, and kaolinite, whose detection limits are approximately 2 per cent. However, among the minerals specified in Figure 6, only albite, quartz, ankerite and rarely, potassium feldspar and amphibole can be considered as major components; they commonly exceed 20 weight per cent. Chlorite, epidote, and calcite commonly assume a subordinate role, forming 10 to 20 per cent of the rock, whereas mica, native copper, the oxides, sulphides, and particularly the clay minerals frequently occur in amounts that are just discernible on the diffractograms.

One prominent feature of the mineral distributions illustrated in Figure 6 is the dominance of northwesterly trends and, to a lesser extent, northeasterly trends of the boundaries of the mineral domains. These trends parallel trends of the major faults throughout the Iron Mask pluton, which controlled the emplacement of various intrusive phases. The northwesterly trend in particular is parallel to the intrusive contact of the Iron Mask pluton with Nicola Group rocks. A comparison with Figure 5 reveals that the montmorillonite boundary coincides with that of the Tertiary sediments, and that kaolinite is abundant in an area dominated by Tertiary volcanic rocks. Consequently, the presence of these clays elsewhere may be a result of contamination from the Tertiary rocks. Narrow northwesterly trending bands of kaolinite in the southwestern quadrant of the pit may be caused by near-surface alteration related to faulting during the Tertiary period.

Ignoring the clay minerals and native copper, and allowing for minor exceptions, the open pit can be divided diagonally into two parts with different mineral assemblages. Potassium feldspar, epidote, hematite, magnetite and, to a lesser extent, clinopyroxene dominate the northeastern half whereas the southwestern half is characterized by ankerite and/or amphibole and pyrite. Obviously, a great proportion of the hematite is derived from alteration of magnetite; epidote and at least some of the potassium feldspar and magnetite are either deuteric or hydrothermal in origin. However, it is not clear whether the occurrence of clinopyroxene and amphibole in different domains reflects an obscure geological contact or is simply a result of *in situ* differentiation. Among the ubiquitous minerals, quartz is more abundant in the southwest while calcite is more concentrated in the northeast. Albite, chlorite, and mica are rather evenly distributed, except where carbonate alteration is intense.

The micas occur in rather small amounts, and cannot be distinguished with respect to kind and type based on evidence obtained from bulk sample diffractograms. In addition, because the copper sulphides have generally diffuse diffraction patterns which hinder separation of interfering reflection peaks, they are not described in Figure 6. These limitations, however, can readily be eliminated by detailed thin section and polished section studies of specimens collected from the same general area.

Figures 7a to 7d depict the mineral distributions as determined from petrographic examinations of 173 specimens taken from the 640 to 613-metre levels. Despite sporadic exceptions, these reaffirm the general abundance of clinopyroxene, epidote, and potassium feldspar in the northeastern half and hornblende and ankerite in the southwestern quadrant of the pit. Hornblende pseudomorphs made up of chlorite, a mica-like mineral (hydrobiotite?) and carbonates are also abundant in the northwestern quadrant. Figure 7a shows that biotite is also concentrated in the northeastern half whereas sericite/muscovite replacement is more abundant in the southwestern half of the pit. In a similar fashion, Figure 7d shows that supergene copper minerals (native copper ± chalcocite) are more characteristic of the northeastern half whereas hypogene sulphides (bornite ± chalcopyrite ± pyrite ± minor molybdenite) are more abundant in the southwestern half. The sparsely sampled region between them is characterized by high-grade oxidized ore. Chlorite associated with the supergene assemblage is of the iron-rich variety, occurs as yellowish, fine-grained aggregates and exhibits normal interference colours. Chlorite associated with the hypogene assemblage, in contrast, is typically a coarse-grained magnesium-iron chlorite with anomalous brown interference colour. Regarding the accessory minerals, apatite is more or less ubiquitous; tourmaline is only found adjacent to zones of intense carbonate alteration; sphene is more common in rocks of the northeastern portion of the open pit. The distribution of minerals generally characteristic of low-grade metamorphism, like pumpellyite and prehnite, is rather sporadic but is clearly antipathetic to zones of intense carbonate alteration.

Minor to moderate amounts of dominantly amorphous material, and trace amounts of gypsum are commonly associated with the supergene copper ores. The amorphous material includes reddish, earthy hematitic clay, greenish and poorly crystalline mixed-layer illite-montmorillonite clays, and rarely trace amounts of suspected amorphous matter that may be copper sulphate. The gypsum, copper sulphate hydrates and some late fracture-filling calcite are probably products of recent weathering.

VERTICAL DISTRIBUTION OF MINERALS

Figures 8 and 9 illustrate the major patterns of mineralization and alteration with depth. Figure 8 results mainly from detailed core logging aided by X-ray diffractometry and depicts the presumably high temperature hydrothermal alterations relative to the 0.5 per cent copper isopleth and host rock lithologies in the eastern half of the pit. Other than

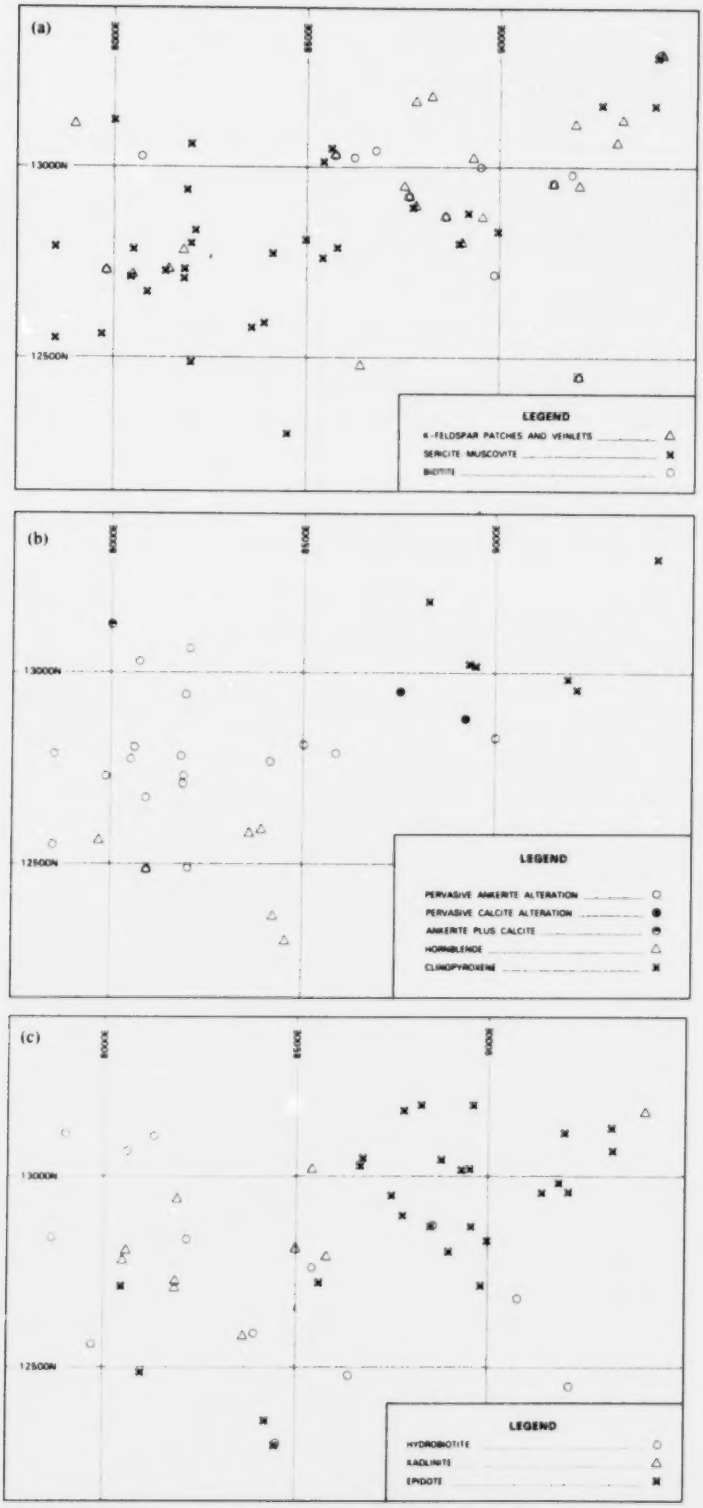

Figure 7(a-c). Distribution of selected minerals as determined from petrographic examination of 173 specimens from the 613–640-metre levels of the Afton open pit. The sample sites are shown in Figure 5.

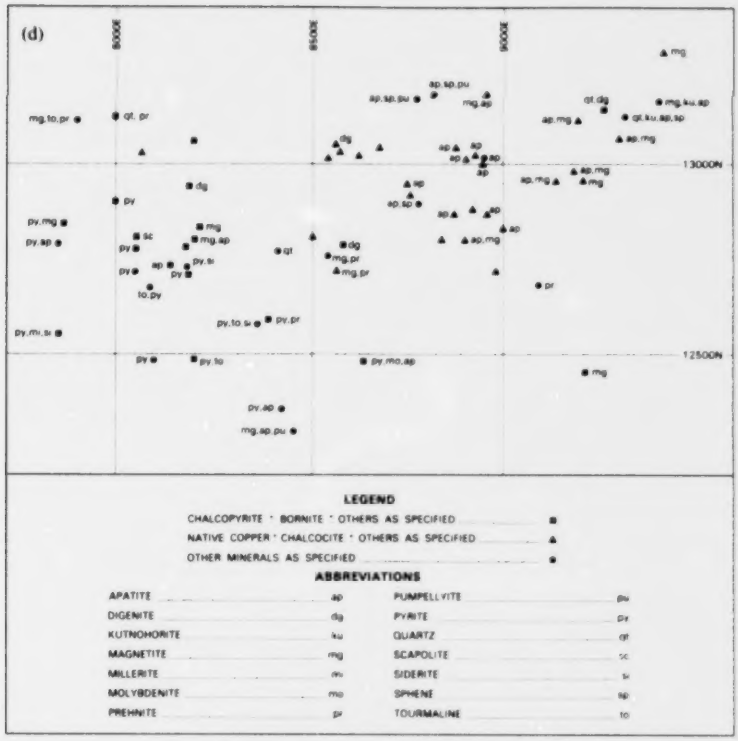

Figure 7(d). Distribution of ore and accessory minerals in the 613–640-metre levels of the Afton open pit. Petrographic examination aided by X-ray diffractometry has been used in the identification of the specified minerals.

the ubiquitous occurrence of chlorite and the apparent development of a pyrite zone about the orebody, both near the surface and at depth, occurrences of abundant potassium feldspar, biotite, epidote, and carbonates appear to be sporadic. In detail, however, several features are worth noting. First, epidote, which frequently extends well beyond the orebody, shows a positive correlation with the occurrence of magnetite. Wherever disseminated magnetite is abundant, or in the vicinity of magnetite veins in excess of 30 centimetres in width, epidotization is pervasive. To the east of reference line "H" in the diagram, epidote is closely associated with magnetite veinlets too small to be shown. Second, the boundary of biotite appearance closely approximates that of the hypogene ore zones. As large structural displacements are not recognized, the separation of these hypogene zones probably results from fracture-controlled supergene alteration. Third, whereas most rocks that have undergone intense carbonate alteration are barren, a few carry a small amount of tennantite, chalcopyrite, and pyrite. In fact, tennantite appears to occur only in or adjacent to rocks replaced by carbonate. Fourth, though described as ubiquitous, chlorite is nearly absent in most carbonate-affected rocks and it is much less conspicuous in latites. Last, though not depicted in the diagram, very small amounts of clinoptilolite and ferrierite occur as fracture fillings, that are particularly obvious in drill hole 73–23, associated with the more potassium-feldspar-rich sections; some celadonite has been observed in drill hole 73–39, again associated with the potassium-feldspar-rich sections; latite dykes in drill hole 73–43, on the other hand, contain marcasite lining microfractures. These, together with hematite and amorphous clay alteration, that are particularly abundant east of drill hole 73–9, are interpreted to result from low temperature hydrothermal events or supergene alteration. The association of alteration minerals with specific wallrocks may reflect buffering of the reacting fluids by the host rocks.

Figure 9 is a section across the western half of the pit; it is modified from Figure 3B (after Carr and Reed, 1976). The distribution of alteration minerals is derived mainly from petrographic studies of thin sections and rock slabs supplied by Afton Mines Ltd. Sporadic distribution of alteration mineral domains is again obvious. In comparison with that noted in the eastern section, however, hydrothermal biotite, although confined within the orebody, extends well into the supergene zone. The development of carbonate alteration is more extensive, both near the surface and at depth, thus it partially surrounds the orebody. The fact that biotite survived supergene alteration under the apparent blanketing effect of the carbonate suggests that the presence of abundant carbonate might have affected the solution chemistry during the supergene event. The equigranular diorite beneath the orebody and west of reference line "G" also contains abundant biotite. However, in this case, it is primary and poikilitic in contrast with the clusters of fine-grained hydrothermal biotite, which are evidently fracture controlled. Epidote

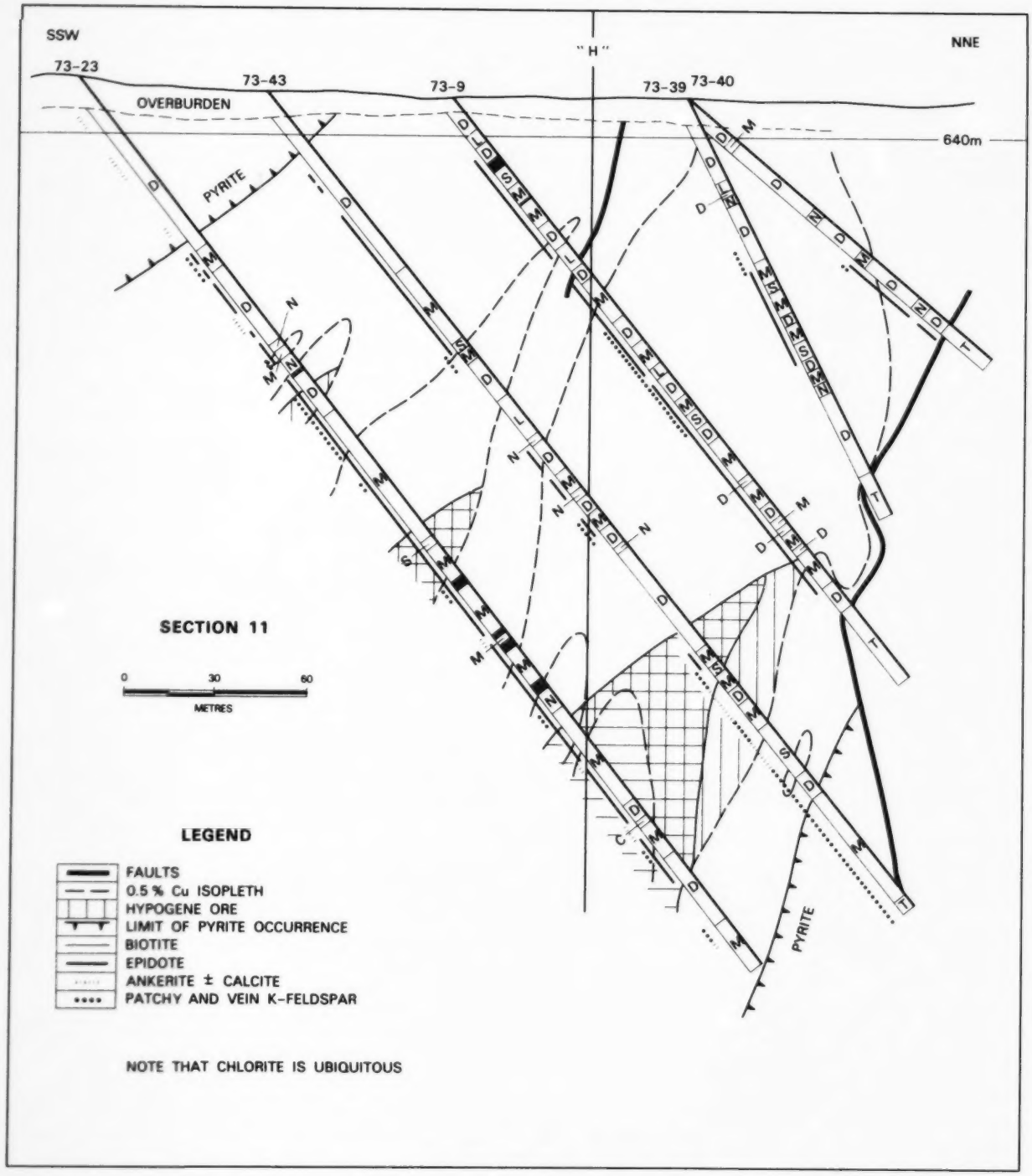

Figure 8. Hydrothermal alteration observed in a geological section (11 in Figure 5) across the eastern portion of the orebody. (Lithologies: D, diorite; M, monzonite; S, syenite; L, latite; N, Nicola Group volcanic rocks; T, Tertiary volcanic and sedimentary rocks; C, ankerite; solid black, magnetite.)

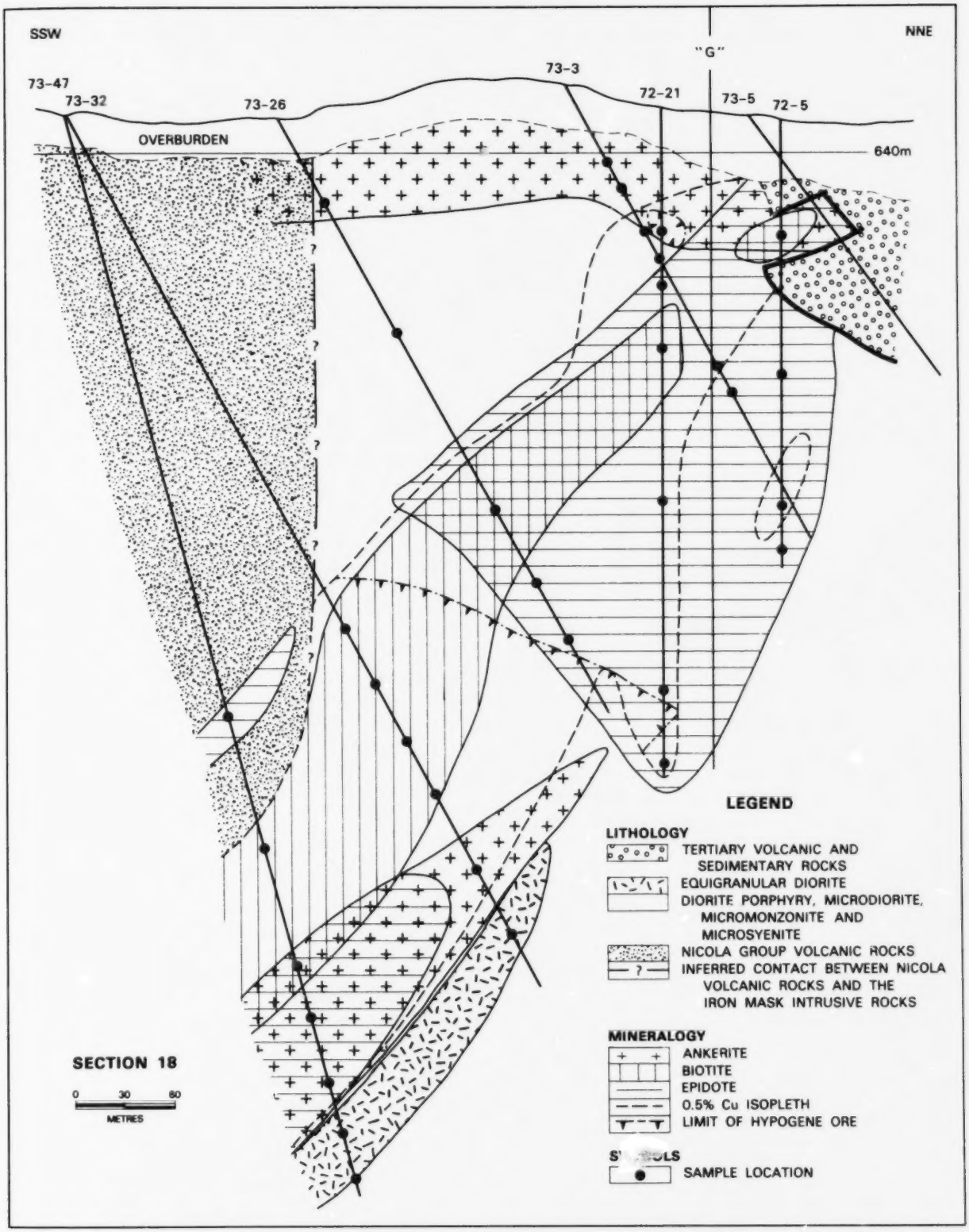

Figure 9. An illustration of vertical distribution of minerals at Afton mine; distribution of high temperature alteration minerals in a geological section (18 in Figure 5) across the western portion of the orebody. Note that only minerals occurring in excess of about 5% by volume are depicted in the diagram.

again extends beyond the orebody and chlorite, while still ubiquitous, occurs in greatly diminished amounts. Finally, pyrite is more concentrated in rocks above the orebody, but also occurs in small amounts in highly carbonatized rocks.

Reed (1983) reported an increase in chalcopyrite relative to bornite toward the footwall of the orebody in the hypogene zone. This is evident in drill holes 73–47 and 73–32 depicted in Figure 9. However, the abundance of chalcopyrite here appears to correlate with the appearance of intense carbonate (ankerite) alteration.

DETAILS OF ORE MINERALIZATION

As a prerequisite for interpreting ore-wallrock relationships, the distribution of alteration minerals must be correlated with the mode of occurrence of the ore minerals. Relevant features of the latter are briefly described as follows:

At Afton mine, supergene mineralization dominates to a depth of approximately 400 metres in the western and 250 metres in the eastern portions of the orebody. It is characterized by a native copper to chalcocite ratio in excess of 2:1. Chalcocite in this zone is mostly of the sooty variety and occurs mainly in veins less than 3 millimetres wide. Native copper occurs in stockworks as scales, films and dendrites, and also as granules associated with specularite. In the east end of the pit, isolated specks of native copper occur in magnetite, which occurs as veins, patches, and rare disseminations. Whereas native copper and chalcocite commonly occur in the same horizon, they rarely occupy the same vein. Thus replacement features between the two are uncommon; in crosscutting relationships, veinlets of native copper are always younger. Thin coatings of cuprite are found on many native copper crystals; malachite, azurite, conichalcite, and some poorly crystalline copper sulphate hydrates (?) occur locally in trace amounts. These minerals, like minor amounts of gypsum and late calcite veinlets, are probably products of post-supergene alteration processes.

In the hypogene zone, bornite and chalcopyrite are equally abundant and chalcocite is subordinate. Bornite commonly encloses chalcopyrite in carbonate-free veins cutting highly chloritized rocks or as sulphide patches located within chloritized mafic phenocrysts themselves; chalcopyrite enclosing bornite is less common. In either case, bornite commonly exhibits exsolution rims of chalcocite and covellite. Bornite and grey chalcocite, either together or separately, also occur as disseminations in feldspar-rich monzonitic rocks that have accessory secondary biotite. Detailed studies of polished sections indicate that these sulphides do not occur as individual globules but as impregnations connected by microfractures.

In addition to its association with bornite, chalcopyrite also occurs with pyrite in carbonate veins and is particularly abundant in epidote-rich rocks. At the southern rim of the open pit at an elevation of 610 metres, there are isolated occurrences of chalcopyrite and molybdenite, and chalcopyrite and hematite veins about 1 centimetre wide. These veins commonly show a 2-centimetre-wide potassium-feldspar selvedge. Rare monomineralic chalcopyrite veins up to 2 centimetres wide exhibit prominent albite selvedges. In rocks intensively replaced by carbonate, chalcopyrite locally accompanies tennantite and/or pyrite. This assemblage also survived locally in the supergene zone.

Whereas gold and silver are significant byproducts of the copper ore, their mode of occurrence is still open to speculation. In the eastern portion of the orebody, only one example of native gold coating disseminated bornite, which is incompletely altered to chalcocite, has been observed. The textural relationship involved is illustrated in Plate 1. Limited spectrochemical analyses also indicate a positive correlation between copper sulphides and gold. Possibly, native gold occurs as microdispersions in the sulphide phases and aggregates visible only after partial destruction of the host minerals. This would explain the concentration of gold within the copper orebody as shown in Figure 10, but the highest ore grades for the two elements do not necessarily coincide (Reed, 1983). Tennantite, commonly observed in carbonate-altered and adjacent rocks, is also a likely host for silver and some gold. As suggested by Hoiles (1978), quantitatively insignificant sulphosalts, associated with the copper sulphides, may also play a significant role in hosting the gold and silver contained in the ore.

DISCUSSION AND INTERPRETATION

In the lithologic description of the host rocks, it was argued that they represent a roof pendant characterized by intricate and sporadic distributions of rock types. Whereas detailed distinction of rock types provides little help in finding ore, details of the distribution of alteration minerals should reveal important aspects of the copper mineralization. In the following, the significance of a few prominent distributional features is suggested.

(a) Absence of abundant sericite and clay minerals

In contrast to the alteration mineralogy in the Lowell and Guilbert (1970) model for calc-alkaline porphyry copper deposits, strong phyllic and argillic alteration assemblages are absent at Afton, which is hosted by alkaline plutonic rocks. In the diorite model of Hollister (1978) for alkaline porphyry coppers, the differences in alteration patterns are explained in terms of the disparity in chemical composition of the host rocks. From extensive studies of oxygen and hydrogen isotopic composition of minerals from porphyry deposits throughout North America, Sheppard *et al.* (1969, 1970), however, concluded that secondary biotite from the centres of several deposits formed in equilibrium with dominantly magmatic water, whereas sericite and hypogene clay minerals generally found peripheral to the core of potassic alteration formed in equilibrium with a large component of meteoric water. At Afton, the generally quartz-free (when unaltered) nature and the more mafic composition of the host pluton in comparison to most other porphyry copper deposits should result in a higher temperature of solidification and a lower viscosity of the intrusive magma. A low magma viscosity, coupled with intrusion along steep fracture zones, would give rise to a greater likelihood of formation of sheet-like bodies, the detailed shape of which would be ultimately dependent on the morphology of the conduit fractures. In any case, a more rapid rate of cooling would lead to less time and opportunity for the intervention of meteoric water. In short,

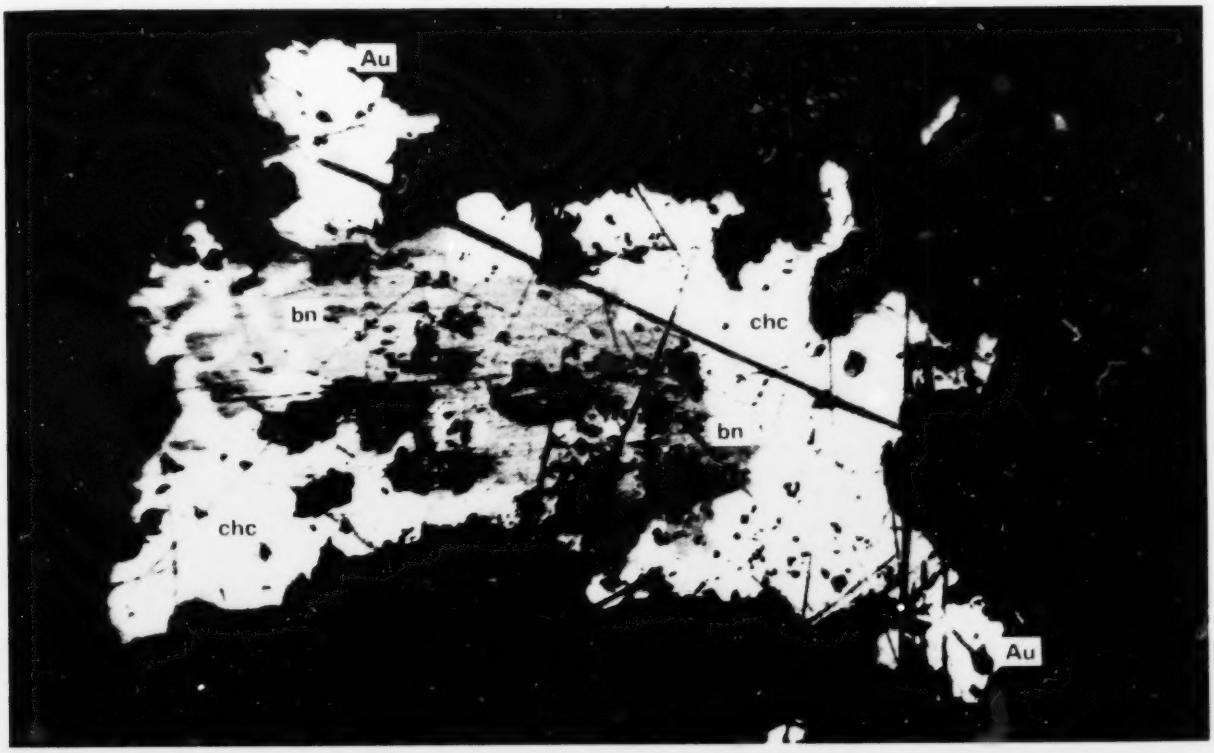

Plate 1. Native gold (white) coating chalcocite (light grey) which incompletely replaces bornite (dark grey). Length of the photograph 10 millimetres.

though ultimately related to the chemical composition of the host pluton, the immediate cause of the lack of phyllic and argillic alteration at Afton is probably due to the scarcity of meteoric water to participate in the hypogene hydrothermal alteration event.

(b) Preferential association of minerals

In the hypogene zone, the predominance of chlorite where magnetite is not abundant, and the preferential correlation of epidote with magnetite, suggest that host rock mineralogy controlled the formation of secondary minerals during hydrothermal alteration. Magnetite, in the present case, probably limited the oxygen fugacity so that the presence of abundant magnetite stabilized epidote in preference to chlorite ± plagioclase. In other words, a low ratio of fluid to rock is inferred to have accompanied the hypogene alteration. The frequent patchy occurrence of potassium feldspar, mostly rimming plagioclase rather than as discrete veins, may also indicate epimagmatic activity with a minimal amount of silicate-free fluid being available. Formation of chalcopyrite veins with albite selvedges may signify the final stage of the transition of a supercritical solution into a hydrothermal solution, a transition which is generally characterized by a change from high-temperature potassium to sodium metasomatism (Beus and Grigorian, 1977). However insignificant it might be in comparison with the total amount of rock mass, the hydrothermal fluid was apparently able to leach most primary sulphides (and possibly some primary magnetite) and redeposited them in the form of veins and fracture-controlled impregnations at a temperature of about 300 degrees Celsius, as indicated by the sulphur isotope data of Hoiles (1978). By analogy with the study of Brimhall (1980) on the deep hypogene oxidation of porphyry copper potassium silicate protore at Butte, Montana, it can be inferred that the low fluid-to-rock ratio accompanying hypogene mineralization at Afton would result in a minimal displacement of the ore elements from the protore zone. Consequently, studying the magmatic processes involved in the formation of the various phases of the Iron Mask batholith in order to recognize the exact stage of primary sulphide precipitation should help in evaluating its exploration potential.

Similarly, the supergene alteration appears to be controlled by the composition of the wallrocks. The concentration of native copper ± chalcocite in the eastern half of the open pit at the 610 to 640-metre levels reflects the presence of abundant magnetite which, when oxidized to hematite together with the coupled reduction of hypogene bornite and chalcopyrite, produces native copper and chalcocite. The frequent persistence of hypogene sulphide assemblages in the western half of the pit seems to be related to the buffering effect of the carbonates present. If a low ratio of fluid to rock is again inferred, either the supergene alteration must have taken place in a semi-arid environment comparable to the present climate at Kamloops, or else the permeability of the host rocks must be very low. The predominant occurrence of supergene minerals in veins and stockworks, with relatively few replacement features, suggests dissolution of the hypogene sulphides and redeposition of the ore elements as

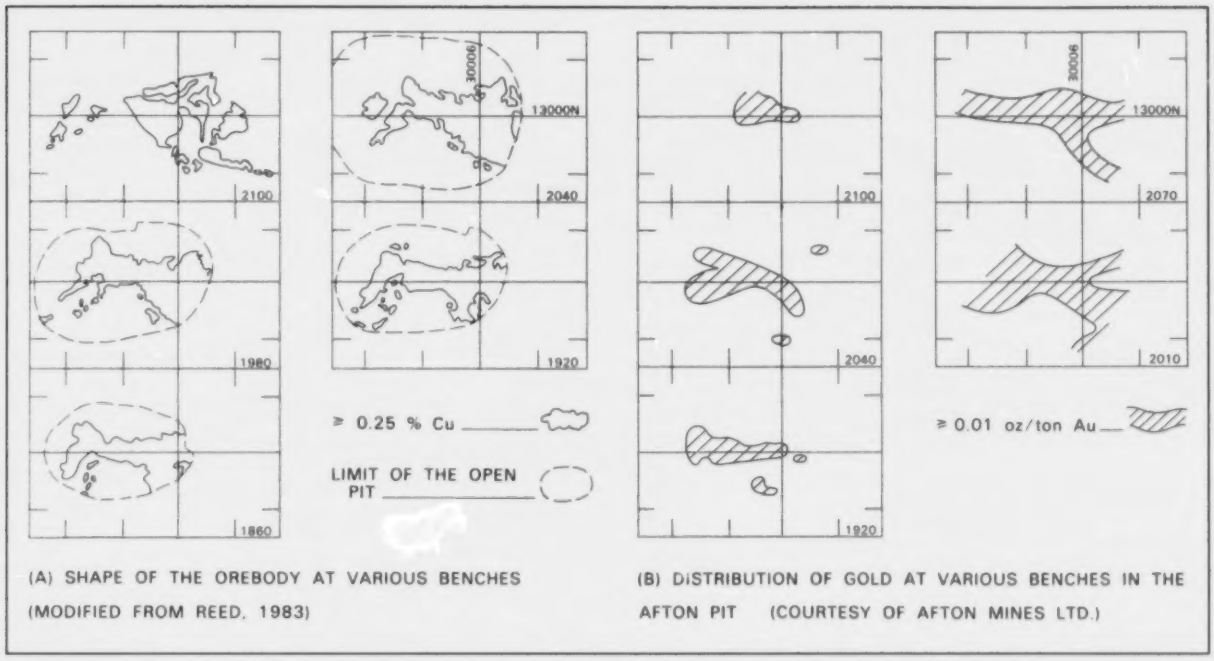

Figure 10. Distribution of copper and gold at various benches in the Afton pit. Note that the gold is concentrated roughly within the limit of the copper orebody at the corresponding benches.

supergene minerals. It should therefore be possible to simulate the supergene event in terms of mineral-solution interactions making use of available thermochemical data.

(c) Timing of the carbonate alteration

Implicit in the suggestion that the carbonates influence the survival of hypogene sulphides in the supergene zone is the implication that the carbonates are high temperature alteration products. Evidence abounds to support the interpretation. First, carbonate alteration is pervasive and particularly abundant in the western half of the pit. The supergene and post-supergene carbonate is calcite, rather than ankerite, and is mainly vein forming. Second, minerals associated with ankerite suggest elevated temperature of formation. Where pervasive carbonatization prevails, associated minerals are tourmaline, mica (mainly muscovite and mariposite), quartz, feldspar, and rarely chlorite and scapolite. Such an assemblage indicates the participation of magmatic volatiles in their crystallization. Finally, in the southwestern quadrant of the open pit, intense carbonate replacement is cut by a pre-Tertiary latite dyke. Thus, major carbonate alteration preceded the supergene event. The fact that part of the latite is also carbonatized, and that mafic minerals in the Tertiary volcanic rocks are also replaced by ankerite, can be interpreted in terms of contemporaneity of the carbonate alteration and the latite intrusion and that similar processes are involved in the evolution of carbon dioxide during Mesozoic magmatism and Tertiary volcanism. In other words, the most probable source of carbon dioxide causing the carbonate alteration is the fluid evolved during secondary boiling associated with the crystallization of different magmas. As reviewed by McMillan and Panteleyev (1980) for models of porphyry copper deposits, multiple boiling events are common in an orthomagmatic hydrothermal system.

(d) Sporadic distribution of hydrothermal minerals

Given a roof pendant environment and a low fluid-to-rock ratio, sporadic distribution of secondary minerals is to be expected. In the case of Afton mine, at least one more factor is a possible cause of sporadic mineral distributions; the Cherry Creek phase of the Iron Mask pluton, which hosts the Afton orebody, consists of a variety of rocks resulting from multiple intrusive events, rather than a single large intrusion. Paragenetically later intrusions, with their associated hydrothermal activities, are likely to alter patterns developed earlier. Consequently, one must examine the development of alteration patterns at Afton in the perspective of an ever-changing wallrock environment. However, the overall alteration did not involve significant displacement of elements from the protore, hence the formation of ore would coincide with the trapping of magmatic fluids. At Afton, the pervasive carbonate replacement (dominantly ankerite with minor amounts of calcite), is a hydrothermal alteration product, hence a good indicator of local concentration of hydrothermal activity. As indicated by the infrequent trapping of specks of chalcopyrite or its alteration product, native copper, in magnetite, primary copper sulphides probably precipitated from the Iron Mask magma shortly after magnetite began to crystallize. Therefore, areas bounded by abundant magnetite on the one hand and intense ankerite replacement on the other are attractive exploration targets for similar copper ores in the Iron Mask batholith. A more detailed model of the copper mineralization at Afton will be presented following the discussion of geochemical data.

SUMMARY AND CONCLUSIONS

In summary, the petrography of the wallrocks of the Afton orebody has been outlined with emphasis placed on the distribution of minerals. It is concluded that the mineralizing process occurred in a roof pendant environment. Within the boundary of large-scale zoning of pyrite and magnetite established by Carr and Reed (1976), ore appears to be most consistently associated with hydrothermal biotite. Other than that, primary and hydrothermal minerals in and near the orebody are sporadically distributed, particularly in the vertical dimension. Nevertheless, several conclusions can be drawn:

(1) The absence of intense phyllic and argillic alteration at Afton reflects the lack of a major meteoric water component during the hypogene mineralizing event.

(2) High-temperature hydrothermal alteration at Afton proceeded with a low fluid-to-rock ratio such that primary mineralogy influenced the type and abundance of secondary minerals formed.

(3) The nature and extent of carbonate (ankerite with a minor amount of calcite) alteration at Afton are delineated. As an indicator of concentrated hydrothermal activity, and because it is readily recognizable, pervasive carbonate alteration could be of great value as a guide to ore in similar copper deposits in alkaline intrusions.

(4) Supergene alteration at Afton appears to be dominated by irreversible mineral-solution interactions. The extent of alteration at depth is largely fracture controlled. Mineral distributions presented previously serve as background field data for testing the feasibility of reconstructing the supergene alteration event through a thermodynamic approach, which involves mass-transfer calculations making use of available thermochemical data on relevant mineral and solution species.

CHAPTER 4

MAJOR ELEMENT GEOCHEMISTRY

INTRODUCTION

The Iron Mask batholith has long been known for its magnetite and copper mineralization (Cockfield, 1948 and Carr, 1956). Studies by Preto (1967 and 1972) and Northcote (1974, 1976, and 1977) furnished detailed information on the geology of various phases of the batholith and their associated mineralization. Upon studying the trace element contents of magnetite from the Iron Mask pluton, Cann (1979) suggested a comagmatic relationship between the iron and copper mineralization, and the diorite and syenite-dominant phases of the pluton, respectively. However few major element geochemical data were presented in these studies to support the various interpretations made. In this chapter, major element compositions of the prominent phases of the batholith are presented and discussed in conjunction with the host rock geochemistry of the Afton orebody. Relevant petrographic features (summarized in Table 1) are also considered to aid interpretations of field and geochemical relationships. The main purpose of the study is to determine the processes involved in the evolution of the Iron Mask batholith and their significance to copper mineralization.

Sampling for this geochemical study has been limited to the Iron Mask pluton mainly because there is good exposure of various rock units. Conclusions subsequently drawn, however, also apply to the related Cherry Creek pluton which consists dominantly of rocks of the Cherry Creek unit.

RESULTS OF MAJOR ELEMENT ANALYSES

Forty-five samples from the Iron Mask pluton and its vicinity, and 58 samples from the Afton property itself, were analysed for nine major elements using the atomic absorption spectroscopic method described in Ralph and Chaudhry (in preparation). The results are tabulated in Appendix I together with a brief description of each sample analysed. The chemical data are also summarized in Table 2, where each rock group is described by the mean and standard deviation of each of its nine constituent major oxides. Assuming that alteration of the rocks results mainly in the addition of volatile components, the deviation of the sum of major oxides from a hundred can be interpreted to indicate the extent of alteration. In this respect the intrusive rocks, with the exception of those collected from the Afton property, are less altered than the extrusive ones. The group of altered Cherry Creek rocks at Afton consists mostly of mineralized samples taken from the open pit; their nine major oxides sum to less than 93 per cent by weight. The group of fresh Cherry Creek rocks at Afton, on the other hand, are the least altered samples collected adjacent to the orebody and shows little sign of copper mineralization. These two groups of rocks will be referred to as altered and fresh Afton host rocks respectively. The group of Iron Mask Hybrid rocks includes the most abundant varieties of coarse-grained fragments in the agmatitic exposures, fine to medium-grained and magnetite-rich intrusive breccia, and coarse-grained diorite believed to be transitional to rocks of the Pothook unit. The heterogeneity of rock types analysed is reflected in higher variability in most of the nine major elements in comparison to that of the other rock groups. Whereas data presented in Table 2 shed light on the variation within a rock group and differences among the groups with respect to chemical composition, compositional trends and subtle differences among related rock groups are more readily revealed in variation diagrams. To allow comparisons to be made, data presented in Appendix I have been recast to a dry basis before being plotted onto the variation diagrams discussed following.

Figure 11 presents Harker plots of the analyses of the Iron Mask Hybrid, Pothook, Sugarloaf, and Cherry Creek units of the Iron Mask batholith, which are considered to bear close genetic relationships (Northcote, 1974, 1976, and 1977 and Cann, 1979). In general, instead of clustering to form discrete domains, analyses of successive rock phases tend to have significant overlap. However, it is evident that progressively younger units have higher silica contents. Furthermore, considering the analyses as a whole and allowing for minor exceptions, several smooth evolutionary trends are readily discernible from the plots. Thus, CaO, MgO and total iron as Fe_2O_3 show a prominent decrease with increasing silica content. Similar variations of MnO and TiO_2 with silica are less convincing because of the relatively greater scatter and smaller range of variability of the data. With the exception of a few silica-poor samples of the Iron Mask Hybrid unit, which contain moderate to very low alumina, the alumina content of the analysed rocks does not vary much with silica. K_2O and Na_2O generally increase with silica but much scatter is evident in the high-silica end of both plots. For the P_2O_5 versus SiO_2 plot, rocks of the Iron Mask Hybrid unit are distinctly low in P_2O_5. Otherwise, scatter of data precludes any significant correlation.

Compositional trends in the Harker plots are depicted by solid lines. These have been constructed by fitting a smooth curve (estimated by eye) through the average analysis (arithmetic mean of all analyses) of each rock group. Distribution of data points in the Harker plots for K_2O, Na_2O, and TiO_2 suggests that alternative trends are possible for analyses with greater than about 55 per cent silica. At this apparent threshold silica content, the K_2O and Na_2O variation curves branch out into two, one sympathetic and the other antipathetic with silica. For TiO_2, a local maximum occurs at about 57 per cent silica. These alternative interpretations of trends are depicted in each Harker plot by broken lines. Because differentiation of a mafic magma generally leads to a progressive increase in silica content in the more evolved liquid (except for the late differentiates of an undersaturated alkalic magma), compositional trends established in Figure 11 are approximations to

TABLE 1.
PETROGRAPHIC CHARACTERISTICS OF VARIOUS ROCK UNITS OF THE IRON MASK BATHOLITH

Rock Unit*	Mineralogy	Texture
Picrite	olivine phenocrysts >20% clinopyroxene phenocrysts frequently >15% feldspar practically absent accessory phlogopite and magnetite	porphyritic with aphanitic to very fine-grained matrix in excess of 35%, compare basalt occasional layered appearance
Iron Mask Hybrid	fragments of variable composition but gabbro is most common; typical modes: clinopyroxene 55% plagioclase ≥25% magnetite ≥10% accessory hornblende ± biotite no olivine	mostly agmatitic with medium to coarse-grained diorite as matrix gabbro fragments frequently show apparent segregation banding
Pothook	clinopyroxene 25% plagioclase 50% magnetite 6–15% accessory biotite, hornblende ± K-feldspar	medium to coarse grained, partly cumulate (Cann, 1979)
Sugarloaf	hornblende ≥45% plagioclase ≤45% accessory magnetite and K-feldspar	porphyritic; typically hypabyssal with aligned plagioclase and hornblende
Cherry Creek	total feldspar ± 70% with K-feldspar generally ≥20% clinopyroxene 2–30% but generally <15% magnetite 2–10% variable amounts of accessory biotite and hornblende	typically fine grained, porphyritic; microvarieties common; occasional breccia
Latite dykes at Afton	total feldspar ≥60% K-feldspar generally ≥20% hornblende generally >20% quartz 5–10% no magnetite	invariably massive, fine grained and slightly porphyritic interstitial and eyes of quartz and K-feldspar common

* Note that the rock units, with the exception of Picrite, are listed in order of oldest to youngest to emphasise the resemblance of the sequential mineralogical change to Bowen's reaction series.

the differentiation trends of the Iron Mask pluton if the investigated units were derived from the same parent magma. No more elaborate method of derivation of the compositional trends has been used for three reasons. First, instead of being representative specimens collected from a well-layered intrusive body, the suite of samples analysed represents only typical varieties of rocks in each major unit of the Iron Mask pluton, and each unit is distinguished mainly on textural evidence. The limited number of samples analysed and the intragroup variations evident in outcrop argue against the usefulness of detailed regression analysis of any individual data group. Second, the compositional trends are constructed mainly to serve as a reference for comparison of data with other related rock groups. The simple approach presented here serves the purpose satisfactorily. Third, although highly altered samples have been excluded, most rocks analysed still show signs of minor alteration, which could be deuteric, metasomatic, hydrothermal, or metamorphic, but the net change in major element geochemistry resulting from these minor alterations is probably small.

Figure 12 depicts the variation of the analyses of the four major intrusive phases of the Iron Mask pluton in a triangular AFM plot. With a few exceptions, analyses of successive units follow a path subparallel to the trend of differentiation of a calc-alkaline magma. If the four units share a common source magma, then the differentiation of the Iron Mask pluton involved little iron enrichment.

Figure 13 compares analyses of the two groups of Afton intrusive host rocks, the latite dykes of the Afton pit, the Nicola Group volcanic rocks, and the Picrite samples, with those of the four major intrusive phases of the Iron Mask pluton. The compositional fields of the latter are approximated by constructing the smallest convex polygon containing all analyses of the same unit. To allow for alternative trends in the variation of K_2O and Na_2O with silica, a reentrant polygon is drawn to contain the Cherry Creek analyses in the Harker plots for these two oxides. In general, the range in silica of the analysed rocks of the Nicola Group approximates that of the Sugarloaf intrusive phase. The Afton host rocks show a large range in silica but most analyses lie close to a region of overlapping Sugarloaf and Cherry Creek analyses of which the corresponding rock specimens were collected away from the Afton property. Most analyses of both the Nicola volcanic rocks and the Afton host rocks fall close to most of the compositional trends established in the Harker plots for the four major intrusive phases of the Iron Mask pluton. The most obvious exception is MnO, in which some of the Afton host rocks are apparently enriched. Because the sum of nine major oxides of these rocks is generally low compared to that of the fresh intrusive rocks, the apparent MnO enrichment may be partially caused by the renormalization of the raw data. Otherwise, hydrothermal alteration and/or weathering probably concentrated manganese in these rocks, in preference to other elements. One Nicola basalt sample (from near the southeastern tip of the batholith) is also exceptionally high in magnesia and low in alumina. Taking the other oxide components into consideration, it appears that this sample is either akin to or contaminated by material of the Picrite unit.

Lying in the low and high silica end of the Harker plots respectively, the analyses of the Picrite unit and the latite

TABLE 2.
MAJOR ELEMENT GEOCHEMISTRY OF VARIOUS ROCK UNITS MAKING UP OR ASSOCIATED WITH THE IRON MASK PLUTON

	SiO_2	Al_2O_3	Fe_2O_3	MgO	CaO	K_2O	Na_2O	TiO_2	MnO	Total
Tertiary Volcanics										
$\bar{x}_1$	53.48	16.77	8.44	3.89	5.85	2.66	3.79	1.64	0.13	96.72
s	5.47	1.08	3.60	1.29	2.07	1.27	0.17	1.12	0.05	2.45
Tertiary Volcanics at Afton										
$\bar{x}_2$	44.02	14.10	7.28	5.57	7.87	2.19	3.38	1.06	0.13	85.58
s	4.21	0.59	0.73	0.67	1.19	0.01	0.40	0.11	0.02	2.69
Latites[1]										
$\bar{x}_5$	62.38	15.28	4.66	3.34	1.16	2.67	4.41	0.72	0.04	94.65
s	4.03	0.69	1.17	1.29	1.09	0.60	0.68	0.31	0.03	1.17
Fresh Cherry Creek Rocks at Afton (fresh Afton host rocks)										
$\bar{x}_{13}$	52.99	17.90	5.97	3.84	4.87	2.91	5.20	0.75	0.19	94.50
s	3.10	1.13	2.51	1.01	2.25	2.16	1.92	0.12	0.11	1.11
Altered Cherry Creek Rocks at Afton (altered Afton host rocks)										
$\bar{x}_{18}$	49.88	17.13	6.34	4.22	4.58	2.34	5.05	0.77	0.22	90.51
s	3.96	0.99	2.80	1.18	2.20	1.50	1.33	0.10	0.19	2.37
Cherry Creek Rocks										
$\bar{x}_{12}$	57.16	18.04	5.29	2.23	4.72	3.44	5.43	0.60	0.10	97.25
s	4.03	1.24	2.75	1.29	1.75	2.66	1.92	0.19	0.04	1.85
Sugarloaf Rocks										
$\bar{x}_4$	49.37	17.13	10.47	5.34	7.71	2.44	3.57	0.64	0.09	96.77
s	2.92	1.51	4.19	0.99	1.76	0.90	0.84	0.12	0.03	1.04
Picrite										
$\bar{x}_3$	41.16	5.65	9.87	29.00	5.91	1.18	0.34	0.25	0.17	93.64
s	1.67	1.40	0.65	4.86	2.45	0.35	0.18	0.09	0.03	0.53
Pothook Diorite										
$\bar{x}_9$	46.19	16.77	11.58	5.64	10.74	1.89	2.85	0.85	0.21	98.14
s	3.42	1.53	1.82	0.93	1.28	0.84	1.01	0.13	0.03	0.64
Iron Mask Hybrid Rocks										
$\bar{x}_{10}$	43.05	16.20	13.11	7.49	14.38	1.01	1.38	0.94	0.16	97.81
s	3.62	4.43	4.50	2.61	2.82	0.77	1.04	0.16	0.04	0.92
Nicola Volcanics[2]										
$\bar{x}_6$	47.61	15.44	9.23	6.93	8.94	2.19	2.94	0.68	0.19	94.55
s	2.77	3.06	1.68	5.86	1.00	0.99	0.85	0.13	0.04	2.48

Symbols: $\bar{x}_n$ = mean of n samples
s = standard deviation

[1] Only five least altered samples are included.

[2] Nicola volcanic rocks within the Afton open pit are not included.

dykes within the Afton pit show significant deviation from the outlined compositional trends in all but the MnO and possibly the K_2O plots. These rocks, in contrast to most Nicola volcanic rocks and the Afton host rocks, are probably not genetically related to the major intrusive phases of the Iron Mask pluton.

In detail, the majority of samples of the two groups of Afton host rocks are apparently slightly enriched in Na_2O, MgO, TiO_2, and Al_2O_3 and depleted in CaO and total iron (as Fe_2O_3) relative to the major intrusive units of the pluton. Comparing the fresh and altered groups of Afton host rocks, the altered rocks appear to be relatively enriched in Na_2O.

Finally, Figure 14 is a total alkali versus silica plot for the analyses of pertinent groups of relatively fresh rocks related to the Iron Mask pluton. While most of the data points of the Picrite unit and latite dykes within Afton lie within the subalkaline field, almost all data points for the rest of the analysed rocks lie in the alkaline field. With a few exceptions, analyses with low silica content lie closer to the dividing line for discriminating alkaline from subalkaline rocks (MacDonald, 1968) than those characterized by high silica. If the plotted rocks are genetically related at all, it appears that their geochemical affinity is better defined with more advanced degree of differentiation.

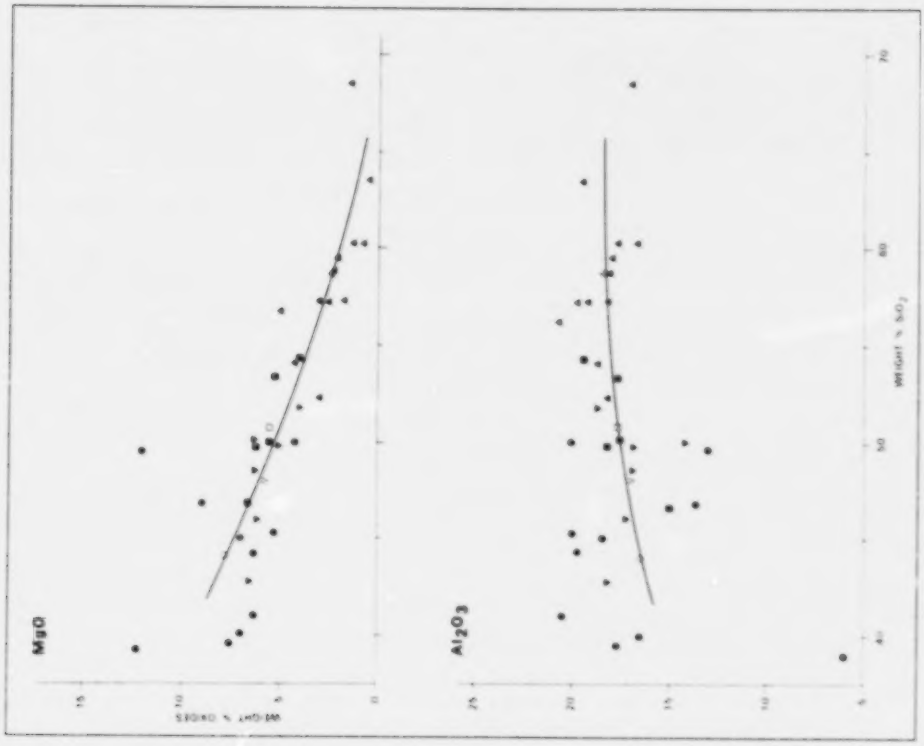
MgO
Al_2O_3

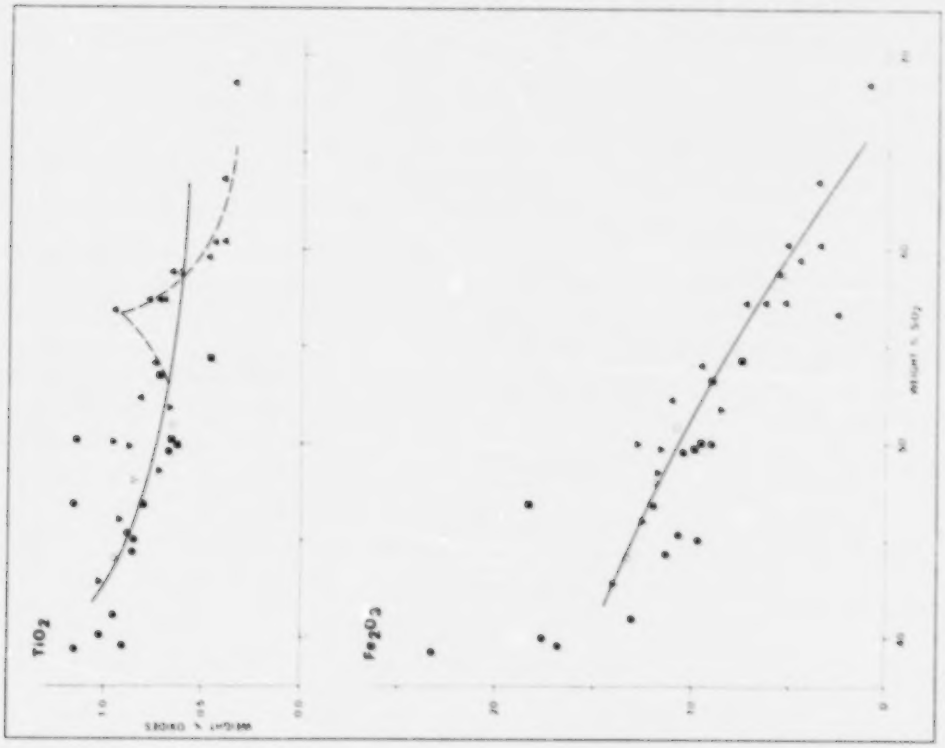
TiO_2
Fe_2O_3

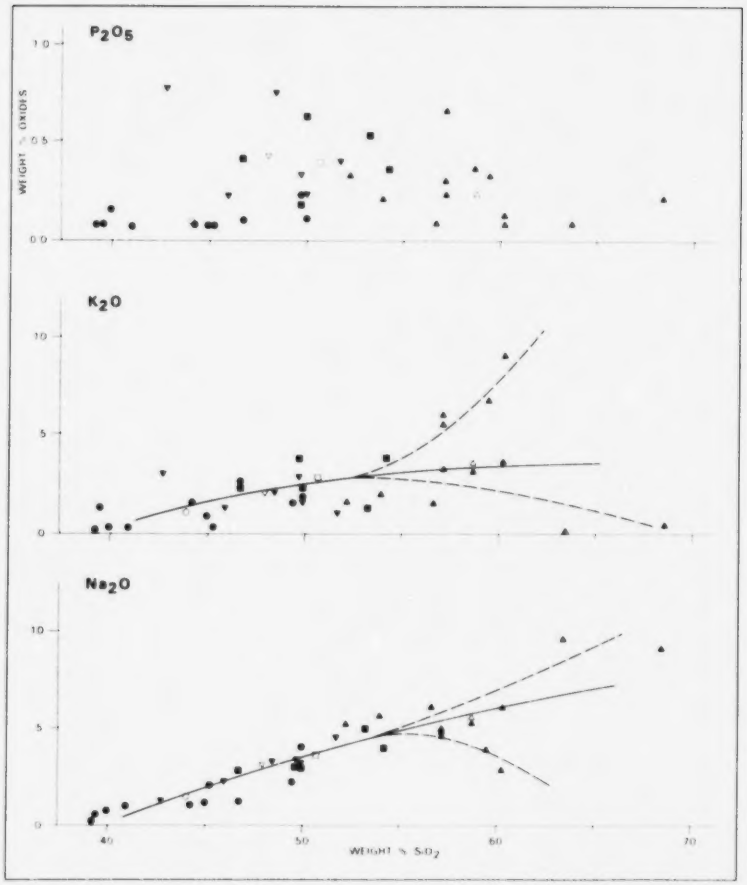

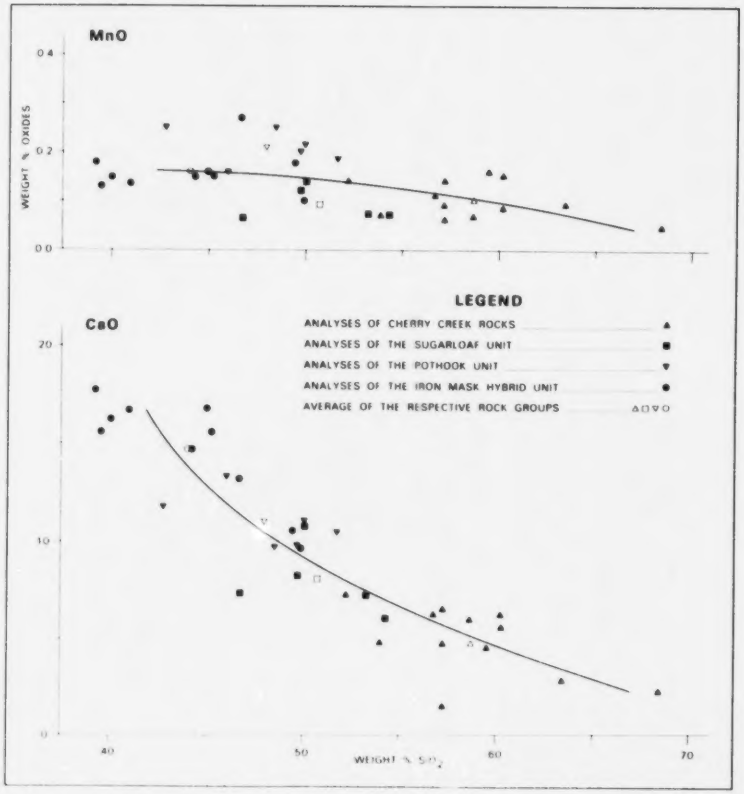

Figure 11. Harker plots of analyses of the major intrusive phases of the Iron Mask pluton. Compositional trends (solid lines) have been constructed by fitting a smooth curve (estimated by eye) through the average analysis of each rock group. Alternative interpretations in the respective K_2O, Na_2O and TiO_2 versus SiO_2 plots are shown in broken lines.

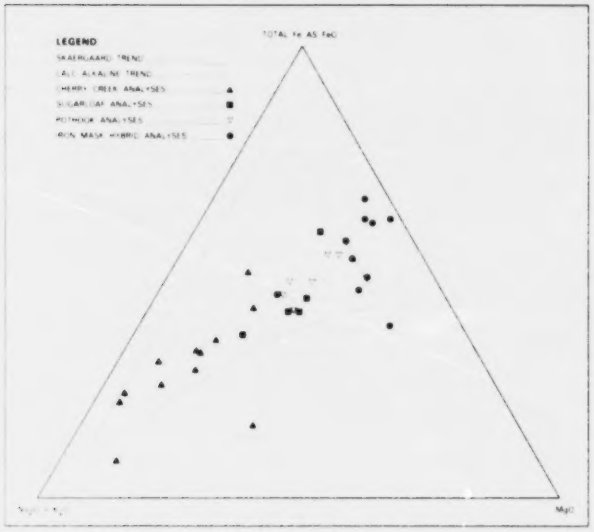

Figure 12. A total alkali-total iron-magnesia plot of the analyses of the four major intrusive phases of the Iron Mask pluton. The Skaergaard and idealized calc-alkaline trends are adapted from Ernst (1976, figure 4.50).

DISCUSSION AND INTERPRETATION

EVOLUTION OF THE IRON MASK BATHOLITH

Three phases of the Iron Mask batholith, namely the Iron Mask Hybrid, Pothook and Cherry Creek units, have been dated by the potassium-argon method (Preto *et al.*, 1979) and shown to be indistinguishable in age using that technique. Field evidence (Petro, 1967 and Northcote, 1974, 1976, and 1977) indicates that the relative age sequence is Iron Mask Hybrid followed by Pothook, then Sugarloaf, and lastly Cherry Creek. Moreover, gradational contacts are common between the Iron Mask Hybrid and Pothook units and, to a lesser extent, between the Sugarloaf and Cherry Creek units. These intimate age and geological contact relationships, combined with the smooth compositional trends and the overlapping compositional boundaries observed among these four phases in the Harker plots, suggest a common parent magma. Many coarse-grained specimens of the Iron Mask Hybrid unit examined by the writer show aligned clinopyroxene and/or plagioclase with or without segregation bands of magnetite, suggestive of crystal settling. Cann (1979) also reported cumulus texture in some rocks of the Pothook unit. In addition, upon describing the coarser grained batholithic rocks, which in the present context are equivalent to those of the Iron Mask Hybrid and Pothook units, Carr (1956, p. 49) noted, "An inconstant banding is developed in place,...". These observations suggest that the batholith evolved mainly by the process of fractional crystallization. Disrupted development of cumulus texture and the overall decrease in grain size from rocks of the Iron Mask Hybrid unit to those of the Pothook unit could have resulted from slow upward movements of the cooling magma initiated shortly after the commencement of crystallization. In contrast, porphyritic and hypabyssal textures, characteristic of most rocks of the Sugarloaf unit, suggest rapid transfer of a cooling magma to shallow depths. The analyses of most Nicola Group volcanic rocks, while conforming to the compositional trend of the major intrusive phases of the batholith, most closely resemble Sugarloaf analyses. Therefore venting of some magma during the Sugarloaf stage seems likely. One consequence of the venting event may have been the localization of some magma in a subvolcanic environment where the Cherry Creek phase started to crystallize. Continuous build up of volatile pressure apparently caused periodic rupture of the roof of the magma chamber, resulting in the formation of breccias and rocks with different textures and chemical compositions.

The genetic relationship of the Picrite unit and latite dykes with the four major intrusive units of the batholith is more difficult to assess. Data points are mainly incompatible with the established trends in the Harker plots and fall mostly in the subalkaline field in the plot of total alkali versus silica, hence they may be genetically distinct from the batholithic rocks. However, their mineralogy and texture (Table 1) could represent both end members of the petrographic sequence for the main phases of the batholith, analogous to Bowen's (1928) reaction series. Preto (1967) bracketed the relative age of the Picrite unit as being between the Pothook and Sugarloaf units. For the Picrite unit to be included in the genetic scheme of the Iron Mask batholith, a two-stage process has to be involved:

(i) Following the precipitation of olivine and some clinopyroxene, the parent Iron Mask magma was transferred to a secondary magma chamber where the differentiation series of Iron Mask Hybrid – Pothook – Sugarloaf – Cherry Creek proceeded, as discussed before.

(ii) The crystal mush left behind in the primary magma chamber later intruded the solidified Iron Mask Hybrid and Pothook phases prior to venting that occurred during the Sugarloaf stage of differentiation. For the case of latite dykes, it is possible that during ascent of the bulk magma a small portion was trapped, locally differentiated at depth with a slightly different trend, and then intruded into the Cherry Creek rocks. With the composition of a parent magma lying close to the alkaline-subalkaline dividing line (Figure 14), straddling of the derivative liquids in either composition field is not difficult to rationalize, especially if differentiation proceeded under high pressure or hydrous conditions. However, the simplest hypothesis remains that the picrites and possibly the latites are unrelated to other intrusive rocks of the batholith.

In short, with the possible exception of the Picrite rocks and the latite dykes, the major rock units of the Iron Mask batholith appear to have derived from a common parent magma and to be related by a single cycle of fractional crystallization. Textural evidence suggests, however, that the formation of the Sugarloaf and Cherry Creek phases took place at a much shallower depth than that required for the crystallization of the Iron Mask Hybrid and Pothook rocks. Periodic venting of the Sugarloaf phase could explain the extrusion of compositionally similar rocks within the Nicola Group and introduction of the embryonic Cherry Creek phase into a subvolcanic environment.

EVOLUTION OF COPPER MINERALIZATION WITHIN THE IRON MASK BATHOLITH

At this time, Afton mine is the only producer located within the Iron Mask batholith. Consequently, the relationship of the evolution of the batholith to its associated copper mineralization will be discussed with reference to the Afton orebody.

Data presented in Figure 13 indicate that Cherry Creek rocks at Afton are compatible with the compositional trends defined by the major phases of the batholith. This implies that the Afton rocks are also products of fractional crystallization of the same source magma. As indicated by the position of the data points in Figure 13, the formation of Afton rocks probably took place in the transitional stage between the Sugarloaf and Cherry Creek phases of intrusion. Copper mineralization found in Afton mine could therefore be a modified byproduct of magmatic differentiation. This view warrants a discussion of certain details of the differentiation process.

Consider first that the AFM plot (Figure 12) shows no prominent iron enrichment in the residual liquids involved in the formation of the four successive major phases of the Iron Mask pluton. A reasonable explanation is that magnetite precipitated continuously, starting with the earliest events recorded. This results in concomitant silica enrichment of the melt. Such an explanation is in agreement with field observations that magnetite is prominent in all four major units of the batholith, but is particularly abundant in rocks of the Iron Mask Hybrid unit (Table 1). The continual precipitation of magnetite as the magma crystallized has three important effects on the formation of copper mineralization. These are outlined as follows:

(i) It influences the solubility of sulphides. In mafic magmas, the saturation and subsequent separation of an immiscible sulphide liquid is antipathetic with the FeO content of the cooling melt (Haughton *et al.*, 1974). Consequently, during crystallization of the parent Iron Mask magma, a continual decrease in sulphide solubility is expected to accompany magnetite precipitation. Whereas the separation of the bulk of copper sulphides might be delayed to the early Cherry Creek or Afton stage, minor amounts of sulphides are expected to be found in other phases of the batholith, with the possible exception of the very first cumulus phase. Moreover, if the differentiating magma was moving upward, the separating sulphide globules would remain suspended and eventually be precipitated as disseminated sulphides, unless scavenged by late magmatic fluids to form veins. The mode of occurrence of copper sulphides described earlier strongly suggests that remobilization of some primary sulphides has taken place. Moreover, according to Northcote (1974, 1976, and 1977), minor copper mineralization characterizes all phases of the Iron Mask batholith.

(ii) It influences the composition of the copper mineralization. With abundant iron being fixed in the oxide phase, the separating sulphide should have a relatively low iron content and no abundant hydrothermal iron-rich sulphides should form during the waning stage of magmatic activity unless a new source of iron becomes available. It is thus not surprising to find bornite, with a copper-iron ratio of 4:1, as an essential component in the disseminated, hypogene ore zone of the Afton orebody and that, in comparison with most calc-alkaline porphyry copper deposits, Afton contains significantly less hydrothermal pyrite. This latter feature, however, may also have been caused by the loss of sulphur under subvolcanic conditions.

(iii) It sheds light on the cause of primary sulphide separation. Cann (1979) interpreted the occurrence of magnetite-apatite lodes in the batholith as due to immiscibility within the alkalic magma. In this context, the precipitation of magnetite may have gradually changed the iron-phosphorus ratio in the melt such that the eutectic composition of approximately two-thirds by volume of magnetite and one-third apatite (Philpotts, 1967) necessary for liquid immiscibility was reached. If this melt formed in the early Cherry Creek stage, it would readily explain the slight iron impoverishment of the Afton rocks in comparison with other fresh Cherry Creek rocks, and its formation could cause sulphide precipitation in the conjugate silicate melt by drastically reducing the sulphide solubility. However, in the variation diagram of P_2O_5 versus SiO_2 (Figure 18), other than the apparent depletion of the Iron Mask Hybrid rocks in P_2O_5, there is no obvious variation in phosphorus content among the other phases to substantiate the required apatite precipitation. Therefore, it is unlikely that enough immiscible magnetite-apatite melt separated to affect the overall differentiation trend of the batholith. Rapid rise of the Cherry Creek magma into a subvolcanic environment, with concomitant faster cooling that caused a drastic decrease in sulphide solubility, is a more plausible explanation for triggering formation of the Afton protore.

The lack of iron enrichment in the rock series of the Iron Mask batholith also implies a high oxidation state throughout the course of magmatic differentiation (Muan and Osborn, 1956 and Ernst, 1976). Coupled with the relatively mafic character of the Afton host rocks, this may explain the scarcity of molybdenum in the orebody. The phase equilibria studies of Korenbaum (1970) were quoted by Landergren and Manhein (1978) to explain the hydrothermal transport of molybdenum; at relatively low temperatures, near 200 degrees Celsius, and neutral pH values, molybdenum remains soluble in the form of thiomolybdates, even with relatively high total sulphur (= 1 molal) available in the system. With higher temperatures, near 400 degrees Celsius, the thiomolybdate field retreats toward basic pH values, but under oxidizing conditions the retreat is small; thus molybdenite precipitation takes place only under more acidic conditions and relatively low oxygen fugacity. For the formation of the Afton orebody, neither of these conditions was met, either at the initial stage of primary sulphide separation or during the late stage of hydrothermal redistribution of sulphides. At least for the porphyry copper deposits of south central British Columbia this explanation is a plausible alternative to the proposal that the high gold content and low

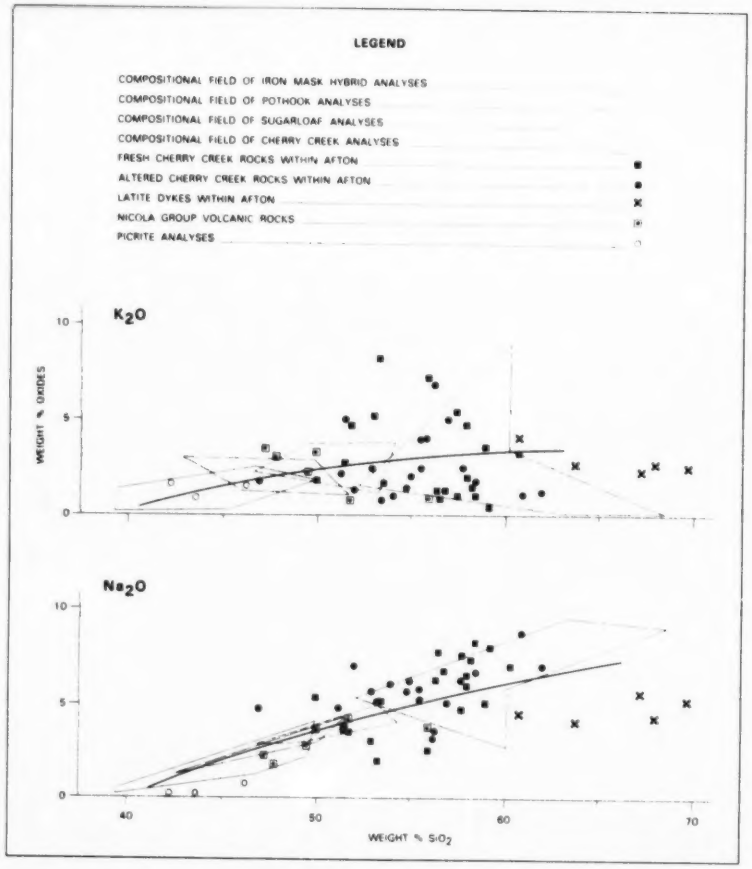
LEGEND
COMPOSITIONAL FIELD OF IRON MASK HYBRID ANALYSES
COMPOSITIONAL FIELD OF POTHOOK ANALYSES
COMPOSITIONAL FIELD OF SUGARLOAF ANALYSES
COMPOSITIONAL FIELD OF CHERRY CREEK ANALYSES
FRESH CHERRY CREEK ROCKS WITHIN AFTON
ALTERED CHERRY CREEK ROCKS WITHIN AFTON
LATITE DYKES WITHIN AFTON
NICOLA GROUP VOLCANIC ROCKS
PICRITE ANALYSES
K2O
Na2O
WEIGHT % OXIDES
WEIGHT % SiO2
10
5
0
40
50
60
70

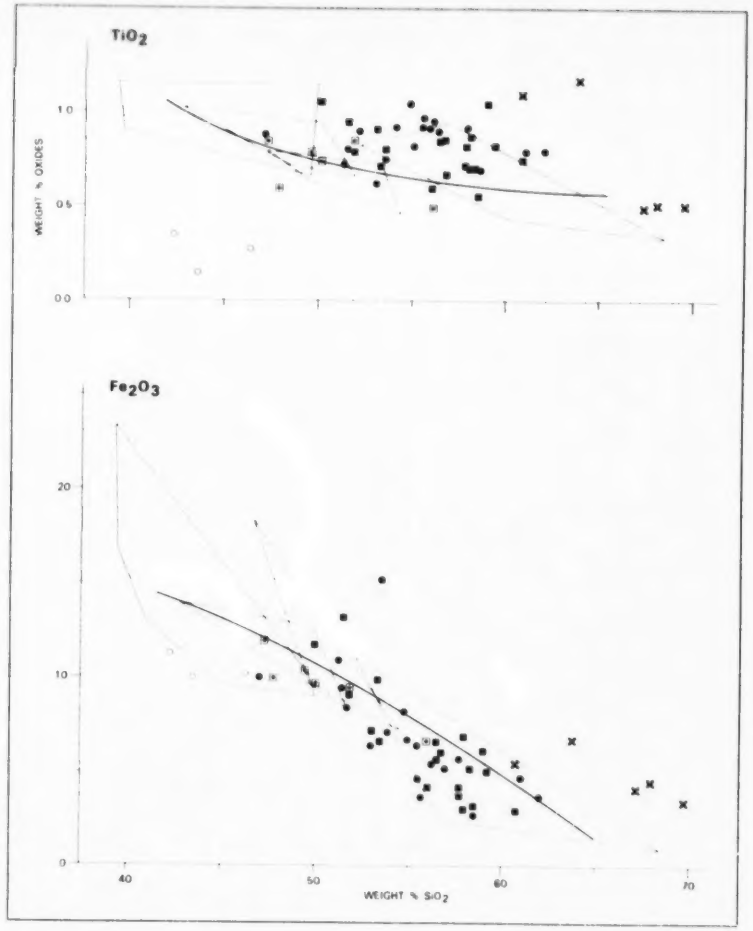
TiO2
Fe2O3
WEIGHT % OXIDES
WEIGHT % SiO2
1.0
0.5
0.0
20
10
0
40
50
60
70

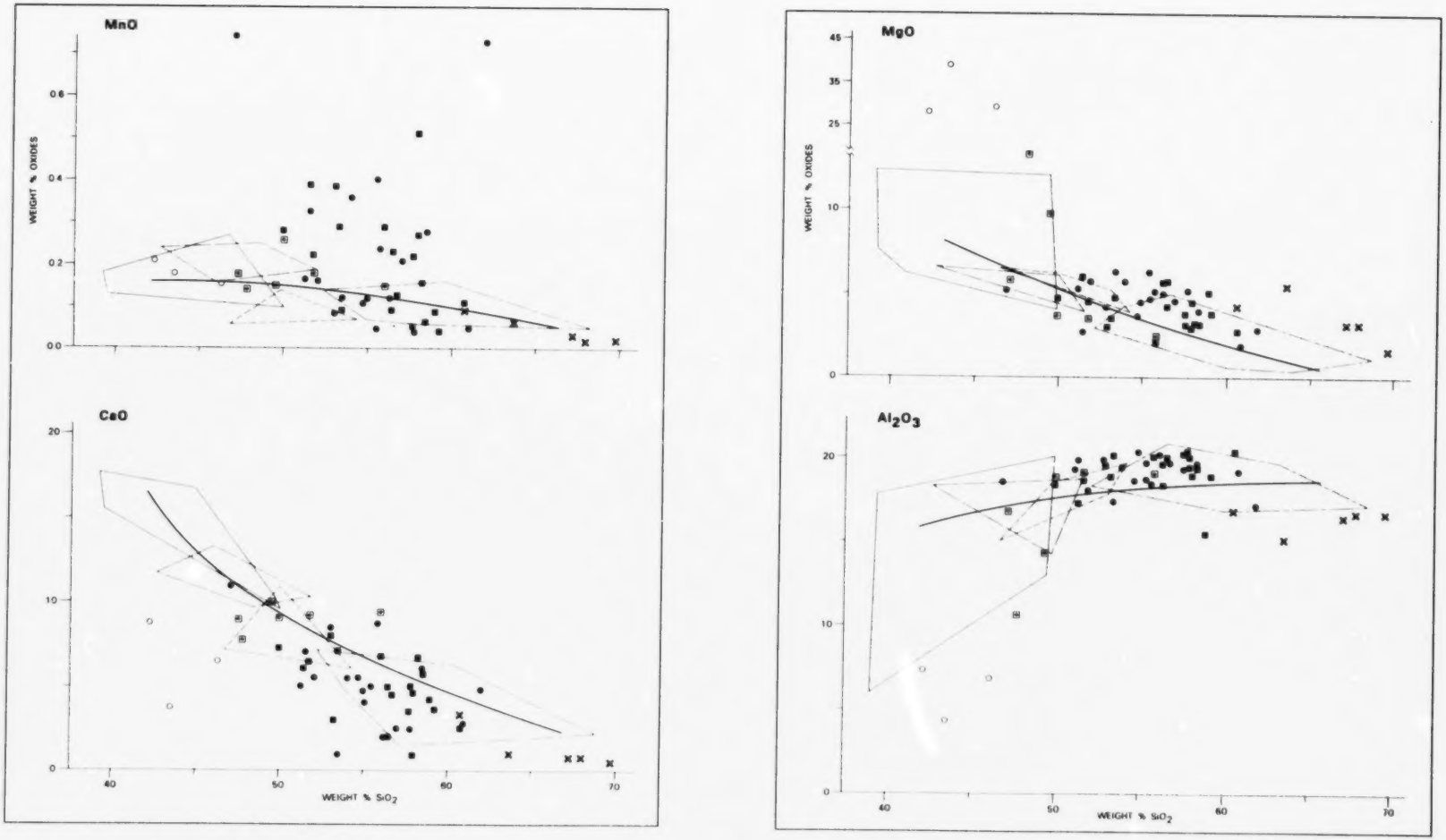

Figure 13. A comparison of analyses of various rock groups related to the Iron Mask batholith with those of the four major intrusive phases of the batholith. The compositional trend of the latter in each Harker plot (solid curve) has been reproduced from Figure 11.

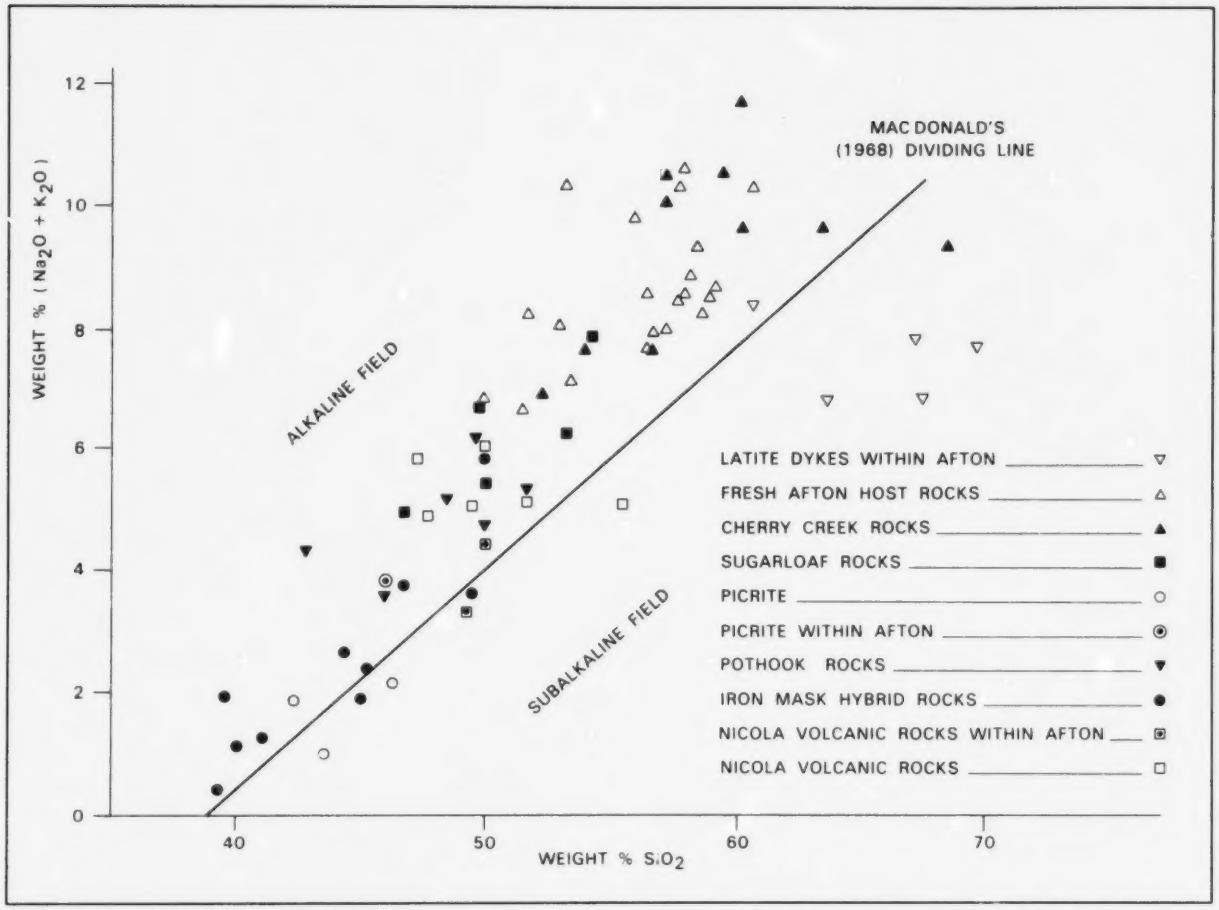

Figure 14. A total alkali versus silica plot for the analyses of various rock groups within the Iron Mask pluton.

concentration of molybdenum in diorite porphyries are the consequence of little sialic crustal contamination (Hollister, 1978). For example, though exhibiting different chemical affinities, both the Guichon Creek batholith (calc-alkaline) and the Iron Mask batholith (alkaline) are closely related in space and time, the age is nearly the same and they have similar initial Sr^{87}/Sr^{86} ratios (Preto *et al.*, 1979). It is difficult to envisage why copper-rich plutons in one were contaminated by sialic crust while those in the other were not. In addition, the common, low initial Sr^{87}/Sr^{86} ratio argues against crustal contamination. More likely, it is the buffering effects of the host rock geochemistry on important parameters of the mineralizing fluid (like pH, f_{O_2}, and f_{S_2} that ultimately determine the kind of ore that will be formed. The more acidic character of the Guichon Creek rocks provides a more suitable geochemical environment for the precipitation of molybdenum while the Afton host rocks are too mafic to do so.

Finally, minor anomalies observed in the variation diagrams also provide information about the evolutionary history of the copper mineralization. The slight relative enrichment of the Afton rocks (particularly the altered ones) in Na_2O rather than K_2O indicates that the copper mineralization was associated with sodium metasomatism rather than potassium feldspar mineralization as previously advocated by Northcote (1974, 1976, and 1977). In view of the high TiO_2 content of hydrothermal biotite associated with the orebody (Appendix II), it is speculated that the apparent enrichment of the Afton rocks in TiO_2 (Figure 13) correlated with the precipitation of biotite. To fully appreciate the significance of the apparent enrichment, however, the composition of primary biotite should also be studied.

SUMMARY AND CONCLUSIONS

Major element geochemical data presented in this section augmented by field observations, lead to the interpretation that the Iron Mask Hybrid, Pothook, Sugarloaf, and Cherry Creek units of the Iron Mask batholith are closely related through the process of fractional crystallization. The differentiation of the original bulk magma is characterized by an absence of iron enrichment as a result of continual magnetite crystallization. A comparison of major element analyses of

the host rocks of the Afton orebody with those of the other intrusive rocks of the batholith indicates that they too follow the same differentiation trend. Their crystallization commenced in the early Cherry Creek stage, where the dominant rock is dioritic and intermediate between the Sugarloaf hornblendites and late Cherry Creek syenites. The evolution of the Afton orebody probably involved three important steps:

(1) Fractional crystallization of an original magma under high oxidation states during its slow ascent, with continual separation of magnetite so as to bring about incipient saturation of copper sulphide phases;

(2) Rapid transfer of portions of the differentiating early stage Cherry Creek magma to a subvolcanic environment where more rapid cooling caused supersaturation with respect to copper sulphides; and

(3) Trapping of late magmatic fluids to remobilize and concentrate the disseminated orthomagmatic copper sulphides to form the stockwork copper ore.

Such a genetic model explains many mineralogical characteristics of the Afton orebody, including the limited occurrence of molybdenite, relative abundance of bornite, and low total pyrite content. The model is also compatible with the sulphur isotope data of Hoiles (1978) who found that sulphides at Afton are characterized by a near zero per mil δS^{34} with a small standard deviation, and the contention that magmatic fluid dominated the hypogene stage of mineralization. Future exploration for similar copper mineralization in the batholith should focus on areas where Cherry Creek diorites are close to major faults; accompanying carbonate alteration and magnetite mineralization are favorable guides for locating targets.

CHAPTER 5

A THERMODYNAMIC SIMULATION OF SUPERGENE ALTERATION AT AFTON MINE

INTRODUCTION AND METHOD OF APPROACH

Afton mine is unusual among porphyry copper deposits in the Canadian Cordillera; it has a significant supergene zone dominated by native copper. To an average depth of about 500 metres, the orebody averages 1 per cent copper, and the main copper minerals are native copper and chalcocite in a ratio in excess of 2:1. Thin smears of cuprite coat native copper locally and malachite, azurite, amorphous hydrated copper sulphates (?) and conichalcite occur rarely. Despite the fact that supergene alteration extends to a considerable depth, the zone is not generally enriched in copper in comparison to the hypogene zone. Carr and Reed (1976) suggested that the coexistence of magnetite and high-sulphur copper minerals could account for the unusual supergene assemblage by facilitating the necessary oxidation-reduction processes. Preto (personal communication), on the other hand, emphasized the absence of abundant pyrite as the prime factor responsible for the lack of supergene enrichment. Ney *et al.* (1976) summarized the general conditions required for enrichment to include abundant hypogene iron sulphides, oxidation under low pH conditions, a water table at considerable depth, high permeability and porosity, absence of reactive wallrocks, and abundant rainfall in a warm climate.

At a given locality and time, solution chemistry (including pH and Eh, in particular) and the associated mineral assemblage are not independent variables. If the overall chemical system is not in equilibrium, or is only in partial equilibrium, mass transfer will occur among the phases in the system, and tend toward equilibrium, that is a state of minimal Gibbs free energy at a given temperature and pressure. Inasmuch as supergene mineralization is a consequence of interactions between downward percolating meteoric water with host rocks containing suitable hypogene mineral assemblages, understanding the process requires consideration of simultaneous reactions involving the bulk rock mineralogy and reacting fluid but not just the sulphides. For this purpose, the mass transfer approach expounded in detail in Helgeson (1968, 1970, and 1979), Helgeson *et al.* (1969), and Helgeson *et al.* (1971) will be utilized. In essence, the approach makes use of thermodynamic constraints imposed by local and partial equilibrium to calculate the extent to which components are redistributed among minerals and aqueous solution, as the solution reacts irreversibly with the host rock minerals. Separation of phases caused indirectly by apparently unrelated processes in different parts of the system are readily revealed in the mass transfer calculations. Consequently, cause and effect in the geologic record are more easily related and subtle indicators of favorable environments for ore deposition can be recognized.

Utilizing the detailed mineral distribution data described in Chapter 3 and the mass transfer computer program described in Perkins (1980), this chapter presents a thermodynamic simulation of the development of supergene alteration at Afton mine. For comparison, interaction between a hypothetical mineralized monzonite and rain water under similar conditions is also presented. Similarities and discrepancies between the simulation results and the actual field observations are elaborated. Parameters controlling the supergene enrichment at Afton mine in particular, and other porphyry copper deposits in general, are then evaluated and discussed. The essence of this presentation has been published elsewhere (Kwong *et al.*, 1982). However, since supergene alteration is an integral part of the evolution history of the Afton deposit, it is repeated here.

SPECIFICATIONS FOR COMPUTER RUNS

Tables 3A and 3B summarize the compositions of the initial reactant solids and fluids for three critical simulation runs which, as will be demonstrated later, outline the variations in style of supergene alteration. The mineralogical compositions for the two portions of the Afton open pit have been estimated from field mapping, and from petrographic and X-ray diffraction studies of samples collected at various stages of stripping of the orebody; limited areas of intensive

TABLE 3A.
COMPOSITION OF STARTING MATERIAL
(in modal per cent)
USED IN COMPUTER SIMULATION
OF SUPERGENE ALTERATION

	1 East Pit Rock	2 West Pit Rock	3 Hypothetical Monzonite
Feldspar	60 ($Ab_{.98}Or_{.03}An_{.02}$)	60 ($Ab_{.98}Or_{.03}An_{.02}$)	65 ($Ab_{.69}Or_{.24}An_{.07}$)
Epidote	12	—	—
Chlorite	5	20	—
Biotite	5	2	7
Magnetite	5	—	—
Chalcopyrite	1	1	3
Bornite	1	1	2
Chalcocite	1	1	—
Carbonates	4	5	—
Pyroxene	5	—	—
Hornblende	—	5	10
Pyrite	—	3	10
Quartz	—	1	3
Apatite	(1)	(1)	—

TABLE 3B.
COMPOSITION OF HYPOTHETICAL RAINWATER USED IN SIMULATION RUNS

	Run 1	Run 2	Run 3
$\log f_{O_2}$	-0.69, that is, in equilibrium with oxygen in the atmosphere		
$\log f_{CO_2}$	-3.5, that is, in equilibrium with carbon dioxide in the atmosphere		
pH	—	7	—
Cu^{++}	1×10^{-8} m	1×10^{-11} m	1×10^{-9} m
Mg^{++}	—	1.48×10^{-5} m*	—
SO_4^{--}	—	1.25×10^{-5} m*	—
Ca^{++}	—	2.42×10^{-5} m*	—
K^{+}	—	6.6×10^{-6} m*	—
Na^{+}	—	4.78×10^{-5} m*	—
Al^{+++}	1×10^{-12} m	1×10^{-11} m	1×10^{-11} m
H_4SiO_4	1×10^{-8} m	1×10^{-11} m	1×10^{-12} m
Fe^{+++}	constrained by the presence of hematite		

* From Wedepohl, 1966.

carbonate replacement and magnetite veining have been deliberately excluded from the average. These estimates are rough, but are considered to be more realistic than artificial approximations.

For minerals commonly exhibiting solid solution, microprobe analyses tabulated in Appendix I indicate that composition variations are frequently evident in grains in the same thin section. Nevertheless, the following approximations in terms of end members can be made: pyroxene is 0.8 diopside and 0.2 hedenbergite; epidote is 0.8 epidote and 0.2 clinozoisite; ignoring its relatively high titanium content, biotite is low in fluorine and is roughly 0.8 phlogopite and 0.2 annite; the compositions of feldspars are explicitly stated in Table 3A; carbonates in the east pit are mainly calcitic and are taken as 0.95 calcite, 0.03 magnesite, and 0.02 siderite; in the western portion of the pit, ankerite is more prominent and the carbonates are expressed as 0.6 dolomite, 0.1 siderite, and 0.3 calcite; hypogene chlorite is mainly pycnochlorite with an average magnesium/iron ratio of 2:1; the magnesium portion is represented by 7A clinochlore and the iron is expressed by a corresponding amount of annite biotite due to lack of thermodynamic data on end-member iron chlorites (the additional potassium introduced into the system through this substitution is considered to be insignificant, because the amount of potassium feldspar actually present in the wallrocks is so variable); hornblende is 0.7 pargasite and 0.3 ferrohastingsite, but available thermodynamic data on file, force one to treat it as pure pargasite. Apatite survives the supergene alteration and is therefore not included as a reactant mineral. After these adjustments, the total number of solid reactants considered in each of the three runs is 18, 16, and 10 respectively.

The data used for the composition of rain water have been adapted from Wedepohl (1966). The missing but required independent components have been arbitrarily assigned small values. Some of these, as shown in Table 3B, are allowed to vary slightly to bring out the point that as long as the initial concentrations are low enough, the reacting rain water derives its constituent ions through reactions with the host rocks and these ions determine the sequence of precipitation of various solid products. For the case of iron, calculations on initial distribution of species have shown that under atmospheric conditions and an assumed pH of 7, water is saturated with respect to hematite at a total iron content as low as 1×10^{-23} molal. Soon after the initial contact of rain water with the relatively iron-rich reacting rocks, hematite, among all the iron minerals considered in the system, will be the first reaction product to precipitate out; for convenience, therefore, it is assumed to be in equilibrium with the rain water in the supergene environment.

Finally, all the mass transfer calculations presented here have been performed assuming isobaric and isothermal conditions in a closed system. Reaction products are not separated from the bulk system after their initial precipitation but are allowed to participate in subsequent reactions accompanying changes in composition of the reacting fluid. The pressure and temperature specified for all the three runs are 1 bar and 25 degrees Celsius respectively. Thermodynamic data for various aqueous and solid phases involved in the calculations are derived mainly from Helgeson (1969) and Robie *et al.* (1978).

RESULTS AND INTERPRETATION

GENERAL ASPECTS

The results of interactions of rain water with the three reacting rock compositions obtained from mass transfer calculations are portrayed in Figures 15 to 17. The progress variable, ξ, is a measure of the extent of a given reaction. It is numerically equal to the number of moles, n, of a given reactant that has been converted into products by the reaction, divided by the stoichiometric coefficient of the reactant. Since the stoichiometric coefficient is a constant, the following differential equation can be written:

$$\frac{dn}{d\xi} = k \text{ where k is constant.}$$

Consequently, in the figures, all the reactants exhibit a positive slope of 1 until they become saturated with respect to the reacting fluid. For the sake of simplicity, only two reactants are depicted in each diagram (broken lines). Each product mineral except hematite, which is assumed to be already in equilibrium with the initial reacting solution, has an initial infinite slope, indicating its first appearance as a new solid phase in the system considered. The net amount of any product mineral present in the system at any instant during overall reaction can be read off from the corresponding evolutionary curve of the mineral (solid lines and labelled to the right of that portion of the curve indicating its initial precipitation). The portion of the curve with a positive slope indicates precipitation while that showing a negative slope indicates subsequent dissolution due to changes of solution chemistry. The variation in activity of a selected species, in the aqueous phase, as the reaction progresses, is also plotted as solid lines. Note the sequential change in copper mineralogy (tenorite-cuprite-native copper-chalcocite) accompanying the monotonic decrease in oxygen fugacity and concomitant increase in sulphur fugacity. This change takes place in nature when the downward percolating rain water has

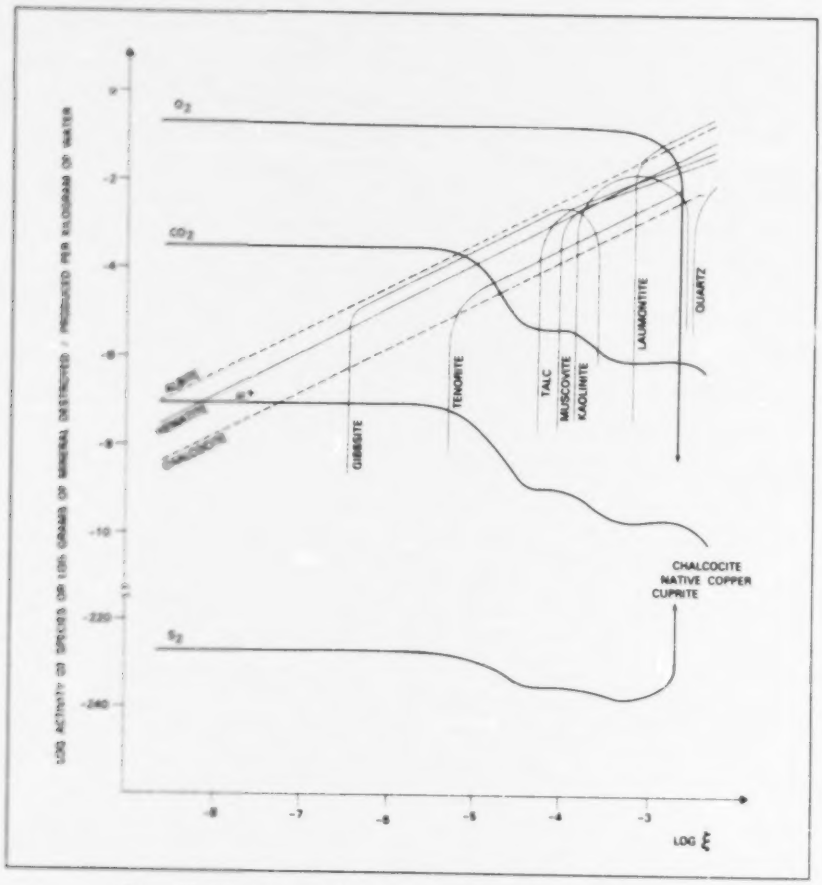

Figure 15. Changes in solution chemistry and the production and destruction of minerals as a result of rain water — rock interactions at 25°C and a pressure of 1 bar (east pit). ξ is the reaction progress variable discussed in the text.

been depleted of most of its dissolved oxygen due to reaction with incompatible minerals encountered in the wallrocks. Limited by the scale of the horizontal axis, the evolutionary paths of the copper-containing minerals cannot be plotted fully in Figures 15 to 17. Details of the sequential change will be described and discussed with respect to a later log f_{O_2} versus log f_{S_2} diagram (Figure 18).

Before leaving Figures 15 to 17, please note the difference in evolution patterns of the hydrogen ion activity in the cases illustrated. Because pH is defined as the negative logarithm of the activity of the hydrogen ion, if one reads the absolute value of the vertical axis, the H^+ variation curve depicts the variation in pH as the reaction progresses. Note that in Run 1 pH tends to increase throughout the process; Run 2, though alkaline throughout, shows a maximum pH value of about 9; and in Run 3 pH decreases, passes through the neutral point, then finally reverses its course after the saturation of chalcocite. As will be discussed following, these differences have a very strong effect on the extent of development of supergene enrichment. Lastly, note that none of the runs have been carried through to reach overall equilibrium. However, the curves shown establish trends that would be followed.

ENRICHMENT VERSUS NONENRICHMENT AND DOMINANCE OF A PARTICULAR PHASE

Figure 18 shows the paths of evolution of the reacting rain water over the stability fields in the iron-copper-sulphur-oxygen system, at 25 degrees Celsius and a pressure of 1 bar, for the three simulations described. Bornite is stable in a thin shell around the stability field of chalcopyrite, but is omitted from the diagram for clarity. The two parallel thick lines, designated by constant products of the activity of sulphate ion and the square of the activity of hydrogen ion, are approximations to the compositional "limits" of aqueous solutions commonly found in a supergene environment. They are derived as follows:

For the reaction,

$$2\,H^+ + SO_4 = {}^3/_2\,O_2 + {}^1/_2\,S_2 + H_2O$$

$$\log K = {}^3/_2 \log f_{O_2} + {}^1/_2 \log f_{S_2} + \log a_{H_2O} - 2 \log a_{H^+} - \log a_{SO_4} \quad (1)$$

where K = equilibrium constant of the reaction, and f_x, a_x = fugacity and activity of species x respectively. Also, log K is related to the equilibrium constant of formation, $K_{f,x}$, of individual species x involved in the reaction by

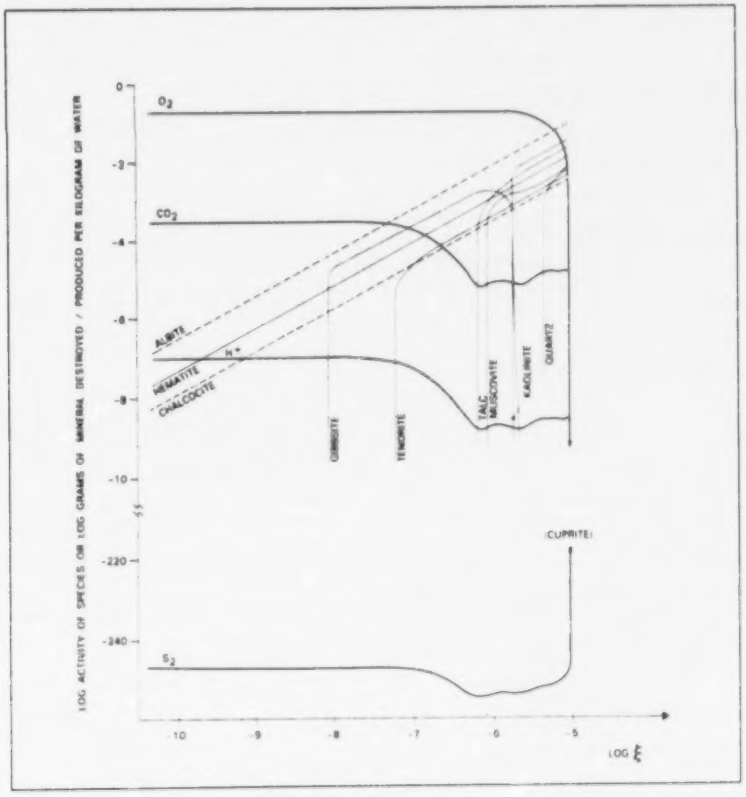

Figure 16. Changes in solution chemistry and the production and destruction of minerals as a result of rainwater — rock interactions at 25°C and a pressure of 1 bar (west pit). ξ is the reaction progress variable discussed in the text.

$$\log K = {}^3/_2 \log K_{f,O_2} + {}^1/_2 \log K_{f,S_2} + \log K_{f,H_2O} - 2 \log K_{f,H^+} - \log K_{f,SO_4} \quad (2)$$

Upon substitution of relevant data at 25 degrees Celsius and a pressure of 1 bar from Robie *et al.* (1978), the equation (2) gives

$$\log K = -95.87 \quad (3)$$

Substituting (3) in (1) and assuming that $a_{H_2O} = 1$, one gets

$${}^3/_2 \log f_{O_2} + {}^1/_2 \log f_{S_2} = -95.87 + 2 \log a_{H^+} + \log a_{SO_4} \quad (4)$$

Arbitrarily setting $a_{SO_4} = 1$, the upper boundary curve (A) corresponds to the case of an extremely acidic environment characterized by pH = 0,

that is, $a^2_{H^+} \cdot a_{SO_4} = (10^{-0})^2 \cdot 1 = 1$

which, upon substitution into equation (4), gives

$${}^3/_2 \log f_{O_2} + {}^1/_2 \log f_{S_2} = -95.87$$

and the lower boundary curve (B) depicts an extremely basic environment characterized by pH = 14,

that is, $a^2_{H^+} \cdot a_{SO_4} = (10^{-14})^2 \cdot 1 = 10^{-28}$

which, upon substitution into equation (4), gives

$${}^3/_2 \log f_{O_2} + {}^1/_2 \log f_{S_2} = -95.87 - 28 = -123.87$$

Strictly speaking, these "limiting" curves apply only to situations where sulphate ion is the dominant sulphur-containing species in solution. Under such conditions, the possible change in order of magnitude of the activity of sulphate ion is small compared to that of hydrogen ion. Consequently, the activity of sulphate ion is less important than pH in affecting the position and shape of the "limiting" curves.

Figure 19 shows that sulphate ion in fact dominates over other sulphur-containing species over a wide range of pH and f_{O_2} conditions at 25 degrees Celsius and 1 bar and thus accounts for the fact that most natural solutions plot within the "limiting" curves of Figure 18. Under extremely reducing conditions, that is, f_{O_2} less than about 10^{-70} and considerably higher at slightly elevated temperature, diminishing abundance of sulphate ion in solution would lead to a deflecion of the "limiting" curves toward lower f_{S_2} values in Figure 18.

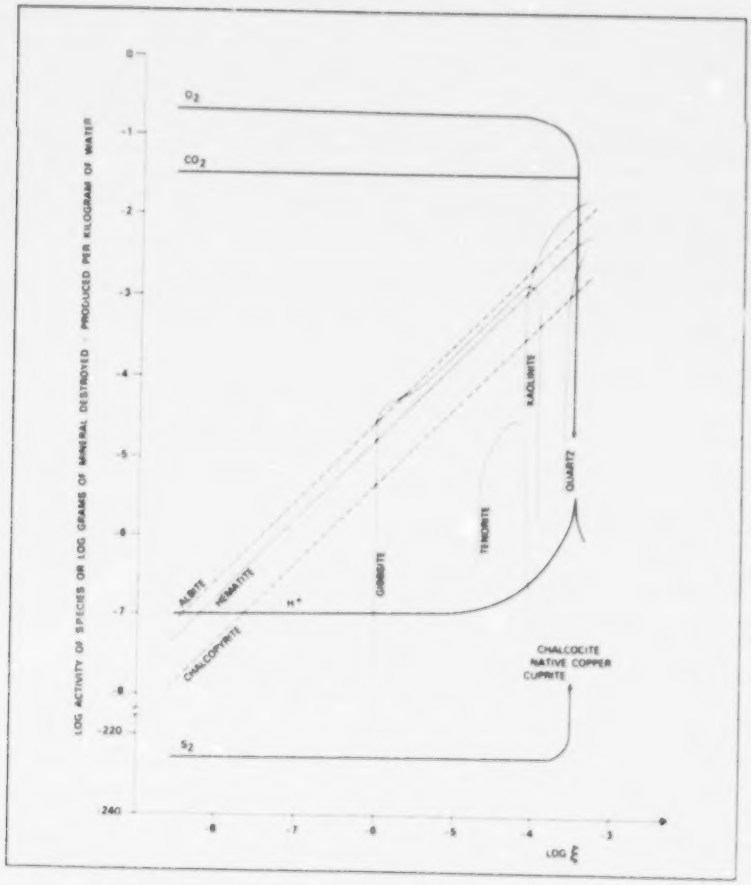

Figure 17 Changes in solution chemistry and the production and destruction of minerals as result of rainwater — hypothetical monzonite interactions at 25°C and a pressure of 1 bar. ξ is the reaction progress variable discussed in the text.

Lines labelled 1 to 3 in Figure 18 correspond to the evolutionary paths of rain water in the three simulation runs. Broken portions indicate that though, within the log f_{O_2} – log f_{S_2} framework, the composition of the solution plots in the stability field of the relevant solid copper phase, actual precipitation would not take place because the solution is not saturated with respect to the mineral concerned; copper still remains as appropriate ions in solution. In contrast to Run 3, initial water-rock interactions in both Run 1 and Run 2 lead to a decrease in sulphur fugacity in the liquid phase. Subsequent reaction paths in all three cases, however, are subparallel to the arbitrary boundary curves A and B; this parallelism reflects the controlling effect of pH on supergene alteration. The pH domain of the process is determined by reactions between the host rocks and percolating water. Because the hydrolysis of primary sulphide furnishes a ready source of hydrogen ion, it is valid to assume that the presence of primary sulphides controls the extent of supergene enrichment. This is readily brought out by comparing the results of the three runs.

Reactants in the three runs differ primarily in the proportion of sulphides and mafic minerals. In Run 1, the deficiency in pyrite and the relative abundance of mafic silicates result in a high and increasing pH along the calculated path. Tenorite is precipitated soon after hematite and in turn is succeeded by cuprite, native copper and chalcocite. Because a copper mineral is stable at each stage of the alteration, relatively little copper is held in solution; supergene enrichment is consequently suppressed. Run 2 shows a very similar behaviour except that the presence of more pyrite brings about slightly lower, though still basic values of pH; supergene enrichment is again negligible. In both these runs, early co-precipitation of tenorite with hematite would preclude extensive development of a copper-deficient leached capping. In Run 3, the hydrolysis effect of abundant sulphides outweighs that of mafic silicates. pH is acidic and decreases continually until chalcocite becomes stable with respect to the reacting water. A very minor amount of tenorite that is initially co-precipitated with hematite is quickly redissolved and copper is held in solution until the composition of the reacting solution plots well into the stability field of cuprite. Subsequently, the usual sequence of native copper and chalcocite follows. In this instance, supergene enrichment is first evident at the cuprite zone which should be overlain by a

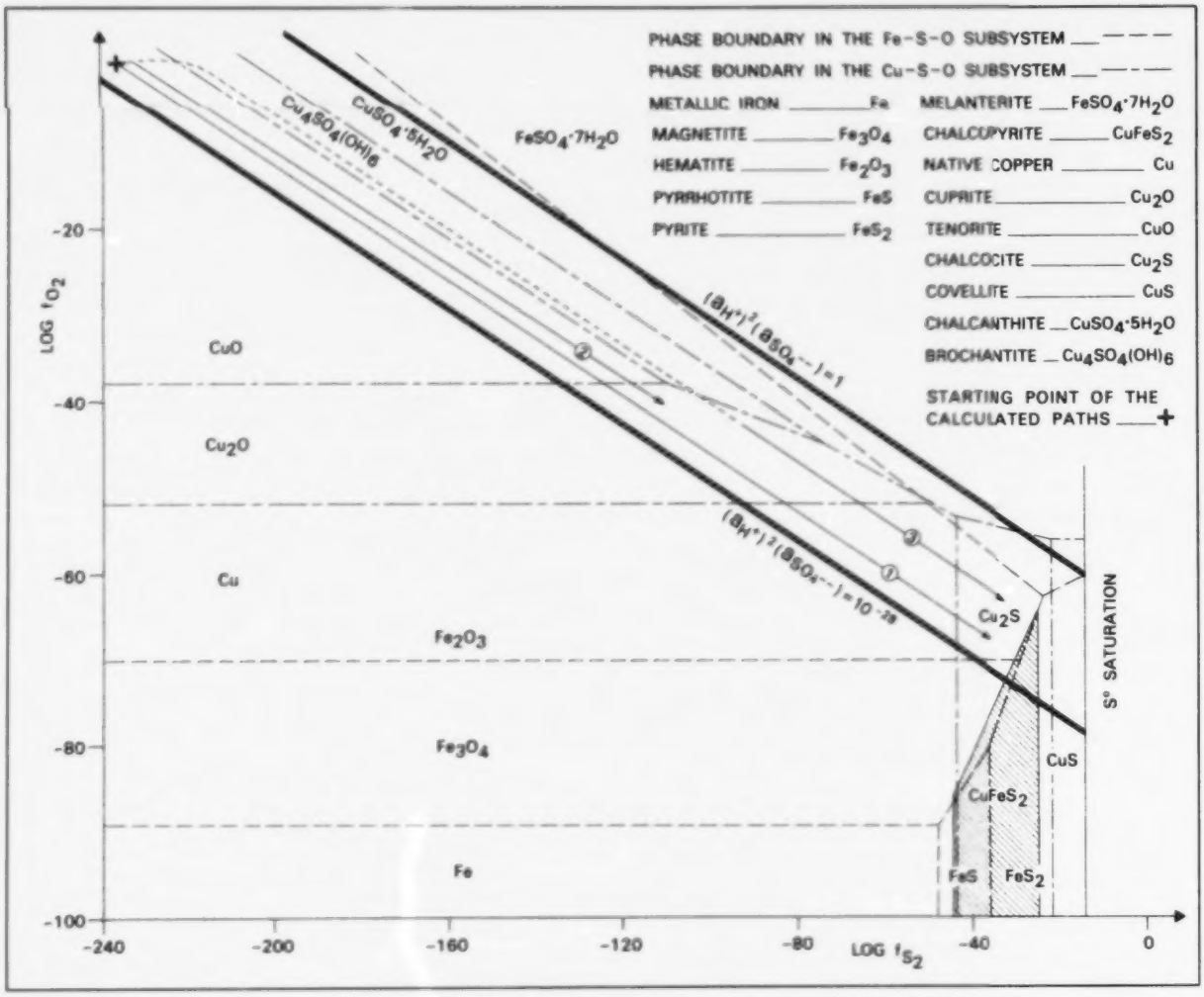

Figure 18. The evolutionary paths of the reacting solutions for the three simulation runs over the stability fields of minerals in the Cu-Fe-S-O system at 25°C and a pressure of 1 bar. Phase boundaries in the Fe-S-O and Cu-S-O subsystems are depicted in broken lines and broken lines with dots, respectively. The chalcopyrite stability field is shaded. The two parallel thick lines are approximations to the compositional "limits" of aqueous solutions commonly found in a supergene environment. *See* text for detailed discussion.

well-developed leached cap characterized by abundant hematite and/or limonite.

The reaction path of Run 1 also differs from that of Run 3 in another aspect; it crosses the stability field of native copper over a much greater range of f_{O_2} and f_{S_2} than the latter. This implies that Run 1 would be characterized by a greater abundance of native copper, with the consequently reduced chance that it would be completely replaced by later chalcocite. This is the prime reason for the preponderance of native copper and the lack of supergene enrichment at Afton mine. The situation with Run 2 is intermediate between Runs 1 and 3 but a little closer to the former. Staying in the native copper stability field for a much shorter interval, the reacting solution in Run 2, in comparison to that of Run 1, is more readily brought into equilibrium with the copper sulphides. Recalling that the reactants used in Runs 1 and 2 represent primary mineralogy of the two portions of the open pit (Table 3A), the simulation results explain why native copper is more widespread in the eastern portion of the open pit than in the western part, where locally some primary sulphides are preserved intact.

The dominance of native copper at Afton mine could also have been enhanced by penetration of the rain water along deep fractures where the ambient temperature was in excess of 25 degrees Celsius. As briefly mentioned previously, higher temperature diminishes the stability field of SO_4 and deflects the "limiting" curves in Figure 18 toward lower values of f_{S_2} at the same f_{O_2}. Evolution of the reaction paths of solutions in Runs 1 and 2 parallel to the lower "limiting" curve would then follow a lengthened path in the stability field of native copper (because the reaction paths are deflected into it). Consequently, more native copper would be produced in the process.

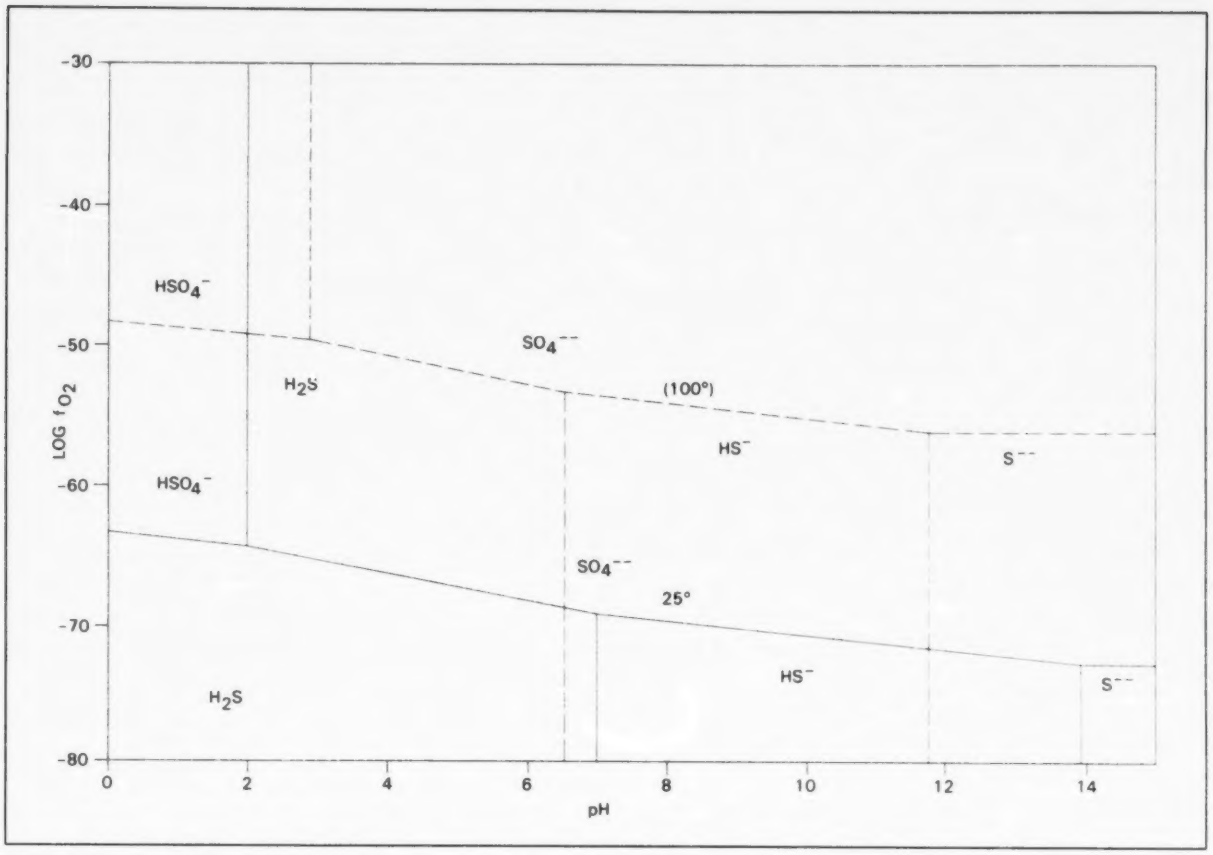

Figure 19. Distribution of sulphur species at 25°C (phase boundaries depicted in solid lines) and 100°C (phase boundaries depicted in broken lines) as a function of oxygen fugacity, f_{O_2}, and solution pH. Thermodynamic data used in the construction of the diagram are from Helgeson, 1969.

In the case of the El Salvador porphyry copper deposit in Chile (Gustafson and Hunt, 1979), the reaction path of the downward percolating water probably plots close to the upper "limiting" curve, so the stability field of native copper is bypassed altogether. Precipitation of abundant limonite and jarosite in the leached cap probably hinders the separation of chalcanthite and melanterite. Copper is kept in solution until the stability field of chalcocite is encountered, leading to the formation of an enriched blanket of supergene ore. Moreover, since the projected reaction path misses both the bornite and chalcopyrite stability field, but passes through that of pyrite, it explains why at appropriate levels of the deposit, supergene sulphides replace bornite and chalcopyrite but leave pyrite intact. Such a textural relationship is not prominent at Afton mine.

DISCREPANCIES BETWEEN THEORETICAL AND OBSERVED MINERAL ASSEMBLAGES

Figure 20 summarizes the paragenesis of product minerals resulting from the water-rock interaction calculations depicted in Figures 15 to 17. The theoretical mineral assemblage closely associated with supergene native copper and chalcocite is expected to be composed of talc, muscovite, kaolinite, hematite, quartz ± laumontite. However, the actual minerals observed are specularite, earthy hematite, limonite, iron-chlorite, quartz, carbonates, and a poorly crystalline mixed-layer illite-montmorillonite swelling clay. A minor amount of kaolinite is observed in the western portion of the open pit but is only associated with chalcocite. Talc is suspected in several specimens. Small amounts of zeolites like ferrierite and clinoptilolite have been identified in late fractures in some potash-rich wallrocks and in the Tertiary rocks overlying the orebody; they are considered to be post-ore alteration products.

The discrepancies between the theoretical and observed supergene mineral assemblages are easily explained. In the first place, thermodynamic calculations predict an equilibrium mineral assemblage under specified physical conditions by considering all relevant mineral species present in the data file. They are incapable of predicting any phases which are not included. Due to the lack of thermodynamic data, many species such as iron-chlorite, amorphous clays, and hydrated iron oxides are not considered in the calculations. The predicted assemblage of talc, kaolinite, laumontite, and some hematite, therefore can be interpreted to occur in the real situation as iron-chlorite and montmorillonite. In

the second place, kinetic effects are not accounted for by this thermodynamic model. Commonly, clay minerals precipitating from a solution under low temperature and pressure conditions are amorphous. Thus the predicted muscovite is probably the illite component of the mixed-layer clay, and hematite is manifested as hydrous and anhydrous ferric oxides. The association of well-crystallized specularite with euhedral native copper crystals observed locally at Afton mine, on the other hand, suggests that at some stage of the supergene event, the prevailing temperature was a little higher than 25 degrees Celsius. In the third place, all calculations presented here assume a closed system. At Afton mine, the detailed host rock lithology changes rapidly over a short distance and the highly fractured nature of these rocks introduces much of the reacting water to several mineralogic environments.

Complications brought about by the relaxation of closed system conditions can be illustrated with the results of short exploratory calculations of interactions between the seepage water at the northwest pit wall and the average mineral assemblage of the eastern portion of the pit. Table 4 outlines the composition of the seepage water as furnished by Afton mine in the spring of 1979. After conversion to appropriate units, variables marked with asterisks were applied to the calculations. The missing sodium and potassium data were estimated by assuming a sodium:potassium ratio of 2:1, roughly accounting for the abundance of syenitic rocks in the vicinity, and maintaining at the same time electric neutrality among the major dissolved components. As in Run 1 the required Al^{+++} and H_4SiO_4 components were assigned small arbitrary values. Calculations of initial distribution of species indicated that the water is saturated with respect to dolomite, hematite, and tenorite. This finding was expected because the seepage was collected in an area showing pervasive ankerite alteration. In order to enable the mass transfer calculation to proceed, the independent variables CO_2, Fe^{++}, and Cu^{+} were assumed to be constrained by dolomite, hematite, and tenorite respectively.

Salient results of the spontaneous reactions calculated include the continual separation of dolomite, hematite, and tenorite, and the sequential precipitation of gibbsite and muscovite, followed by an early stabilization of potassium feldspar and phlogopite prior to the monotonic depletion of dissolved oxygen in the reacting solution. If, in accordance with the field observation that calcite is the preferred supergene alteration product, dolomite is suppressed in the calculations, then calcite takes the place of dolomite and the stabilization of phlogopite precedes that of muscovite. Thus an explanation is obtained for the inclusion of carbonates in the actual supergene mineral assemblage and for the localized persistence of biotite in areas having abundant native copper. Since nothing is drastically different from the results of previous runs and the pH throughout the reactions in both exploratory runs has been buffered to a value of slightly greater than 8, no supergene enrichment is to be expected. The projected evolutionary paths of the reacting water of these runs, if plotted in Figure 18, would lie parallel and close to the right of Run 2.

Incidentally, at Afton mine, no discrete intense zones of tenorite or cuprite mineralization exist. Erosion prior to the deposition of the protective Eocene strata is the most likely explanation for their absence.

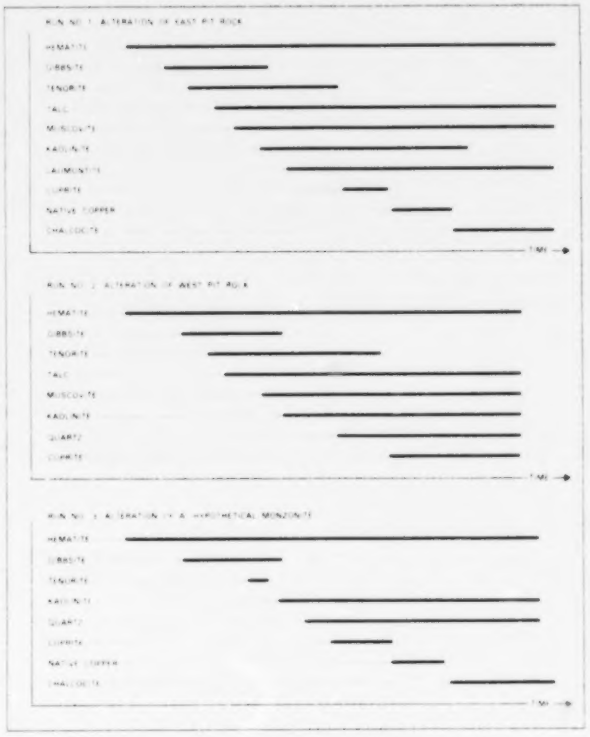

Figure 20. Paragenesis of product minerals resulting from the water-rock interaction calculations.

OTHER CONSIDERATIONS

So far, discussions have been focused on the chemical aspects of supergene alteration, with little attention paid to the physical parameters of porosity and permeability of the host rocks, the depth of the prevalent water table, and climatic conditions accompanying the alteration. Briefly, these parameters affect the rock-to-fluid ratio, which in turn controls the extent of reaction described previously. The case of an extremely low rock-to-fluid ratio, such that wallrock mineralogy fails to affect the chemistry of the reacting solution to any significant extent, is not a viable option here. Other than that, a low ratio of rock to fluid could, if given enough time for reactions to fully proceed, lead to complete destruction of the primary mineral assemblage. In contrast, a high ratio of rock to fluid would result in a ready equilibration of the reacting solution with the wallrock, resulting in preservation of primary sulphides within the supergene zone. In column adsorption chromatography, given identical conditions, a longer column generally facilitates better separation of components. By analogy, the depth of the prevalent water table, coupled with other physical parameters, affects the extent of development of a leached cap, determines whether there is a well-defined succession of secondary copper min-

TABLE 4.
COMPOSITION OF NORTHWEST PIT WALL SEEPAGE WATER
March 14, 1979
(Courtesy of Afton Mines Ltd.)

Physical Parameters		
Field:	Temperature (°C)	11.0*
	pH	8.4*
	Dissolved Oxygen (ppm)	5.6*
	Conductivity (μmhos/cm)	5375
Lab:	pH	8.39
	Turbidity (JTU)	0.3
	Total Suspended Solids (ppm)	1

Major Dissolved Components (ppm)		
Hardness	$CaCO_3$	221* (treated as HCO_3^-)
Calcium	Ca	27.5*
Magnesium	Mg	37.0*
Sodium	Na	—
Potassium	K	—
Sulphate	SO_4^{--}	2380*
Fluoride	F^-	0.64

Metals (ppm):		Dissolved	Total
Arsenic	As	<0.005	<0.005
Copper	Cu	0.002*	0.007
Lead	Pb	0.002	0.005
Mercury	Hg	—	<0.0005
Zinc	Zn	0.002	0.022
Iron	Fe	0.007*	0.034
Molybdenum	Mo	—	—

* Values used in the calculation of interactions with east pit rock.

erals, and determines whether telescoping of alteration mineralogy occurs. The supergene alteration at Afton probably took place along deep fractures characterized by a moderately high ratio of rock to solution, with the consequence that hypogene copper sulphides are locally important in the supergene zone.

SUMMARY AND CONCLUSIONS

In applying the thermodynamic approach to understanding the supergene alteration at Afton mine, although it has not been possible to reproduce the deposition sequence of secondary silicate minerals due to the lack of relevant thermodynamic data, constraints in reaction kinetics and limitations of closed system calculations, valid conclusions regarding the sequential changes in mineralogy in the copper-iron-sulphur-oxygen system can be drawn. The presence of an overwhelming amount of native copper and the lack of supergene enrichment are caused by the combined effect of the relatively mafic composition of the host rocks and the low sulphide content of the hypogene mineral assemblage. As a result, water-rock interactions during the supergene event are constrained to occur within an alkaline pH domain. Supergene alteration of porphyry copper deposits in general can conveniently be interpreted in the framework of a log f_{O_2} – log f_{S_2} plot with respect to two arbitrary "limiting" curves, which are characterized by extreme values of acidic and basic pH respectively. The closer the reacting fluid approaches the upper or acidic limiting curve, the more likely is the formation of a well-developed leached cap with an enriched supergene ore blanket below. In contrast, a reacting fluid evolving close to the lower or basic limiting curve would result in formation of a spectrum of supergene copper oxides and native copper, but little supergene enrichment.

CHAPTER 6

ASSESSING THE MINERAL POTENTIAL OF THE IRON MASK BATHOLITH

COMMODITIES OF INTEREST

The Afton mine dominates metal production from the Iron Mask batholith. Production[1] to the end of 1985 includes 135 900 tonnes of copper, 7714 kilograms of gold, and 30 270 kilograms of silver[2]. Table 5 lists the metal production of previous small-scale mining operations. Figure 21 compares the count of commodities sought among the 66 mineral properties recorded in the MINFILE database of the British Columbia Ministry of Energy, Mines and Petroleum Resources. From these data, it is evident that copper, gold, and silver have always been of great interest while iron and salt deposits have also played a small role in attracting exploration activities to the area. The recent depressed price of copper has accentuated the importance of gold and silver and stimulated new investigations of their distribution (for example, Stewart, 1984). During the course of this study, selected samples from the various phases of the batholith have also been analysed for other precious metals. Detectable amounts of palladium (Pd) were noted in most samples analysed (Table 6). Palladium is an attractive byproduct metal if it can be effectively recovered from the mining of prime target metals like copper and gold.

TABLE 5.
METAL PRODUCTION FROM THE IRON MASK BATHOLITH
PRIOR TO 1970
(Data are from National Mineral Inventory Cards unless indicated otherwise.)

Property Name	Production			
	Tonnage Processed	Metals Extracted (kg)		
	(in tonnes)	Cu	Ag	Au
Iron Mask and Erin	1.66×10^5	2.45×10^6	4.66×10^2	1.22×10^2
Galaxy Copper	48.08	2.55×10^3	0.93	—
Python	27.22	2.18×10^3	—	—
Larsen	29.94	2.90×10^3	0.84	0.26
Iron Cap	2.39×10^2	4.80×10^3	13.95	6.72
Pothook	9.07	4.35×10^2	0.16	0.03
Maxime	29.94	3.04×10^3	1.19	0.03
Copper King*		1.78×10^5	61.8	33.5
Magnet	3.68×10^3 (crude iron)			
Glen Iron*	13.6×10^3 (magnetite)			
Total	17.28×10^3 (crude iron)	2.644×10^6	544.87	162.54

* Data from Cockfield, 1948.
[1] Data source: Canadian Mines Handbook, 1979–1986.
[2] The 1985 silver production figure, which was unavailable at the time of printing, is not included.

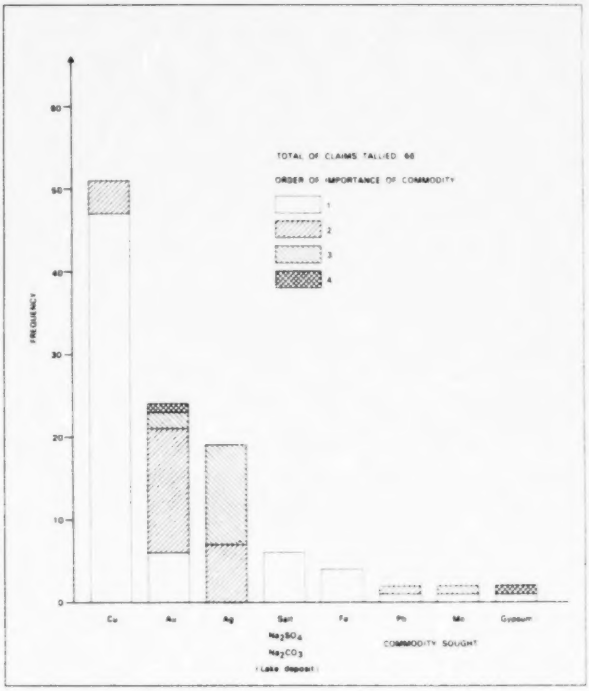

Figure 21. Commodities of interest in mineral claims of the Iron Mask batholith.

With the exception of the Afton deposit, most copper and/or precious metal(s) occurrences in the area are low grade and subeconomic for exploitation by conventional mining methods. However, the ubiquitous presence of mineralization throughout the batholith suggests that the total tonnage could be significant. The production potential of these metals could be greatly enhanced if an efficient, low-cost recovery method could be devised. Heap leaching is one of the methods that offers potential. The semi-arid climate is suitable for open-air facilities for most of the year. The extent of supergene alteration observed in Afton mine suggests that thick deposits of oxidized rocks could be locally preserved. Such oxidized material is particularly amenable to leaching. Leaching techniques for gold, silver, and copper, though not for palladium, have been fairly well established.

Whereas more research is required to test the feasibility of applying these techniques to rocks of the Iron Mask batholith

TABLE 6.
PRECIOUS METALS CONTENT OF SELECTED SAMPLES FROM THE IRON MASK BATHOLITH BY EMISSION SPECTROGRAPHIC ANALYSIS

Sample Number	Brief Description[1]	Precious Metals[2] in ppm Au	Pt	Pd
A. Mineralized and/or altered samples from Afton				
GWA-42	Microdiorite	0.34	N.D.	0.15
GWA-128	Microdiorite	0.34	N.D.	0.15
GWA-147	Quartz-carbonate alteration	0.10	N.D.	0.10
GWA-171	Fine-grained diorite	0.27	N.D.	0.34
PC-1	Picrite	N.D.	N.D.	0.10
B. Barren batholithic rocks				
74KN-27	Cherry Creek microdiorite	≤0.10	≤0.10	0.10
74KN-84 II	Cherry Creek fine-grained diorite	≤0.10	N.D.	0.10
74KN-84 III	Sugarloaf gabbro	N.D.	N.D.	0.10
76IM-131 I	Sugarloaf intrusive breccia	N.D.	N.D.	0.10
76IM-133 IV	Sugarloaf diorite	N.D.	N.D.	0.10
74KN-125	Picrite basalt	≤0.10	N.D.	0.10
74KN-135	Picrite basalt	0.10	N.D.	0.10
74KN-140A	Pothook gabbro	≤0.10	N.D.	0.10
74KN-180	Iron Mask Hybrid gabbro	N.D.	N.D.	0.10
74KN-189	Iron Mask Hybrid leucogabbro	N.D.	≤0.10	≤0.10

[1] See Appendix I for more detailed description.

[2] Rh, Ir, Os were also analysed but not detected in these samples.

and their extrusive equivalents, it is nevertheless worthwhile to consider the possibility while assessing the exploration potential of the area, particularly where semi-oxidized to oxidized materials are encountered.

INDICATORS OF MINERALIZATION

A brief review of the geology of mineralized zones[1] (ranging from major deposits like Afton to scattered minor occurrences) in the Iron Mask batholith indicates that the controlling features of mineralization are invariably structural. These structural features include shear zones along intrusive contacts, brecciated zones within an intrusive phase, intersections of fault zones, oxidation and/or unconformity exposures. The localization of mineralization along these permeable zones reflects the prominance of hydrothermal and/or hydrologic processes in the final concentration of ore elements, regardless of their origin. Exploration in the batholith can be made easier if signatures of the associated alteration are recognized. Various indicators of mineralization are thus assessed in the light of the new findings of this study as follows:

[1] See Appendix III for selected examples.

(1) **Hypogene mineralization** – Geological phenomena that have been observed associated with hypogene mineralization include:

(i) Albitization (Carr, 1956 and Preto, 1967),

(ii) Potassium feldspathization (Northcote, 1974, 1976, and 1977),

(iii) Carbonate alteration (this study),

(iv) Propylitization (Preto, 1967 and Hoiles, 1978), and

(v) Association with rocks of the Picrite unit (Carr, 1956 and Carr and Reed, 1976).

These factors are not necessarily mutually exclusive and are consequently discussed together.

Both albitization and potassium feldspathization occur in two forms, namely pervasive alteration that tends to flood the matrix of porphyritic rocks, and discrete veins with or without associated sulphides. As a whole, pervasive alteration is much more abundant than veining. Because of the ubiquitous presence of secondary iron oxide, the two feldspars are not easily distinguished in unstained specimens. However, in contrast to albitization, pervasive potassium feldspar alteration does not usually affect feldspar phenocrysts and potassium feldspar veins are frequently enveloped by chlorite. Pervasive feldspathization probably results from changes in magmatic composition in the final stages of differentiation, while feldspar veins are undoubtedly of hydrothermal origin. In itself, the feldspar alteration is not an infallible indicator of mineralization, but it offers a recognizable target for exploration. Within the affected area, an associated mineral that may indicate mineralization is fine-grained brownish hydrothermal biotite, which is associated with the hypogene mineralization at Afton and is readily distinguished from coarser grained greenish biotite in barren rocks. Limited microprobe analyses indicate that the brown hydrothermal biotite is particularly titaniferous. Whereas more data are required to substantiate the hypothesis, it appears that chlorite associated with copper mineralization is characterized by a higher magnesium to iron ratio than that in barren rocks. Thus these two phyllosilicates are impoverished in iron where they accompany sulphides.

Like the feldspar alteration, carbonate alteration can be pervasive or vein forming. Depending on the original composition of the altered rocks, pervasive carbonatization is either dolomitic or ankeritic. It was contemporaneous with or slightly later than the pervasive feldspar alteration. Carbonate veining, which postdated the pervasive alteration and recurred several times, becomes more calcitic with time. In the area of the batholith, the carbonate alteration is rarely coincident with sulphide mineralization; it reflects only a hydrothermal process that involved magmatic fluids. At Afton, however, tennantite appears to be preferentially associated with carbonate-altered rocks and may be responsible for some localization of precious metals.

Despite the fact that pyrite-chalcopyrite-calcite veins are occasionally found in rocks affected by propylitization, the alteration is not a good exploration target because of its ubiquitous occurrence. Propylitization generally postdated the feldspar and carbonate alterations and resulted in a mineral assemblage practically indistinguishable from that

TABLE 7.
COPPER AND GOLD CONTENTS OF A SUITE OF SAMPLES FROM THE JOKER CLAIM: A SYSTEMATIC CHIP-SAMPLING OF A SMALL PORTION OF THE WEST SIDE OF A GULLY ALONG ANDERSON CREEK

Field Number	*Brief Description*	Cu (%)	Au (ppm)
Joker-1	Up to 6 metres of massive, though slightly fractured, microdiorite; trace malachite along fractures near the bottom of the unit	0.01	0.3
Joker-2	0–1 metre of brecciated microdiorite(?) with prominent reddish ochreous alteration	0.27	1.7
Joker-3	3–5 metres of friable microdiorite with prominent malachite stain	1.63	1.5
Joker-4	About 50 metres downstream; same horizon as Joker 3; heavy malachite stain, overlying rock and loose material bleached white	6.96	7.4
Joker-5	Grab float sample from the floor of the gully: microdiorite breccia with prominent hematite, native copper, goethite, siderite, and minor malachite	5.75	3.8

produced by regional metamorphism which is especially evident in the surrounding Nicola Group volcanic rocks. Prominent sulphide mineralization associated with propylitization appears to be limited to the contact zones of the intrusive and extrusive rocks.

Inasmuch as wallrocks act as proton sinks during hydrothermal alteration, the presence of picrite, particularly if fractured to enhance the reacting surface area, is important in the mineralization process. This is because its interaction with a hydrothermal solution is capable of bringing about a rapid increase in pH which would cause sulphide precipitation. In fact, picrite bodies, though not well exposed, are generally found within 300 metres of most prospects in the district (Carr and Reed, 1976). The controlling factor then is whether or not the hydrothermal solution that came into contact with picritic rocks was ore bearing. Similarily, highly mafic country rocks, like some of the Nicola volcanic rocks around the southeastern end of the Iron Mask batholith, are also effective in causing sulphide precipitation if they come into contact with an ore-bearing solution.

(2) **Supergene alteration** – From the detailed analysis of supergene alteration at Afton, it can be inferred that a barren leached cap is unlikely to develop in oxidized material of the Iron Mask batholith, which is more mafic relative to most copper-bearing calc-alkaline intrusions. Supergene mineralization, if present, should be found close to the oxidation surface. If chemical weathering has gone on for a long time, the stable products are native copper and hematite with or without cuprite and siderite. Incipient oxidation observed in many parts of the batholith is indicated by malachite associated with remnant chalcopyrite and bornite. Deep oxidation profiles of batholithic rocks are readily distinguished from barren Tertiary rocks by the characteristic presence of red ochreous alteration resulting from oxidation of the ubiquitous magnetite. However, the reddish coloration is sometimes so intense that it makes recognition of native copper and cuprite difficult.

As a consequence of complex, postbatholithic deformations affecting the area, buried ore-bearing oxidation profiles are a distinct possibility that should be considered. Table 7 shows the analyses of chip samples collected from a gully along Anderson Creek on the Joker claim, located about 1.3 kilometres southwest of Separation Lake. Here about 6 metres of friable, oxidized microdiorite, with anomalous copper and gold, is partially overlain by up to 6 metres of relatively fresh and massive Cherry Creek diorite. In explaining the repeated occurrence of supergene mineralization in a portion of the Afton orebody, Preto (1972) suggested that landslides occurred. Whereas more detailed mapping is needed here to interpret the structure involved, mineralization can easily be missed if studies are confined to outcrops alone. Geochemical sampling of stream sediments and along abandoned natural drainage systems may be fruitful in locating shallowly buried oxidized ore in the batholith.

SUMMARY AND CONCLUSIONS

While copper, gold and silver remain the main commodities mined and sought in the Iron Mask batholith, palladium is a potential byproduct metal that could be developed with proper extraction techniques. In addition to relatively high-grade mineable deposits like the Afton orebody, widespread but localized concentrations of these metals might be amenable to recovery by heap leaching. Indicators of mineralization to aid exploration in the batholith are intense potassium feldspathization, albitization, and carbonatization; these reflect concentrated hydrothermal activity that might, in some stages involve ore formation. Moreover, picrite bodies, especially if fractured, are effective in causing sulphide precipitation if they interact with ore-bearing solutions. For supergene ore, oxidized rocks exhibiting red ochreous alteration or intense malachite staining deserve careful examination. To explore for shallowly buried mineralization, geochemical sampling of stream sediments and old drainage systems is recommended. Taking the overall geological environment into consideration, it is concluded that the southeastern end of the Iron Mask pluton is a prime exploration target for another Afton-type deposit.

BIBLIOGRAPHY

Barr, D.A., Fox, P.E., Northcote, K.E., and Preto, V.A. (1976): The Alkaline Suite Porphyry Deposits — A Summary; *in* Porphyry Deposits of the Canadian Cordillera, A. Sutherland Brown, editor, *Canadian Institute of Mining and Metallurgy*, Special Vol. 15, pp. 359–367.

Bence, A.E. and Albee, A.L. (1968): Empirical correction factors for the electron microanalysis of silicates and oxides, *Analytical Chemistry*, Vol. 76, pp. 382–403.

Beus, A.A. and Grigorian, S.V. (1977): Geochemical Exploration Methods for Mineral Deposits, *Applied Publishing Ltd.*, Wilmetti, Illinois, 287 pp.

Bowen, N.L. (1928): The Evolution of the Igneous Rocks, *Princeton University Press*, Princeton, N.J.

Brimhall, G.H., Jr. (1980): Deep Hypogene Oxidation of Porphyry Copper Potassium-silicate Protore at Butte, Montana: A Theoretical Evaluation of Copper Remobilization Hypothesis, *Economic Geology*, Vol. 75, pp. 384–409.

Campbell, R.B. and Tipper, H.W. (1970): Geology and Mineral Exploration Potential of the Quesnel Trough, British Columbia, *Canadian Institute of Mining and Metallurgy*, Bull., Vol. 63, No. 699, pp. 785–790.

Cann, R.M. (1979): Geochemistry of Magnetite and the Genesis of Magnetite-apatite Lodes in the Iron Mask Batholith, B.C., unpub. M.Sc. thesis, *The University of British Columbia*, 196 pp.

Carr, J.M. (1956): (Copper) Deposits Associated with the Eastern Part of the Iron Mask Batholith near Kamloops, *Minister of Mines, B.C.*, Ann. Rept., 1956, pp. 47–69.

Carr, J.M. and Reed A.J. (1976): Afton: A Supergene Copper Deposit, *in* Porphyry Deposits of the Canadian Cordillera, A. Sutherland Brown, editor, *Canadian Institute of Mining and Metallurgy*, Special Vol. 15, pp. 376–387.

Cockfield W.E. (1948): Geology and Mineral Deposits of Nicola Map Area, British Columbia, *Geological Survey of Canada*, Mem. 249.

Ernst, W.G. (1976): Petrologic Phase Equilibria, *W.H. Freeman & Co.*, San Francisco, 333 pp.

Ewing, T. (1982): Geology of the Kamloops Group near Kamloops, Preliminary Map No. 48 and accompanying notes, *B.C. Ministry of Energy, Mines and Petroleum Resources*, 19 pp.

Gustafson, L.B. and Hunt, J.P. (1975): The Porphyry Copper Deposit at El Salvador, Chile, *Economic Geology*, Vol. 70, pp. 857-912.

Haughton, D.R., Roeder, P.L., and Skinner, B.J. (1974): Solubility of Sulfur in Mafic Magmas, *Economic Geology*, Vol. 69, pp. 451–467.

Helgeson, H.C. (1968): Evaluation of Irreversible Reactions *in* Geochemical Processes Involving Minerals and Aqueous Solutions — I. Thermodynamic Relations, *Geochimica et Cosmochimica Acta*, Vol. 32, pp. 853–877.

_____ (1969): Thermodynamics of Hydrothermal Systems at Elevated Temperatures and Pressures, *American Journal of Science*, Vol. 267, pp. 729–804.

_____ (1970): A Chemical and Thermodynamic Model of Ore Deposition in Hydrothermal Systems, *Mineralogical Society of America*, Special Paper 3, pp. 155–186.

_____ (1971): Kinetics of Mass Transfer Among Silicates and Aqueous Solutions, *Geochimica et Cosmochimica Acta*, Vol. 35, pp. 421–469.

_____ (1979): Mass Transfer Among Minerals and Hydrothermal Solutions, *in* Geochemistry of Hydrothermal Ore Deposits, H.L. Barnes, editor, *John Wiley & Sons, Inc.*, pp. 568–610.

Helgeson, H.C., Garrels, R.M., and MacKenzie, F.T. (1969): Evaluation of Irreversible Reactions in Geochemical Processes Involving Minerals and Aqueous Solutions — II. Applications, *Geochimica et Cosmochimica Acta*, Vol. 33, pp. 455–481.

Helgeson H.C., Brown, T.H., Nigrini, A., and Jones, T.A. (1971): Calculation of Mass Transfer in Geochemical Processes Involving Aqueous Solutions, *Geochimica et Cosmochimica Acta*, Vol. 34, pp. 569–592.

Hoiles, H.K. (1978): Nature and Genesis of the Afton Copper Deposit, Kamloops, British Columbia, unpub. M.Sc. thesis, *University of Alberta*, 186 pp.

Hollister, V.F. (1978): Geology of the Porphyry Copper Deposits of the Western Hemisphere, *American Institute of Mining, Metallurgy and Petroleum Engineering Inc.*, New York, 219 pp.

Kwong, Y.T.J. (1982): A New Look at the Afton Copper Mine in the Light of Mineral Distributions, Host Rock Geochemistry and Irreversible Mineral-solution Interactions, unpub. Ph.D. thesis, *The University of British Columbia*, 121 pp.

Kwong, Y.T.J., Greenwood, H.J., and Brown, T.H. (1982): A Thermodynamic Approach to the Understanding of the Supergene Alteration at the Afton Copper Mine, South-central British Columbia, *Canadian Journal of Earth Science*, Vol. 19, pp. 2378–2386.

Korenbaum, S.A. (1970): Fiziko-khimicheskie Usloviya Kristallizatsii Mineralov Volframa i Molybdena v Gidrotermalnykh Sredakh. Moscow: Izdat. Nauka.

Landergren, S. and Manhein, F.T. (1978): Molybdenum, *in* Handbook of Geochemistry, K.E. Wedepohl, editor, *Handbook of Geochemistry*, Vol. II/4, pp. 42 B-0.

Lowell, J.D. and Guilbert, J.M. (1970): Lateral and Vertical Alteration-mineralization Zoning in Porphyry Ore Deposits, *Economic Geology*, Vol. 65, pp. 373–408.

MacDonald, G.A. (1968): Composition and Origin of Hawaiian Lavas, *Geological Society of America*, Mem. 116, pp. 477–522.

McMillan, W.J. and Panteleyev, A. (1980): Ore Deposit Models — 1. Porphyry Copper Deposits, *Geoscience Canada*, Vol. 7, pp. 52–63.

Monger, J.W.H. and McMillan, W.J. (1984): Bedrock Geology of Ashcroft (92I) Map Area, *Geological Survey of Canada*, Open File 980.

Muan, A. and Osborn, E.F. (1956): Phase Equilibria at Liquidus Temperatures in the System MgO-FeO-Fe_2O_3-SiO_2, *Journal of American Ceramics Society*, Vol. 39, pp. 121–140.

Nathan, H.D. and Van Kirk, C.K. (1978): A Model of Magmatic Crystallization, *Journal of Petrology*, Vol. 19, pp. 66–94.

Ney, C.S., Cathro, R.J., Panteleyev, A., and Rotherham, D.C. (1976): Supergene Copper Mineralization, *in* Porphyry Deposits of the Canadian Cordillera, A. Sutherland Brown, editor, *Canadian Institute of Mining and Metallurgy*, Special Vol. 15, pp. 72–78.

Northcote, K.E. (1974): Geology of the Northwest Half of the Iron Mask Batholith, *in* Geological Fieldwork, 1974, Paper 1975-1, *B.C. Ministry of Energy, Mines and Petroleum Resources*, pp. 22–26.

_____ (1976): Geology of the Southeast Half of the Iron Mask Batholith, *in* Geological Fieldwork, 1976, Paper 1977-1, *B.C. Ministry of Energy, Mines and Petroleum Resources*, pp. 41–46.

_____ (1977): Preliminary Map No. 26 (Iron Mask Batholith) and accompanying notes, *B.C. Ministry of Energy, Mines and Petroleum Resources*, 8 pp.

Perkins, E.H. (1980): A Reinvestigation of the Theoretical Basis for the Calculation of Isothermal-isobaric Mass Transfer in Geochemical Systems Involving an Aqueous Phase, unpub. M.Sc. thesis, *The University of British Columbia*.

Philpotts, A.R. (1967): Origin of Certain Iron-titanium Oxide and Apatite Rocks, *Economic Geology*, Vol. 62, pp. 303–315.

Preto, V.A. (1967): Geology of the Eastern Part of the Iron Mask Batholith, *Minister of Mines, B.C.*, Annual Report, 1967, pp. 137–147.

_____ (1972): Report on Afton, Pothook, *B.C. Ministry of Energy, Mines and Petroleum Resources*, GEM, 1972, pp. 209–220.

_____ (1979): Geology of the Nicola Group Between Merritt and Princeton, *B.C. Ministry of Energy, Mines and Petroleum Resources*, Bull. 69, 90 pp.

Preto, V.A., Osatenko, M.J., McMillan, W.J., and Armstrong, R.L. (1979): Isotopic Dates and Strontium Isotopic Ratios for Plutonic and Volcanic Rocks in the Quesnel Trough and Nicola Belt, South-central B.C., *Canadian Journal of Earth Science*, Vol. 16, pp. 1658–1672.

Ralph, P.F. and Chaudhry, M.A. (in prep.): Accurate Routine Analysis of Geological Samples Using Atomic Absorption Flame Spectrophotometry.

Reed A.J. (1983): Structural Geology and Geostatistical Parameters of the Afton Copper-gold Mine, Kamloops, B.C., *Canadian Institute of Mining and Metallurgy*, Bull., Vol. 76, No. 856, pp. 45–55.

Robie, R.A., Hemingway, B.S., and Fisher, J.R. (1978): Thermodynamic Properties of Minerals and Related Substances at 298.15K and 1 Bar (10^5 Pascals) Pressure and at High Temperatures, *United States Geological Survey*, Bull. 1452, 456 pp.

Sheppard, S.M.F., Nielsen, R.L., and Taylor, H.P., Jr. (1969): Oxygen and Hydrogen Isotope Ratios of Clay Minerals from Porphyry Copper Deposits, *Economic Geology*, Vol. 64, pp. 755–777.

_____ (1971): Hydrogen and Oxygen Isotope Ratios in Minerals from Porphyry Copper Deposits, *Economic Geology*, Vol. 66, pp. 515–542.

Steward, D. (1984): Afton Orebody Precious Metal Model., Paper 5.4 presented at the *Canadian Institute of Mining and Metallurgy*, Ninth District 6 Meeting, October 24–27, 1984, Kamloops, B.C.

Wedephol, K.H. (1966): Die Geochemie der ä Gewässer, Naturwissenschaften 53, 14, 352–354.

APPENDIX IA.

MAJOR ELEMENT GEOCHEMISTRY AND BRIEF SAMPLE DESCRIPTIONS OF THE MAJOR INTRUSIVE PHASES OF THE IRON MASK PLUTON AND ROCKS IN ITS VICINITY

Field No.	SiO_2	Al_2O_3	Fe_2O_3	MgO	CaO	K_2O	Na_2O	TiO_2	MnO	P_2O_5	Total	Unit	Field Name and Remarks
77KN-2	47.13	17.86	12.51	5.47	8.18	1.32	3.95	2.93	0.19	0.41	99.95	Tertiary	mesocrystalline basalt; compare mesocratic gabbro; strongly magnetic.
77KN-9	58.04	15.71	5.67	3.20	5.11	2.8	13.6	10.87	0.10	0.20	95.32	volanic	dark grey andesite.
77KN-59	55.23	16.74	7.14	3.28	4.25	3.85	3.80	1.12	0.10	0.48	95.99	rocks	dark grey andesite with obvious trachytic texture; slightly magnetic.
77KN-35	44.07	15.56	11.25	5.29	10.49	3.16	2.21	0.77	0.17	0.23	93.20		purplish basaltic andesite; epidote alteration prominent.
76IM11-III	50.03	18.45	9.11	3.39	9.01	0.84	4.06	0.82	0.17	0.61	96.49		yellowish green tuffaceous andesite.
74KN-332	51.59	17.54	6.22	2.27	8.68	1.20	3.38	0.46	0.14	0.50	91.98	Nicola Group	red tuff breccia.
76IM10 I	47.56	13.74	9.95	9.42	9.51	2.09	2.70	0.76	0.17	0.23	96.13		porphyritic dark green flow breccia.
74KN-342	45.85	17.13	9.00	3.45	8.38	2.96	3.48	0.67	0.24	0.76	91.92		reddish tuff breccia.
82-6-11-4	46.56	10.19	9.83	17.73	7.57	2.91	1.80	0.60	0.14	0.24	97.57		massive, dark green basaltic breccia, porphyritic with olivine and pyroxene.
82-6-10-1	56.63	18.11	6.25	2.69	6.30	3.21	4.67	0.71	0.14	0.30	99.01		medium-grained diorite with evenly distributed poikilitic patches of feldspar.
82-6-11U	56.45	17.82	5.42	2.10	5.72	2.88	5.10	0.66	0.07	0.35	97.07		light-coloured, medium-grained diorite; local poikilitic feldspathic patches.
74KN-99 II	60.22	18.20	4.58	1.91	4.67	6.87	3.76	0.48	0.16	0.32	101.17		medium-grained syenite with minor diorite fragments (?).
74KN-28 I	56.72	15.71	3.39	0.70	5.87	8.44	2.56	0.38	0.14	0.07	93.98		porphyritic microsyenite breccia.
74KN-1O4 I	56.29	19.41	5.04	1.74	4.76	5.37	4.45	0.77	0.09	0.22	98.14		micromonzonite, slightly magnetic.
74KN-15 III	62.10	19.15	3.34	0.61	2.69	0.04	9.40	0.39	0.09	0.07	97.88	Cherry	micromonzonite, albitized?
74KN-36	55.27	18.60	6.94	2.92	1.50	5.75	4.39	0.67	0.06	0.62	96.72	Creek	micromonzonite breccia.
74KN-53 I	57.19	16.81	5.02	1.19	5.15	3.44	5.70	0.42	0.08	0.11	95.11		fine-grained monzonite.
74KN-130	54.82	20.03	2.53	4.77	5.97	1.54	5.76	0.91	0.11	0.08	96.52		microdiorite.
74KN-27	51.39	17.99	10.75	2.89	7.21	1.47	5.28	0.81	0.14	0.32	98.25		microdiorite, moderately magnetic.
74KN-49 II	65.98	16.43	0.97	1.24	2.18	0.26	8.70	0.33	0.05	0.18	96.32		medium-grained diorite with epidote patches, albitized?
74KN-84 II	52.30	18.26	9.24	4.04	4.62	1.95	5.41	0.72	0.07	0.18	96.79		fine-grained diorite, slightly magnetic.
76IM255 IV	48.96	17.22	9.23	5.46	10.56	2.30	2.99	0.64	0.14	0.61	98.11		fine-grained gabbro with monzonite fragments, weakly magnetic.
76IM133 IV	45.80	14.73	17.80	6.41	7.03	2.19	2.64	0.79	0.06	0.39	97.84		porphyritic hornblende-plagioclase andesite; moderately magnetic.
76IM131 I	52.20	17.35	8.75	5.15	7.16	1.23	4.81	0.71	0.07	0.52	97.95	Sugarloaf	porphyritic hornblende intrusive breccia.
74KN-167	52.45	18.94	7.20	3.79	5.86	3.68	3.88	0.46	0.07	0.34	96.67		hornblende porphyry.
74KN-84 III	47.43	17.41	9.39	5.90	7.95	2.80	3.55	0.59	0.11	0.16	95.29		porphyritic hornblende gabbro, moderately magnetic.
74KN-62	47.93	16.83	11.54	6.13	9.68	1.91	3.11	0.71	0.25	0.73	98.82		dark grey, coarse-grained diorite, weakly magnetic.
74KN-14	41.50	17.84	13.70	6.40	11.50	2.89	1.32	1.00	0.23	0.76	97.14		dark grey, coarse-grained diorite, magnetic.
74KN-42	50.79	18.51	8.29	4.02	10.28	0.89	4.32	0.67	0.19	0.39	98.35	Pothook	dark grey, medium-grained diorite.
74KN-140A	44.82	16.96	12.16	6.08	12.93	1.22	2.18	0.90	0.16	0.22	97.63		coarse-grained greenish diorite.
82-6-10-4	48.98	14.06	12.52	6.19	10.52	1.58	3.01	0.94	0.21	0.17	98.18		massive, dark grey, medium-grained gabbro.
82-6-10-6	49.11	16.43	11.25	4.99	9.53	2.87	3.13	0.86	0.20	0.32	98.69		grey, medium-grained diorite, moderately magnetic.
82-6-8-4	39.48	16.23	17.34	6.80	16.10	0.32	0.86	1.01	0.15	0.15	98.44		dark grey, medium-grained magnetite-rich gabbro; local coarse-grained patches.
74KN-51	43.85	18.10	9.49	6.93	16.43	0.69	1.13	0.83	0.16	0.08	97.69		coarse-grained, dark grey gabbro with minor epidote-albite veins.
74KN-189	38.53	17.26	16.27	7.26	15.12	1.32	0.55	0.88	0.13	0.08	97.40		very coarse grained leucogabbro dominated by plagioclase and pyroxene.
74KN-182	39.04	5.97	23.12	12.16	17.73	0.07	0.29	1.14	0.18	0.08	99.78	Iron	massive, magnetite and pyroxene-rich gabbro.
76IM7-II	47.86	12.68	10.10	11.53	10.14	1.40	2.11	0.65	0.17	0.22	96.86	Mask	fine-grained intrusive breccia with prominent chlorite alteration.
74KN-126	45.60	13.35	11.74	8.68	13.02	2.39	1.22	1.12	0.26	0.09	97.47	Hybrid	gabbro, magnetic.
74KN-203 II	40.14	20.13	12.69	6.20	16.39	0.30	0.88	0.92	0.14	0.07	97.86		intrusive breccia, magnetic; epidote + prehnite alteration common.
74KN-180	43.16	19.37	10.92	6.16	14.53	1.55	0.97	0.84	0.15	0.07	97.72		magnetite-rich gabbro.
74KN-214	48.33	19.29	8.76	4.08	9.08	1.70	3.90	1.10	0.10	0.11	96.45		coarse-grained diorite with discontinuous magnetic bands.
74KN-304 II	44.47	19.63	10.64	5.11	15.24	0.35	1.86	0.87	0.15	0.07	98.39		medium-grained magnetite-rich gabbro with patchy epidote alteration.
74KN-125	40.80	4.06	9.46	34.60	3.43	0.78	0.19	0.15	0.17	0.08	93.72		black, porphyritic basalt, slightly magnetic.
74KN-135	42.98	6.19	9.53	26.00	5.98	1.38	0.54	0.26	0.14	0.08	93.08	Picrite	black, porphyritic basalt, slightly magnetic.
6-11-1	39.69	6.71	10.62	26.39	8.33	1.38	0.30	0.33	0.20	0.18	94.13		dark green, porphyritic basalt, local magnetite-rich inclusions.

APPENDIX IB.
MAJOR ELEMENT GEOCHEMISTRY AND BRIEF SAMPLE DESCRIPTIONS OF ROCKS COLLECTED FROM THE AFTON PROPERTY

Sample No.	SiO_2	Al_2O_3	Fe_2O_3	MgO	CaO	Na_2O	K_2O	TiO_2	MnO	Total	Field Name and Remarks
6-3-3	53.49	17.85	5.31	4.88	2.15	5.69	2.21	0.85	0.04	92.47	medium-grained diorite; magnetite veinlets with calcite envelope common.
6-2-4	51.11	17.96	5.95	4.28	4.67	4.88	2.23	0.85	0.05	91.98	brownish grey, medium-grained diorite; pyrite veinlets common.
GWA-4O	40.02	15.72	8.53	4.56	9.32	3.95	1.59	0.74	0.63	85.06	fine-grained diorite with disseminated chalcocite; mafic minerals replaced by chlorite and calcite.
6-3-1	46.73	17.89	8.55	2.40	6.28	3.32	4.55	0.72	0.30	90.74	pale greenish brown, medium-grained monzonite with pervasive carbonate alteration.
GWA-171	45.34	15.74	7.43	5.87	4.75	6.05	1.12	0.79	0.14	87.23	porphyritic diorite breccia with abundant carbonate patches and chalcopyrite veinlets.
GWA-27	47.37	17.73	10.21	4.72	4.62	4.39	2.18	0.66	0.15	92.03	porphyritic monozodiorite with medium-grained matrix; epiodote-pyrite veinlets common.
GWA-87	49.94	18.63	6.22	4.00	3.71	5.62	1.74	0.74	0.11	90.71	pale green, fine-grained diorite with disseminated and vein pyrite.
6-4-8	49.38	17.96	8.93	4.30	6.08	3.23	4.53	0.74	0.21	95.36	medium-grained monzonite with no obvious mineralization.
GWA-6	50.55	17.88	5.00	4.52	1.79	3.13	6.03	0.81	0.11	89.82	diorite breccia with disseminated bornite and chalcopyrite; K-feldspar and chlorite alteration.
GWA-32	57.35	18.21	4.82	3.63	3.54	7.77	0.54	0.79	0.09	96.74	porphyritic diorite with pyrite and chalcopyrite veinlets; chlorite alteration common.
GWA-95	55.75	15.92	5.05	3.09	6.56	6.86	1.50	0.66	0.15	95.54	medium-grained diorite; streaks of K-feldspar and epidote common.
GWA-22	54.05	18.88	4.08	2.95	3.19	4.55	5.10	0.68	0.21	93.69	micromonzonite breccia; chlorite alteration prominent.
GWA-31	47.75	15.60	3.27	4.40	7.60	2.76	3.42	0.79	0.21	85.80	carbonatized intrusive breccia; compare Nicola Group volcanic rocks.
GWA-7	50.40	17.01	7.50	3.37	5.14	6.13	1.38	0.96	0.10	91.99	porphyritic diorite with fine-grained matrix; patchy K-feldspar and chalcocite common.
6-2-5	54.94	19.32	3.61	3.59	4.75	7.01	0.99	0.76	0.05	95.02	light grey, coarse-grained diorite with minor fracture-lining pyrite.
6-1-13	49.61	16.07	14.05	5.80	0.90	4.86	0.67	0.70	0.11	92.77	chloritized medium-grained diorite breccia with included Nicola volcanic fragments.
6-4-6	47.30	17.23	11.00	4.48	6.85	4.89	1.55	0.98	0.26	94.54	microdiorite with chlorite and epidote alteration; trace disseminated chalcocite also present.
GWA-128	52.41	17.92	4.84	4.34	2.30	4.62	4.57	0.87	0.19	92.06	reddish brown micromonzonite with disseminations and veinlets of chalcocite.
GWA-102	56.75	15.46	3.32	2.64	4.27	6.45	1.20	0.72	0.67	91.48	reddish brown microdiorite breccia with prominent native copper veinlets.
GWA-161	54.80	17.90	3.06	3.12	5.39	7.75	0.93	0.51	0.06	93.52	rather fresh, light grey, medium-grained diorite.
GWA-37	52.74	18.13	6.21	5.39	1.95	7.13	0.79	0.79	0.08	93.21	fine-grained and tuffaceous-looking monzonite; chalcopyrite veinlet with albite envelope observed.
GWA-14	49.94	18.78	6.19	4.53	6.45	4.95	1.71	0.73	0.08	93.36	massive porphyritic monzonite with fine-grained matrix; trace pyrite along fractures.
GWA-35	51.07	17.20	4.41	5.85	4.45	4.31	3.60	0.89	0.37	92.15	microdiorite breccia with patchy K-feldspar; disseminated fine-grained biotite and native copper veinlets.
GWA-43	53.03	18.50	5.52	4.05	4.31	6.20	1.21	0.64	0.12	93.58	porphyritic hornblende microdiorite; minor pyrite along fractures.
GWA-77	54.01	18.58	2.71	4.22	4.35	6.11	1.76	0.81	0.47	93.02	fine-grained diorite breccia with very minor native copper veinlets.
GWA-98	49.46	17.68	6.71	5.24	5.07	5.43	1.03	0.84	0.33	91.79	microdiorite breccia with pervasive epidote alteration; native copper veinlets common.
GWA-20	47.22	16.80	5.90	3.71	7.67	5.04	2.16	0.56	0.07	89.13	fine-grained diorite breccia with chalcoprite ± pyrite ± carbonate veinlets and trace molybdenite.
GWA-29	56.56	17.73	4.50	1.68	2.55	8.14	0.83	0.75	0.05	92.79	carbonatized microdiorite breccia with chalcopyrite.
6-3-2	57.11	19.00	2.80	2.50	2.26	6.66	2.98	0.70	0.10	94.11	pale greenish brown micromonzonite with fracture linings of calcite and chalcocite.
30-1	50.38	17.81	9.45	3.41	2.96	1.85	7.91	0.69	0.27	94.73	pinkish, fine-grained syenite; chlorite + epidote alteration prominent; trace disseminated magnetite.
GWA-86	56.90	14.98	6.08	4.83	4.16	4.93	3.29	1.01	0.09	96.27	light brown porphyritic monzonite with fine-grained matrix; nonmineralized.
6-4-7	49.31	18.07	6.86	2.80	7.42	2.69	4.79	0.84	0.36	93.14	medium-grained syenite with prominent epidote alteration.
6-1-2	54.96	18.22	6.71	2.90	0.95	5.60	4.42	0.67	0.26	94.69	fine-grained syenite with prominent chlorite alteration.
GWA-126	52.67	18.81	4.10	2.21	6.24	2.36	6.88	0.56	0.27	94.10	porphyritic syenite with fine-grained matrix; mafic minerals replaced by epidote patches.
GWA-42	52.15	17.46	2.35	3.57	5.28	6.06	1.54	0.60	0.25	89.26	highly altered microdiorite breccia (?); abundant native copper + chalcocite + amorphous matter.
6-2-21	54.07	17.55	5.62	5.59	4.67	5.98	1.27	0.81	0.22	95.78	medium-grained monzonite with pervasive epidote alteration and very minor native copper veinlets.
GWA-76	48.09	16.17	10.59	5.53	5.72	3.56	2.57	0.88	0.36	93.47	microdiorite breccia with intense chlorite + epidote alteration and specks of copper.

Tertiary Volcanic Rocks											
GWA-101	46.99	14.52	6.76	5.09	7.03	3.65	2.19	1.13	0.11	87.48	greenish grey tuffaceous andesite with minor carbonate veins.
GWA-9	41.04	13.68	7.79	6.04	8.71	3.10	2.18	0.98	0.15	83.67	massive, medium grey andesite; mafic minerals replaced by carbonate.
Latites											
GWA-5	60.24	14.06	6.44	5.08	1.05	3.74	2.64	1.10	0.06	94.41	reddish porphyritic hornblende latite; chlorite alteration common.
GWA-86	3.95	15.54	4.18	2.98	0.59	3.93	2.49	0.49	0.02	94.17	fresh, massive porphyritic hornblende latite.
GWA-90	66.88	15.79	3.40	1.60	0.48	5.05	2.29	0.50	0.02	96.01	reddish latite, slightly porphyritic with hornblende; some quartz and K-feldspar eyes.
GWA-139	64.26	15.55	4.14	3.05	0.61	5.23	2.22	0.49	0.03	95.58	reddish latite, slightly tuffaceous looking; miarolitic cavity filled with chlorite and copper.
GWA-150	56.55	15.45	5.15	3.97	3.08	4.10	3.69	1.02	0.08	93.09	pink latite with eyes of quartz and carbonate.
GWA-154	50.39	14.73	6.88	7.21	4.83	3.44	2.89	0.92	0.09	91.38	dark green porphyritic hornblende latite, compare lamprophyre.
GWA-4	41.85	13.03	6.15	5.45	9.23	1.46	3.72	1.01	0.14	82.04	massive latite with pervasive carbonate alteration.
GWA-24	42.90	12.88	6.35	6.56	8.55	2.03	2.64	1.07	0.14	83.12	light grey porphyritic latite; carbonate veins and alteration common.
Carbonates											
GWA-147	32.15	5.39	8.01	9.03	15.63	0.06	1.45	0.28	0.23	72.23	essentially a quartz-ankerite rock; relic texture comparable to picrite; minor sulphides observed.
6-2-2	49.68	18.54	4.61	2.73	4.79	3.86	3.50	0.69	0.07	88.47	pinkish porphyritic microdiorite (?) with pervasive carbonate alteration.
GWA-155	52.55	18.74	1.80	2.64	4.94	6.45	2.37	0.64	0.20	90.33	pervasively altered, flesh-coloured diorite breccia (?).
6-1-1	46.07	15.65	8.02	3.58	5.23	3.95	2.68	0.63	0.50	86.31	brownish, fine-grained diorite breccia (?) with intense carbonate alteration.
30-10	56.44	15.40	2.61	2.95	5.14	0.15	4.27	0.54	0.07	87.57	carbonatized, greyish white microdiorite (?) with green spots (mica?).
Nicola Volcanics											
6-11-3	44.58	10.51	6.25	6.16	9.55	0.09	3.03	0.63	0.17	80.97	porphyritic hornblende andesite with pervasive carbonate alteration.
6-11-4	40.46	9.71	10.79	10.89	8.07	0.18	1.89	0.56	0.21	82.76	porphyritic hornblende andesite with intense carbonate alteration.
6-3-11	46.50	11.12	12.12	12.81	7.73	2.29	0.84	0.80	0.27	94.48	hornblende-rich lapillistone.
6-11-6	47.45	14.42	12.01	8.57	7.43	3.91	0.27	0.81	0.23	95.10	hornblende-rich tuffaceous andesite; epidote alteration prominent.
Picrite Basalts											
PC-1A	40.84	6.43	8.72	24.91	4.78	0.18	3.17	0.33	0.15	89.51	porphyritic green nodule with abundant clinopyroxene and serpentinized olivine.
PC-1B	41.61	6.68	8.76	21.75	6.83	0.43	3.01	0.33	0.15	89.55	fine-grained, yellowish green, friable crust surrounding the fresher looking nodules.

Note: The KN and IM series of samples included above were collected by K.E. Northcote and the GWA servies by G.E.P. White.

APPENDIX II.
RESULTS OF MICROPROBE ANALYSES OF SELECTED MINERALS[1]

Mineral analysed	Biotite[3]			Epidote[2]		
Sample number	GWA 35	GWA 38	GWA 112	GWA 2	GWA 112	GWA 22
Number of analyses	5	3	6	4	4	3
Na_2O	0.30 ± 0.02	0.27 ± 0.04	0.24 ± 0.03	0.01 ± 0.01	—	—
MgO	19.67 ± 1.25	18.49 ± 0.52	18.81 ± 0.73	0.03 ± 0.03	0.04 ± 0.01	0.03 ± 0.02
Al_2O_3	12.93 ± 0.46	14.87 ± 0.08	13.29 ± 0.23	23.84 ± 0.21	23.38 ± 0.18	23.54 ± 0.28
SiO_2	38.91 ± 0.54	36.74 ± 0.37	38.63 ± 0.33	37.54 ± 0.05	37.25 ± 0.02	37.25 ± 0.22
K_2O	9.28 ± 0.58	9.61 ± 0.13	9.59 ± 0.22	—	0.01 ± 0.01	0.01 ± 0.01
CaO	0.03 ± 0.03	—	0.02 ± 0.05	23.43 ± 0.24	22.83 ± 0.01	23.12 ± 0.15
TiO_2	6.83 ± 1.48	6.28 ± 0.66	5.37 ± 0.80	0.02 ± 0.02	0.01 ± 0.01	0.01 ± 0.01
Cr_2O_3	0.03 ± 0.01	0.01 ± 0.01	0.07 ± 0.06	0.02 ± 0.01	0.02 ± 0.02	—
MnO	0.18 ± 0.05	0.20 ± 0.05	0.24 ± 0.03	0.03 ± 0.02	0.03 ± 0.02	0.02 ± 0.02
FeO	7.41 ± 0.35	8.86 ± 0.25	8.60 ± 0.40	11.82 ± 0.32	12.83 ± 0.40	12.72 ± 0.29
Total	95.57 ± 0.63	95.34 ± 0.04	94.84 ± 0.51	96.74 ± 0.23	96.40 ± 0.20	96.70 ± 0.35
Formulae	$K_{1.66}Na_{.08}$	$K_{1.79}Na_{.08}$	$K_{1.79}Na_{.07}$	$Ca_{1.99}Fe_{.78}$	$Ca_{1.94}Fe_{.85}$	$Ca_{1.97}Fe_{.85}$
	$Mg_{4.22}Mn_{.02}$	$Mg_{4.02}Mn_{.02}$	$Mg_{4.07}Mn_{.03}$	$Al_{2.25}Si_{2.98}$	$Al_{2.19}Si_{2.96}$	$Al_{2.21}Si_{2.97}$
	$Fe_{.99}Ti_{.74}$	$Fe_{1.08}Ti_{.60}$	$Fe_{1.08}Ti_{.59}$	$O_{12}(OH)_{1.03}$	$O_{12}(OH)_{1.15}$	$O_{12}(OH)$
	$Si_{5.66}Al_{2.19}$	$Si_{5.36}Al_{2.65}$	$Cr_{.01}Si_{5.64}$			
	$O_{20}(OH)_4$	$O_{20}(OH)_4$	$Al_{2.36}O_{20}(OH)_4$			

Mineral analysed	Clinopyroxene		Chlorite			Amphibole	
Sample number	GWA 38	GWA 100	GWA 95	GWA 32	GWA 20	GWA 145	GWA 73
Number of analyses	4	2	6	5	6	5	5
Na_2O	0.55 ± 0.20	0.51 ± 0.06	0.01 ± 0.01	0.01 ± 0.01	0.01 ± 0.01	2.45 ± 0.07	2.45 ± 0.04
MgO	14.75 ± 1.19	15.60 ± 0.30	19.71 ± 0.63	21.19 ± 1.23	22.17 ± 1.10	13.59 ± 0.40	14.72 ± 0.24
Al_2O_3	2.14 ± 0.54	1.82 ± 0.15	18.86 ± 0.48	17.70 ± 1.23	18.47 ± 0.27	12.75 ± 0.06	11.88 ± 0.12
SiO_2	52.10 ± 0.55	52.56 ± 0.32	27.91 ± 0.32	29.29 ± 1.11	29.15 ± 0.43	41.66 ± 0.50	41.89 ± 0.25
K_2O	0.01 ± 0.01	0.01 ± 0.01	0.03 ± 0.02	0.11 ± 0.13	0.02 ± 0.01	0.97 ± 0.01	0.89 ± 0.04
CaO	23.28 ± 0.10	23.20 ± 0.08	0.05 ± 0.04	0.03 ± 0.03	0.13 ± 0.09	11.66 ± 0.14	11.53 ± 0.12
TiO_2	0.35 ± 0.10	0.35 ± 0.05	0.20 ± 0.19	0.23 ± 0.18	0.04 ± 0.01	2.65 ± 0.44	3.10 ± 0.14
Cr_2O_3	0.04 ± 0.04	—	0.02 ± 0.02	0.01 ± 0.01	0.01 ± 0.01	0.02 ± 0.01	0.02 ± 0.03
MnO	0.40 ± 0.12	0.47 ± 0.03	0.03 ± 0.06	0.44 ± 0.05	0.06 ± 0.03	0.19 ± 0.02	0.13 ± 0.01
FeO	6.39 ± 1.04	5.39 ± 0.21	19.96 ± 0.77	18.07 ± 1.61	17.01 ± 0.71	11.48 ± 0.42	10.14 ± 0.28
Total	99.98 ± 0.35	99.89 ± 0.35	87.04 ± 0.23	87.08 ± 0.40	87.09 ± 0.33	97.41 ± 0.33	96.75 ± 0.41
Formulae	$Na_{.08}Ca_{.93}$	$Na_{.08}Ca_{.92}Fe_{.17}$	$K_{.01}Mg_{6.09}$	$K_{.03}Mg_{6.43}$	$Mg_{6.66}Ca_{.03}$	$Na_{.70}K_{.18}$	$Na_{.70}K_{.17}$
	$Fe_{.20}Mg_{.82}$	$Mg_{.86}Mn_{.01}Ti_{.01}$	$Ca_{.01}Mn_{.05}$	$Ca_{.01}Mn_{.08}$	$Mn_{.01}Fe_{2.67}$	$Ca_{1.85}Mn_{.02}$	$Ca_{1.85}Mn_{.02}$
	$Mn_{.01}Al_{.08}$	$Al_{.08}Si_{1.98}O_6$	$Fe_{3.44}Ti_{.03}$	$Fe_{3.08}Ti_{.04}$	$Ti_{.01}Al_{3.40}$	$Mg_{3.08}Fe_{1.42}$	$Mg_{3.25}Fe_{1.26}$
	$Ti_{.01}Si_{1.93}O_6$		$Al_{4.58}Si_{5.75}$	$Al_{4.25}Si_{5.97}$	$Si_{5.98}O_{20}$	$Ti_{.76}Al_{2.23}$	$Ti_{.75}Al_{2.07}$
			$O_{20}(OH)_{16}$	$O_{20}(OH)_{16}$	$(OH)_{16}$	$Si_{6.13}O_{22}(OH)_2$	$Si_{6.20}O_{22}(OH)_2$

[1] Feldspar and carbonate were also analysed in most samples listed here. The former varies from plagioclase with $Ab_{.85-.96}$ to K-feldspar with $Or_{.96-.99}$. The latter varies from calcite with an average calcite component of 93 mole per cent to ankerite with an average composition of $Ca_{.48}Mg_{.39}Fe_{.13}CO_3$. Distribution of feldspar and carbonate in the Afton open pit is not uniform. Data used for these two minerals in the text are approximations corresponding mainly to the modal abundance in microdioritic rocks which contain well-preserved hypogene ore. Analyses presented here were obtained using an ARL-SEMQ instrument with the following operating conditions: 15-kv accelerating voltage, 10 μm beam diameter, 40nA beam current and 10-second counting time. Data were computer reduced using Bence-Albee correction factors (Bence and Albee, 1968).

[2] FeO has been converted to Fe_2O_3 prior to calculation of chemical formula. H_2O+ is taken as the difference of the sum of the major oxides from a hundred.

[3] Fluorine was also analysed but found to be an insignificant component in these biotites.

APPENDIX III.
A LIST OF MAJOR MINERAL OCCURRENCES IN THE IRON MASK BATHOLITH

(*See* Figure 2 for Location.)

Map No.	Name	Commodity	Reserve/Previous Production	Description	Reference
1	Afton Mine	Cu, Au, Ag	Orebody comprised 30.84 million tonnes ore averaging 1% Cu, 0.58 ppm Au and 4.19 ppm Ag at start-up	The tabular deposit, consisting of shattered Cherry Creek rocks, comprises two zones. The overlying, deeply penetrating supergene zone is characterized by abundant native copper with subordinate chalcocite and the lower hypogene zone is dominated by bornite and chalcopyrite.	Preto, 1972 Carr and Reed, 1976 Kwong, 1982
2	Ajax	Cu, Au, Ag	Not defined	Dissemination and replacement veinlets of pyrite and chalcopyrite occur mainly in porphyritic Sugarloaf microdiorite. Albitization is prominent.	Preto, 1967
3	Copper King	Cu, Au, Ag	1.78×10^5 kg Cu, 61.8 kg Ag, 33.5 kg Au	Pryite, chalcopyrite and bornite occur in steeply dipping NNW-trending zones of Cherry Creek rocks strongly replaced by K-feldspar and laced by magnetite veinlets.	Carr, 1957
4	Galaxy Copper	Cu, Ag	2.55×10^3 kg Cu, 0.93 kg Ag	Highly variable and irregular copper mineralization occurs in albitized volcanic rocks surrounded by microdiorite.	Preto, 1967
5	Glen Iron	Fe	1.36×10^4 kg magnetite	Generally E-trending veins of magnetite with varying amounts of apatite occur in diorite.	Cockfield, 1948
6	Iron Cap	Au, Cu, Ag	4.8×10^3 kg Cu, 13.95 kg Ag, 6.72 kg Au	Veins and stringers of chalcopyrite commonly associated with albite alteration occur in micromonzonite in fault contact with coarser grained Cherry Creek porphyry.	Carr, 1957
7	Iron Mask and Erin	Cu, Au, Ag, Gypsum	2.46×10^6 kg Cu, 466 kg Ag, 122 kg Au	Diorite mineralized with disseminated chalcopyrite is in contact with barren picrite along a breccia zone.	Cockfield, 1948
8	Joker	Cu, Au, Ag	Not defined	Disseminated chalcopyrite and chalcocite occur in altered zones spatially associated with faulting. Supergene alteration is locally prominent.	Preto, 1967 This study
9	Kimberley	Cu, Au, Ag	Not defined	Widely disseminated chalcopyrite occurs in fractured and brecciated monzonite and diorite.	Carr, 1957
10	Larsen	Cu, Au, Ag	2.9×10^3 kg Cu, 0.84 kg Ag, 0.26 kg Au	Chalcopyrite occurs in diorite breccia in contact with picrite.	Carr, 1957
11	Magnet	Fe	3.68×10^3 crude iron	ESE-striking magnetite veins with subvertical dips occur in diorite and monzonite.	Cockfield, 1948
12	Maxime	Cu, Ag	3.04×10^3 kg Cu, 1.19 kg Ag, 0.03 kg Au	Sparse disseminations of pyrite, chalcopyrite and magnetite occur in fragmental and massive [illegible]anic(?) rocks. narrow and widely separated shears in these rocks carry chalcocite.	Cockfield, 1948
13	Pothook	Cu, Au, Ag	435 kg Cu, 0.16 kg Ag, 0.03 kg Au	Precursor to the Afton discovery. Highly variable bornite and chalcocite occur in shattered Cherry Creek rocks.	Preto, 1972
14	Python (Makaoo)	Cu, Ag, Au	2.18×10^3 kg Cu in 1899 Recent estimates*: Python zone: 223 500 tonnes at 1.11% Cu Noonday zone: 609 700 tonnes at 0.74% Cu Copper Head zone: 116 900 tonnes at 1.13% Cu	Chalcopyrite stringers, lenses and disseminations occur in strongly shattered and albitized diorite adjacent to a lens of picrite.	Carr, 1957

* Data source: National mineral inventory card 510596, Mineral Development Sector, Department of Energy, Mines and Resources, Ottawa.